Reports of the Department of Geodetic Science

Report No. 110

INVESTIGATIONS INTO THE UTILIZATION OF PASSIVE SATELLITE OBSERVATIONAL DATA

by

James P. Veach

Prepared for

National Aeronautics and Space Administration
Washington, D. C.
Contract No. NGR 36-008-093
OSURF Project No. 2514

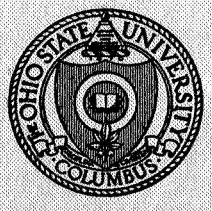

...e Ohio State University
Research Foundation
Columbus, Ohio 43212

...ne, 1968

Reports of the Department of Geodetic Science

Report No. 110

INVESTIGATIONS INTO THE UTILIZATION OF PASSIVE SATELLITE OBSERVATIONAL DATA

by

James P. Veach

Prepared for

National Aeronautics and Space Administration
Washington, D.C.

Contract No. NGR 36-008-093
OSURF Project No. 2514

The Ohio State University
Research Foundation
Columbus, Ohio 43212

June, 1968

PREFACE

This project is under the direction of Professor Ivan I. Mueller of the Department of Geodetic Science, The Ohio State University. Project Manager is Jerome D. Rosenberg, Geodetic Satellites, Code SAG, NASA Headquarters, Washington, D. C. The contract is administered by the Office of University Affairs, NASA Headquarters, Washington, D. C.

Reports of The Ohio State University Department of Geodetic Science related to NASA Contract No. NGR 36-008-093 and published to date are the following:

The Determination and Distribution of Precise Time, Report No. 70, April, 1966

Proposed Optical Network for the National Geodetic Satellite Program, Report No. 71, May, 1966

Preprocessing Optical Satellite Observations, Report No. 82, April, 1967

Least Squares Adjustment of Satellite Observations for Simultaneous Directions or Ranges. Part I: Report No. 86, September, 1967, Part II: Report No. 87, in press, Part III: Report No. 88, December, 1968

Preprocessing Electronic Satellite Observations, Report No. 100, March, 1968

Comparison of Astrometric and Photogrammetric Plate Reduction Techniques for a Wild BC-4 Camera, Report No. 106, March, 1968

Investigations Into the Utilization of Passive Satellite Observational Data, Report No. 110, June, 1968

ABSTRACT

There are several organizations observing satellites for geodetic purposes. Satellites have provided an object at a finite distance which can be used to establish the spatial relationship between several ground stations. This relationship may be extended over much greater distances and is free of many limitations and errors inherent in the classical terrestrial methods of triangulation. It does present new problems of its own however.

This report describes several methods of determining accurate satellite positions optically. Specifically, it deals with passive satellites recorded against the stellar background on the photographic plate of a metric camera. The trail of a passive satellite consisting of several hundred images on a photographic plate may be utilized for geodetic purposes in several ways:

(1) All image coordinates may be fitted to a single polynomial with the time as argument and all the information on the plate is aggregated into a single highly precise fictitious satellite direction. This is the approach of the USCGS using the Wild BC-4 camera plates.

(2) The image coordinates may be divided into 3 - 4 groups and a separate polynomial is fitted to each group. The information on the plate thus is aggregated into 3 - 5 fictitious satellite directions each somewhat less precise than the one in (1). The advantage of this method is that it is possible to deduce 3 - 5 simultaneous observations even from single plates which may yield a solution for the directions between the stations involved. Method #(1) does not provide a solution from single plates. If this method is used, it may be possible to reduce the time which must be spent at each of the observation stations.

(3) Each or selected (e.g., every twentieth) images may be reduced individually and used in the geodetic solution. In this case there will be as many simultaneous observations deduced from each pair of plates as many images were selected. The advantage of this method is the inexpensive plate reduction. It is estimated that to reduce one image costs about $15; thus for the maximum of

15 - 20 images per plate the cost would be $225 - 300, which figure is much less than the amount required to reduce a plate with Method #(1).

(4) The right ascension and declination of each image (this is the form in which for example the BC-4 data is deposited in the Data Center) may be used directly in the short-arc mode.

The paper deals with the results obtained in the four modes mentioned above. The accuracy aspects of the four solutions are investigated.

TABLE OF CONTENTS

LIST OF FIGURES

LIST OF TABLES

1. INTRODUCTION

The purpose of this study was to determine the optimum method of utilizing the observational data from a ballistic camera. The camera studied was the BC-4 used by the Environmental Sciences Services Administration (ESSA).

Two aspects of the subject were studied and are discussed here. The first was how a single or several individual satellite images can be obtained. The second was a data compression process in which the information contained in several satellite images could be condensed into a single, more accurate image.

No entirely new procedures have been developed; neither were any agency procedures copied in total. Those now in use in the United States provided a basis for the investigation. No attempt was made to support the methods of any agency; some criticisms of specific agency procedures and results have been encountered during background research. As these criticisms would apply equally to this study, they have been discussed in the particular section of the report to which they apply.

The ballistic camera and passive satellite combination offer a convenient area of investigation. Up to 600 satellite images and 150 stars appear on each plate, and the plates are rigorously measured and reduced by ESSA.

The BC-4 camera consists of a modified Wild RC-5 aerial camera mounted on a T-4 theodolite base. Originally an Astrotar lens was used, but recently it has been replaced by a lens of longer focal length (300 mm vs. 450 mm). This new lens was designed especially for satellite photography. The camera is equipped with rotating and capping shutters to control the rate and length of exposure. The

rotating shutters are indirectly controlled by a quartz crystal oscillator and are used to chop the satellite image trail into precisely time correlated segments. The capping shutter is used to chop star trails before and after satellite passage; the star images provide the necessary control to determine the orientation of the camera during the satellite pass.

The final product of the BC-4, or any other camera used similarly, is a photographic plate or film from which a satellite direction may be obtained. In this study, a satellite direction is defined as any convenient set of coordinates which determines a direction in space to the satellite. Normally these are the equatorial coordinates—right ascension and declination. In the case of the ESSA data, a satellite direction is expressed in terms of x and y plate coordinates which, together with the camera orientation parameters, define a spatial direction.

In any case, the resulting satellite direction can be used to precisely locate the camera station. First considered is the purely geometric approach, the formulation of which is attributed to Väisälä. Briefly stated, this theory postulates that an elevated target (the satellite) and two ground stations instantaneously determine a plane. Two satellite positions and the two ground stations determine two planes which intersect in a line common to the two stations. Extending this reasoning, the intersection of sufficient planes (five for a unique solution) determines a spatially oriented triangle. Inherent to this method is the requirement for simultaneous observation of the satellite from two or more ground stations.

In practice, certain restrictions must be imposed on the satellite's position at the time of observation. To simplify the refraction problem, it is generally agreed that the zenith distance of the satellite should not exceed approximately 60°. To provide geometric strength to the solution, the distance to the satellite should be approximately equal to the distance between the observing stations; and the two planes forming the triangle sides should intersect in an angle of nearly 60°.

Scale can be introduced into the spatial triangle by measuring the range to the satellite or by measuring the distance between two of the observing stations.

The simplest alternative to the geometric approach is the "short-arc method." This approach has advantages and disadvantages when compared to the purely geometric. One advantage is that simultaneous or very nearly simultaneous observations are not required. This, in turn, allows a less demanding observing program. A disadvantage is that the solution for the station coordinates necessarily involves the potential field of the earth.

The short-arc method implies a series of observations made along the satellite's orbital arc. This arc is instantaneously defined by six orbital elements. These elements are continuously changing. They are a function of air drag, solar radiation pressure, and most importantly, the gravitational field through which the satellite is traveling. Brown states [Brown, 1967, p. 4] that when using arcs of one-third of an orbit or less and reasonably precise coefficients of the geopotential, errors in the final station coordinates due to errors in the coefficients are negligible.

A detailed description of the short-arc theory and practice may be found in [Brown, 1967]. The geometric theory as it is employed by ESSA is described in [Schmid, 1965b].

1.1 Background

There are four agencies in the United States photographing satellites and reducing the resulting plates or film. These agencies are all contributors to the National Geodetic Satellite Program (NGSP). The three agencies in addition to ESSA are the Goddard Space Flight Center of the National Aeronautics and Space Administration (GSFC, NASA), the Aeronautical Chart and Information Center of the United States Air Force (ACIC) and the Smithsonian Astrophysical Observatory (SAO). The NGSP will provide large amounts of observational data and portions of this report are directly applicable to it.

Each agency has developed equipment and procedures particularly suited for its own objectives. Only recently have there been attempts to use data from several agencies in a single station adjustment; such a program is now in progress here at The Ohio State University (OSU). Consequently, there has been considerable

effort to examine the various agency procedures and to document the differences which exist. Capt. Frank D. Hotter developed procedures to rigorously reduce the four agencies' observational data to a common reference system [Hotter, 1967, p. 141]. Capt. Daniel H. Hornbarger further compared the agencies' plate reduction procedures [Hornbarger, 1968] and found that all now give similar results.

Photographic plate reduction can be divided generally into two categories, photogrammetric and astrometric. The photogrammetric technique attempts to identify and model all sources of systematic error. The parameters of the mathematical model are recovered simultaneously with the camera orientation and satellite directions during the final plate reduction. ESSA is the only agency doing a photogrammetric reduction as defined here.

A great deal of effort is expended by ESSA to insure accuracy in timing and plate measurement. A very large amount of observational data is used to orient and to calibrate the taking camera. The camera calibration is performed with every plate using a photogrammetric model of up to 22 parameters (18 normally as ESSA employs the Garfinkel refraction model with four coefficients which are not treated as unknowns in the data available to this author). After this extensive measuring and plate reduction, all satellite images are reduced to a single observation through a curve fitting process. The ultimate accuracy is represented by a standard deviation of between 0".3 and 0".4 for the determination of an individual direction to a fictitious satellite image near the plate center [Schmid, 1965b, p. 19]. This estimate is based on approximately 150 star and 600 satellite images.

In contrast to the photogrammetric is the astrometric plate reduction. This method was developed in the late nineteenth century by astronomers interested in stellar positions and proper motions. It is normally used with cameras of long focal length and small field of view and is generally considered the simpler method of the two.

The astrometric model may assume several different mathematical formulations [Hornbarger, 1968, pp. 40, 68, 76; Brown, 1964, p. 88; Hallert, 1960, p. 15]. Most importantly though, no attempt is made to give a physical interpretation to

the parameters of the mathematical model. When using this method and cameras with a wide field of view, the measured plate coordinates would normally be corrected for known, or predetermined, systematic errors. The parameters of the model (plate constants) would then be expected to absorb the unknown distortions that remain.

In either plate reduction technique, object and image spaces are related through central projection theory. This implies a two-step procedure. First, a plane is constructed tangent to the celestial sphere, the point of tangency being nominally the point of intersection of the camera's optical axis and the celestial sphere. The star and satellite images are projected mathematically to this plane. The second step is to define the projective relationship between the coordinate systems of the photographic plate and the tangent plane.

It is assumed that the reader is acquainted with both the photogrammetric and the astrometric methods of plate reduction. For those interested in detailed discussions of these subjects: for the photogrammetric method see [Schmid, 1959] or [Brown, 1964]; for the astrometric method see [Smart, 1962]. Chapter 3 of [Hotter, 1967] gives a summary of both methods.

This author did not attempt any photogrammetric plate reductions. The ESSA results were used in the sections of this report concerned with the subject. Furthermore, they were used as the accuracy standard for the astrometric reductions.

The astrometric portions of this study are based generally on the conclusions of Hornbarger's report [Hornbarger, 1968, p. 89]. The following are of particular interest to this study:

(1) The astrometric technique cannot be used to reduce an entire photographic plate from a camera with a field of view comparable to the BC-4. This is certainly not a new finding. However, Hornbarger graphically demonstrated this fact for the BC-4.

(2) If the measured plate coordinates are corrected for refraction and lens distortions (radial and tangential), the projective equations produce quite satisfactory results.

(3) If refraction corrections are applied to the updated stellar images (Garfinkel model with four coefficients), the astrometric technique can give satisfactory results for a small area around the plate center.

1.2 Available Data

The entire study was made possible by ESSA who supplied three plates from their BC-4 cameras along with punched card and output listings from their various plate measurement and reduction programs. The three plates constituted a simultaneous observation of the passive satellite Echo II made on November 30, 1965 (see Figs. 1.1, 1.2, 1.3).

The data was supplied to Dr. Ivan Mueller of The Ohio State University Department of Geodetic Science by ESSA in September, 1967. The simultaneous observation (an event) was recorded by cameras equipped with the 300 mm lenses. The stations participating in this event were:

Lynn Lake, Manitoba, Canada	plate 2559
Frobisher Bay, NWT, Canada	plate 6132
Cambridge Bay, NWT, Canada	plate 5205

Accompanying the plates were the output of the various ESSA plate measurement and reduction programs in the form of punched cards and output listings. Included in the data and of interest to this report are:

(1) Updated star positions of all stars on the plate that were measured and identified. These were apparent positions, i.e., updated for precession, nutation, proper motion and annual aberration.

(2) Measured plate coordinates of all stars appearing on the plates and the sidereal times of their observation.

(3) Measured plate coordinates for the satellite images, the sidereal times of observation and an approximate range to the satellite at the time of observation.

(4) "Adjusted" plate coordinates of the satellites. These adjusted coordinates were corrected for:

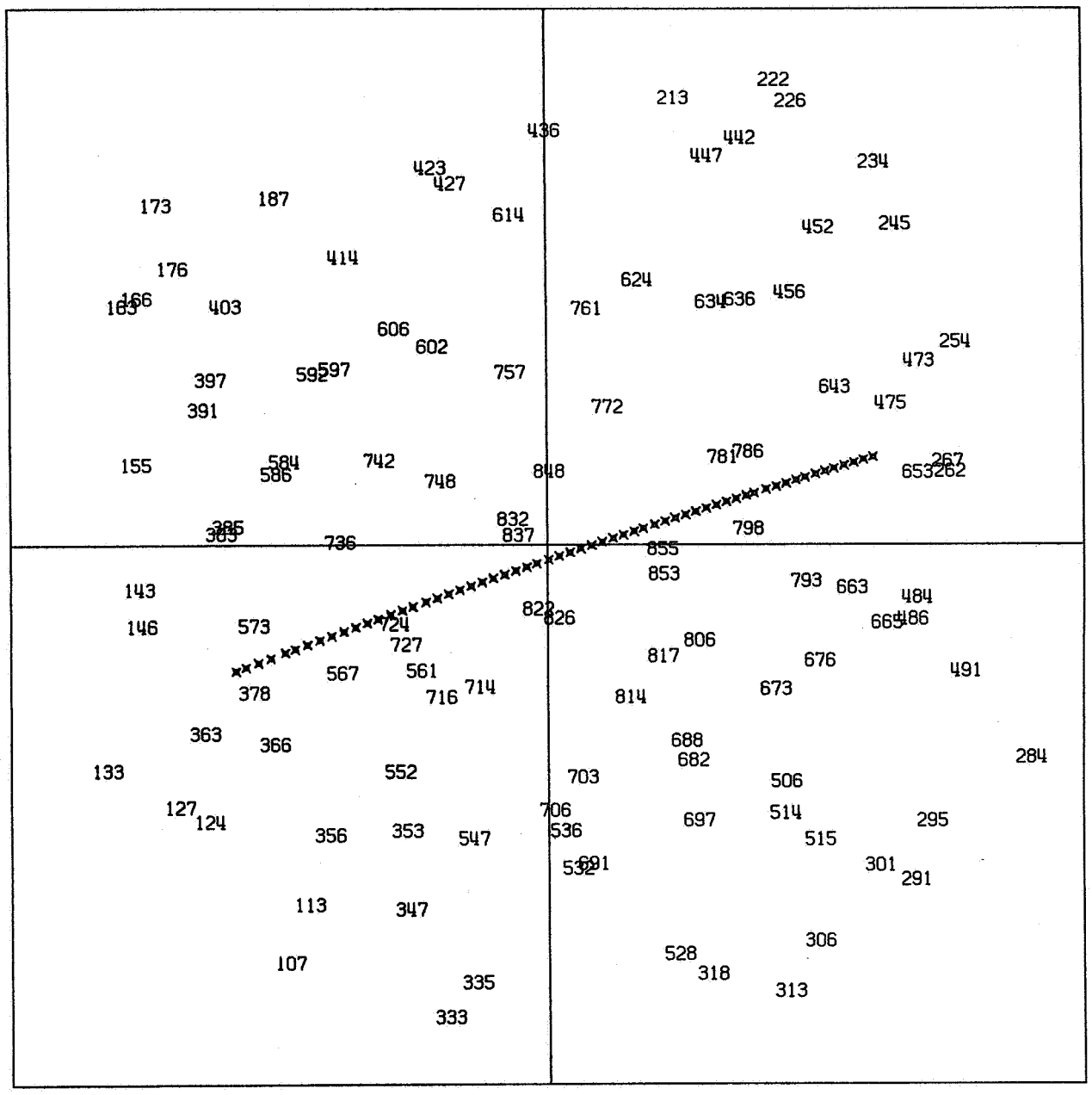

Fig. 1.1 Plate 2559: Star and Satellite Images
Central Star and Every 10th Satellite Image Are Plotted

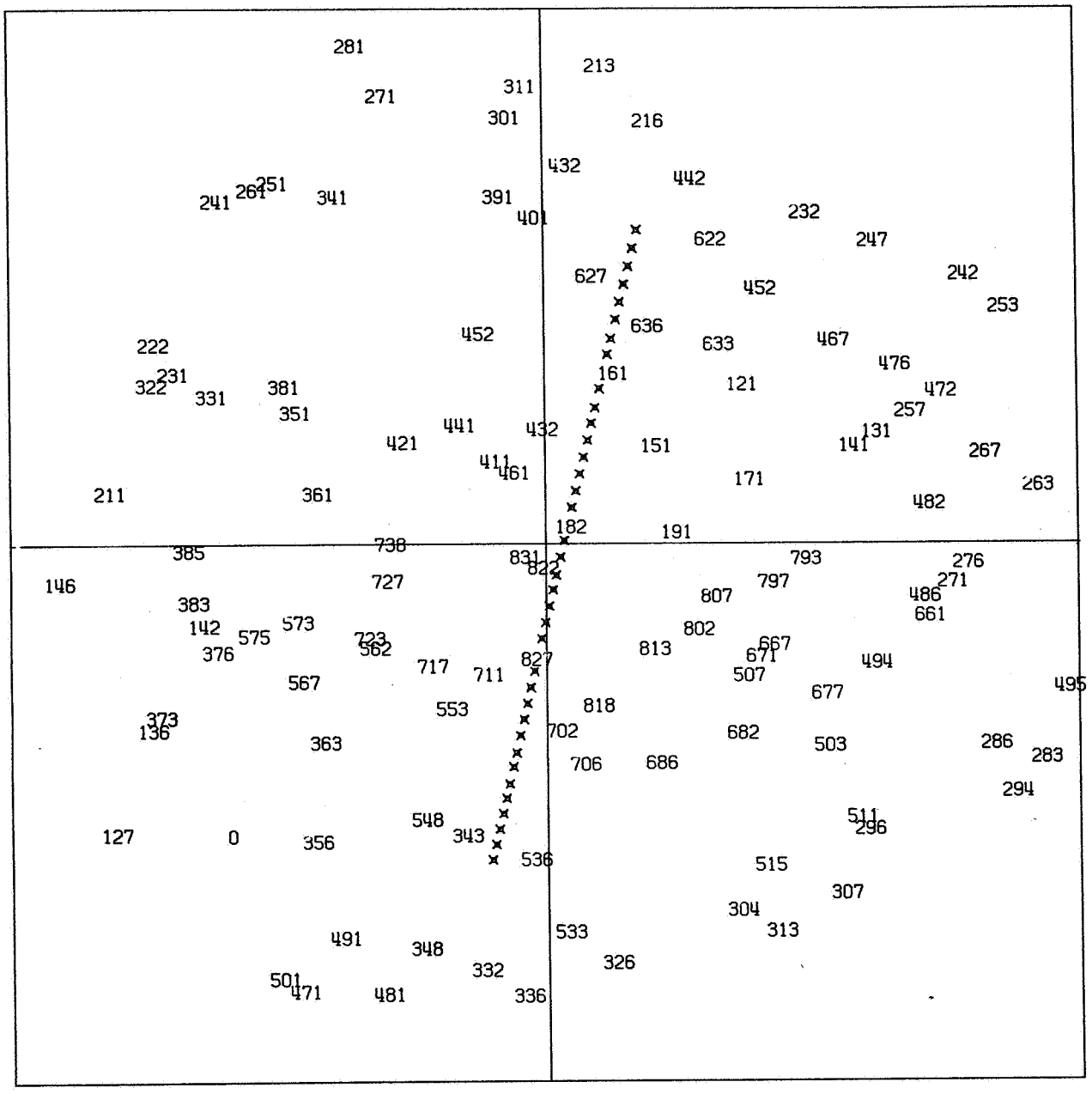

Fig. 1.2 Plate 5205: Star and Satellite Images
Central Star and Every 10th Satellite Image Are Plotted

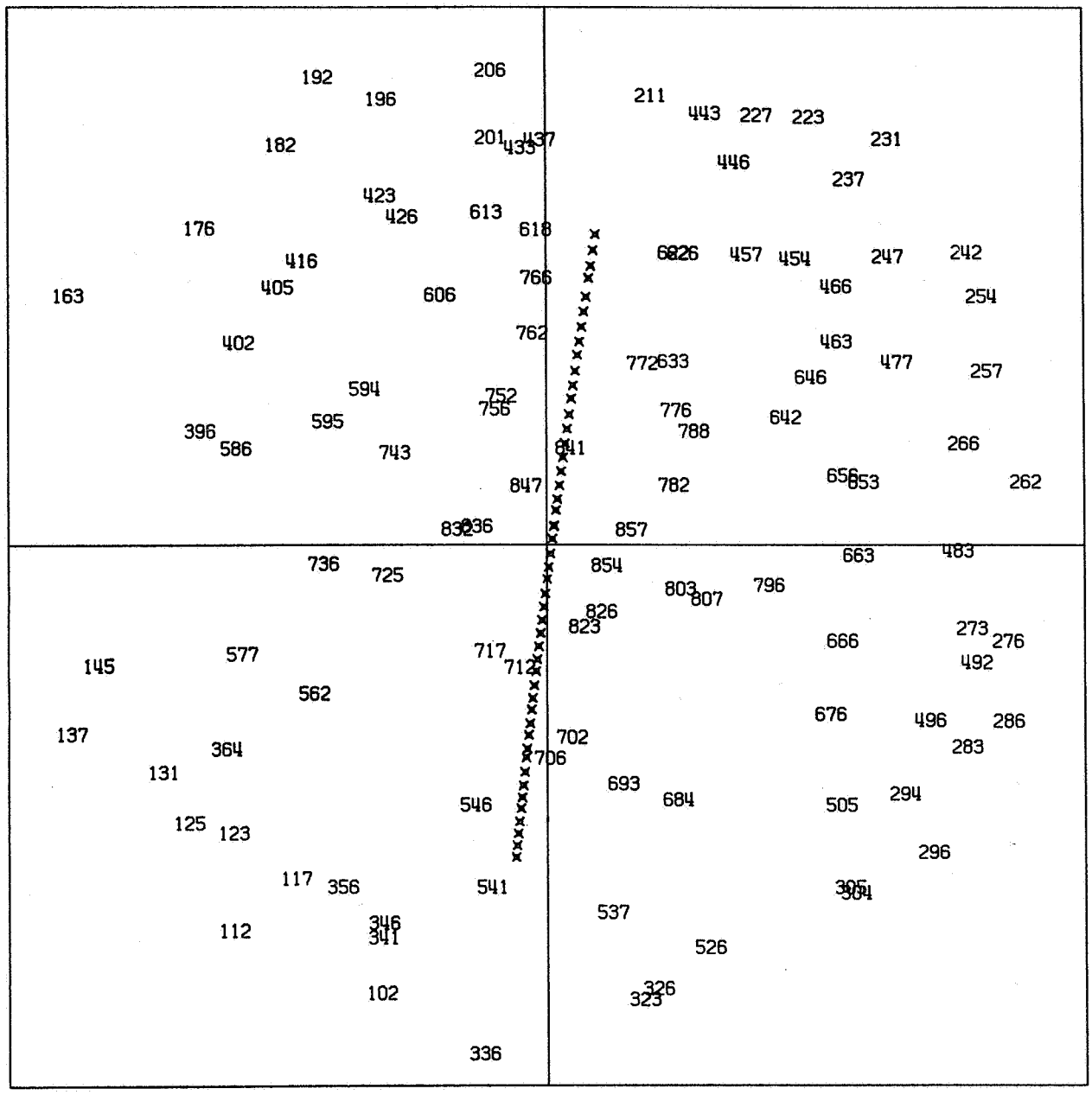

Fig. 1.3 Plate 6132: Star and Satellite Images
Central Star and Every 10th Satellite Image Are Plotted

(a) nonorthogonality of the comparator axis (the comparator used to measure the star and satellite images)

(b) radial and tangential lens distortions

(c) atmospheric refraction (astronomic less parallactic)

(d) phase angle

A detailed description of these corrections can be found in [Hotter, 1967].

(5) Right ascensions, declinations, azimuths and altitudes of each adjusted satellite image.

(6) Station data which included:

(a) latitude and longitude

(b) atmospheric information

(c) station clock corrections

(8) The single camera orientation program. This output listed, in addition to the elements of interior and exterior orientation, the parameters required to apply the corrections listed in (5) above. See [Hotter, 1967, p. 117 or USCGS Technical Bulletin No. 24, p. 13] for a description of this program.

The methods employed by ESSA are well described in Technical Bulletin No. 24 of the USCGS, 1965; and the reader is referred to this publication for a general description of how the data is obtained and reduced.

Also available was a computer tape supplied by the National Space Science Data Center. This tape contained the observational data in the form of satellite right ascensions and declinations from 270 BC-4 plates. It was supplied to the Data Center by ESSA.

The IBM 7094 computer at OSU was used extensively in all mathematical computations.

The Omnitab Computer Program of the National Bureau of Standards (University of Maryland version) was available and used in the curve fitting and statistical analysis of the data as well as in some plotting. The OSU IBM 1620 was also used in the data plotting.

The adjustment program developed by Hornbarger [Hornbarger, 1968] was

modified and used extensively in the astrometric plate reduction portions of this study. In addition, several subroutines written by him were copied in total or modified and included in programs written by this author.

The programs written by this author were in the Scatran language in use at OSU.

2. A SINGLE ASTROMETRIC SATELLITE DIRECTION

No agency in the United States is today obtaining final satellite directions with this method. It is of interest to this study because of its expected accuracies and limitations. It also provides a standard of comparison for the more rigorous alternatives and a convenient area to investigate the systematic and random errors associated with metric cameras.

The only agency doing an astrometric reduction is the Smithsonian Astrophysical Observatory. No direct comparison can be made between their results and those of this author because of dissimilar equipment and reduction methods. However, a brief discussion of the SAO procedure serves as an introduction to the subject.

In the past, the SAO has used the Baker-Nunn camera although they have a new camera under development. The Baker-Nunn is a modification of the Super-Schmidt f/1 telescope so mounted that it can track along any great circle. The focal length is 500 mm, the field of view is $5^{\circ} \times 30^{\circ}$, and film is used against a spherical platen to record the stellar and satellite images [Mueller, 1964, p. 245]. For precise geodetic observations, the camera is normally employed in the stationary mode [Lambeck, 1967, p. 90].

The important difference in the reduction method is the astrometric model used. The SAO uses the Turner's method [Hotter, 1967, p. 103], which is of the form

$$\xi = Ax + By + C$$
$$\eta = Dx + Ey + F$$

where A, B, C, D, E, and F are adjustable plate constants. The Turner equations are applied to a relatively small area around the satellite image.

In this study, the model used was

$$x = \frac{A\xi + B\eta + C}{a\xi + b\eta + 1} \quad ,$$

$$y = \frac{D\xi + E\eta + F}{a\xi + b\eta + 1} \quad .$$

The additional plate constants, a and b, should accommodate nonparallelism of the tangent plane and photographic plate.

It should be pointed out that in an undistorted central projection, a and b are not independent of the original six plate constants. Therefore they should be constrained by the two additional equations [Brown, 1964, p. 88]

$$AB + DE + ab = 0 \quad ,$$
$$A^2 + D^2 + a^2 - B^2 - E^2 - b^2 = 0 \quad .$$

These constraints were not included in the adjustment program available. In an attempt to determine the extent to which these conditions were satisfied, numerical values were computed from the expressions above. The final plate constants from several different sets of data were used. The departures from zero were random and normally very small. They could have been accommodated by slight changes in the plate constants.

It was not clear whether these constraints were applicable in all cases where the adjustment program was used. In the outer areas of the plate, the projection was obviously not undistorted. The constraints were not included. It appeared that if errors were actually introduced by their exclusion, they would not be significant.

2.1 Accuracy Estimates and Error Sources

In data submitted to the Geodetic Satellite Data Center, the SAO estimates an accuracy of a single direction to be 4"; this is probably a conservative estimate. Recent results support accuracies of 2".0 to 2".5 [Lambeck, 1967, p. 96]. It is expected that BC-4 data would yield similar results.

The major sources of error in the computed satellite directions could be timing, plate measuring, image motion (shimmer), uncompensated lens distortions, and the star catalog. Among the other error sources usually considered less important are emulsion shifts and irregularities, plate flatness, phase angle correc-

tions and rapidly varying or differing magnitudes of stellar and satellite images. The following paragraphs will briefly describe the major error sources, their effect on an astrometric reduction and their expected magnitudes in relation to the BC-4 plates. In paragraph 2.16, an accuracy estimate for a single satellite direction is given.

Before proceeding further, it was necessary to establish a reference to which the results of the astrometric reductions can be compared. Generally, ESSA's photogrammetric results accompanying the data were used as a standard.

There was no reason to question any of the ESSA material. For thoroughness and in the course of normal experimentation, Hornbarger verified the ESSA star updating program using Department of Geodetic Science programs. ESSA and this author obtained nearly identical equatorial coordinates from measured or adjusted plate coordinates and the orientation parameters. Other quantities, such as refraction and phase angle corrections agreed very closely in all cases. This led to the conclusion that the final values obtained from the two plate reduction techniques could be compared directly. No systematic differences were introduced by the computational methods or mathematical formulations used in the various data reduction steps.

2.11 Timing Errors

The data acquisition procedures used by ESSA attempt the ultimate in timing accuracy. The value claimed for the star images is 3 to 4 ms referenced to Universal Time (UT); for the satellite images, a maximum error of 100 μs is expected. The 4 ms for the star recordings would result in a maximum directional error of 0".06, a 100 μs error in timing for the satellite would correspond to a directional error of 0".1 or less even for relatively low orbital altitudes [Schmid, 1965b, p. 20].

The problem of satellite timing is critical when using passive satellites in the geometric method with its requirement for simultaneous observations. Active satellites (flashing beacon) obviate this requirement. A widely quoted figure for timing accuracy in the observation of satellites for geodetic purposes is Markowitz's

value of 1 ms [Markowitz, 1963, p. 217]. The BC-4 timing data easily meets this standard.

2.12 Plate Measurement

Plate measurement imposes a very real barrier to the attainable accuracies associated with photographic plates. Schmid's experimentation at ESSA indicates a precision of 1.8 μm for a single coordinate measurement [Schmid, 1965b, p. 19]. This would indicate that the repeatability of a single measurement is not better than 1".2 (arc) for the 300 mm camera. For the Baker-Nunn photographs at the Smithsonian, the comparable figures are 2.5 μm and 1".1 [Lambeck, 1967, p. 76]. For the later model BC-4 camera with 450 mm focal length, the plate measurement error estimate would be reduced to about 0".8. In addition to these "pointing" errors, there may be additional systematic errors introduced by the comparator [Brown, 1967, p. 22].

The obvious way to decrease the effect of the random errors is to increase the number of pointings on each image. To reduce operator and image bias the plate may be measured twice, a rotation of 180° being made between each set of measurements.

ESSA does measure the plates in a direct and rotated position; apparently only one pointing is made on each image in each position however. Redundancy of measurement is obtained indirectly because each star trail is chopped into five segments, each of which is measured and then reduced to a single image. In the ESSA reduction method where all satellite images are compressed into one, the large number of images measured should minimize the effect of their random pointing errors.

In contrast to ESSA, this author normally used just one image from each star trail. A limited sample was obtained using all five star images reduced to a single set of coordinate measurements which corresponded to the time of the central image.

In this chapter where only a single set of star and satellite coordinates were used, the maximum effect of plate measurement error can be expected.

2.13 Lens Distortions

As has been mentioned previously, Hornbarger found that "a confined area no greater than 3 cm (6°) in radius from the plate center can be reduced with good results" [Hornbarger, 1968, p. 89]. This was true for the three BC-4 plates available; more camera and lens combinations would have to be investigated before this statement could be generalized.

For this part of the study his recommendations were followed. A circle of approximately 6° radius was drawn around the center, and the remainder of the plate was not reduced (Figs 2.1, 2.2, 2.3). It was assumed that the lens distortions occurring in this reduced plate area would be adequately accommodated by the astrometric reduction.

2.14 Star Catalog

ESSA uses the Smithsonian Astrophysical Observatory Star Catalog [SAO, 1966] which is referenced to the FK-4 catalog system. Estimates of positional standard deviations are given in the SAO catalog. ESSA has used these estimates to select stars with a positional accuracy of better than 0".4 to use in plate reduction [Schmid, 1966, p. 9]. Only these "good" stars are used in the BC-4 data.

In addition to the random errors, there may be unknown systematic errors in the FK-4 system and further systematic errors introduced when the SAO catalog was compiled from its constituent catalogs. Lambeck estimates 0".3 to be a reasonable figure for these errors [Lambeck, 1967, p. 80].

An astrometric reduction done within a small plate area, and consequently, with a small number of stars, is particularly susceptible to either random or systematic errors of the catalog.

2.15 Image Motions

The magnitude of image motion, or shimmer as it is often termed, is the subject of some controversy. Turbulence in the atmosphere produces random changes in its refractivity; this, in turn, causes a light ray to continuously deviate from its expected path.

Lambeck gives a review of the literature and experimentation regarding the

subject [Lambeck, 1967, Chapter 1.2]. His findings are briefly summarized here:

(1) Image motion is irregular—both amplitude and period vary.

(2) The motion may be categorized generally into long period (one minute) and short period (less than one second) phenomena.

(3) The long period motion is associated with amplitudes of about 0".5 while short period fluctuations reach several seconds of arc.

ESSA results indicate a standard deviation of 1".5 attributable to shimmer [USCGS Sp. Pub. No. 24, 1965, p. 14]. Brown believes a much smaller figure to be valid at the zenith and disagrees with Schmid [Brown, 1967, pp. 122, 126]. It seems that Brown interprets Schmid's 1965 references to image motion as a claim for a much higher standard deviation value, i.e., "two to three seconds of arc" [Brown, 1967, p. 126].

Schmid cites one example [Schmid, 1965b, p. 19] of a total standard deviation for a satellite image of 3.2 μm across track and a slightly larger 3.5 μm along track. The same reference allows a contribution of up to 1.5 μm from plate measurement. If an allowance of 1.0 μm is made for emulsion instability and other random errors (as Brown does), the shimmer effect is only 1".8. If the allowance for emulsion instability is raised to 1.5 μm as Brown does for the PC-1000 camera, the shimmer effect is further reduced to 1".6 Either figure is compatible with extreme values of 3" (see p. 18).

The three BC-4 plates under consideration here have an average standard deviation of about 2".8 along track and 2".5 across track. Using the same allowances as above for the other error sources, the component attributable to shimmer would range between 0".9 and 1".4.

Brown does an analysis of 10 ESSA BC-4 plates which yields a somewhat smaller estimate of "around 0".8" [Brown, 1967, p. 121]. In the same reference he cites, among other examples, the results of a PC-600 camera experiment on a "calm and clear night" in which the effect was much less. Lambeck concludes that for the Baker-Nunn, a relatively large aperture camera, an "average" image

motion of 0".7 is to be expected with an active satellite [Lambeck, 1967, p. 42]. He goes on to point out that Brown's formulations would yield an average value of only 0".1 for the Baker-Nunn and a maximum of about 0".2.

Although the absolute magnitude of image motion may be controversial, there does seem to be general agreement on the factors that influence it. They are atmospheric stability (seeing), exposure time, lens aperture and zenith distance.

The BC-4 data available is characterized by short satellite exposures, relatively large zenith distances and small apertures. A standard deviation estimate of 1".5 is not unreasonable.

2.16 Estimate of Total Error

The error in a satellite direction can be attributed for the most part to the error sources already discussed. Lambeck gives (with changed notation) for the total expected standard deviation [Lambeck, 1967, pp. 74, 80, 81]

$$\sigma_T = [(1 + \gamma^2)\sigma_m^2 + \frac{\sigma_c^2}{n} + \sigma_\psi^2]^{\frac{1}{2}}$$

where

$$\gamma^2 = \frac{\theta'^2 \sigma_t^2}{\sigma_m^2}$$

and

$$\sigma_c^2 = \sigma_s^2 + \frac{\sigma_r^2}{n}$$

θ' being the apparent angular velocity of the satellite, σ_t^2 the timing variance, σ_m^2 the plate measurement variance, σ_s^2 and σ_r^2 the variances associated with systematic and random star catalog errors respectively, σ_ψ^2 the image motion variance and n equal to the total number of stars carried in the reduction.

This author believes an additional term, σ_U^2, is justified for short focal length cameras to consider error arising from emulsion instability or irregularities, plate flatness and other hopefully random error sources.

Estimated values for these terms in relation to the three BC-4 plates under consideration are as follows:

$\theta' = 650''/\text{sec}$ [an average value]

$\sigma_t = 100\mu s$

$\sigma_m = 1''.0$

$\sigma_s = 0''.3$

$\sigma_r = 0''.4$

$n = 16$ [an average number]

$\sigma_\psi = 1''.5$

$\sigma_\upsilon = 0''.7$

These values result in an estimated total standard deviation for a single satellite image near the plate center of

$$\sigma_T = 1''.9 \quad .$$

This is admittedly an optimistic figure. Maximum values or more pessimistic estimates of the quantities above yield values of σ_T from 2".0 to 2".5. Furthermore, these estimates include only random error sources.

If it can be assumed that the total error is normally distributed with a mean of zero and that the above variance estimates are reasonable, tolerance limits for the error can be constructed from

$$e = \bar{e} \pm z\sigma$$

where $\bar{e}$ is equal to zero [Natrella, 1963, pp. 2-13]. At the 90% and 99% confidence levels and with an estimated standard deviation of 1".9, the following tolerance limits are obtained (z from [Natrella, 1963, p. T-3, Table A-2]):

90%, $e = \pm 2''.4$

99%, $e + \pm 4''.4$

If the standard deviation is assumed to be as much as 2".5, corresponding tolerance limits are

90%, $e = \pm 3''.2$

99%, $e = \pm 5''.8$

These figures are of course based on several assumptions, some of which may be only partially true. They are given only to point out that a relatively low estimate of the error variance does not exclude much larger actual errors.

2.2 Procedure

All identified stars within six degrees of the plate centers were used in the astrometric adjustment program. This area is illustrated in Figs. 2.1, 2.2, and 2.3. Satellite image 296 was chosen as the single satellite image of interest; and as can be seen, it is near the center of all three plates.

The number of stars available in this area varied by plate as follows.

plate 2559	16 stars
plate 5205	17 stars
plate 6132	19 stars

Each star generated two observation equations, the minimum degrees of freedom being 24.

The program was run with two different star inputs. The first consisted of the measured x and y coordinates of the middle star image from each trail. In the second run, the five x and the five y coordinates from each star trail were averaged into a single set of coordinates which corresponded to the time of the central image.

2.3 Results

The results of this chapter's experimentation is summarized in Table 2.1 below. Given first are the right ascension and declination of satellite image 296 as computed by ESSA from their photogrammetric reduction. The two remaining columns give the values as computed astrometrically with the different star imputs. Only the astrometric seconds are given, the hours or degrees and minutes were the same as the photogrammetric in all cases.

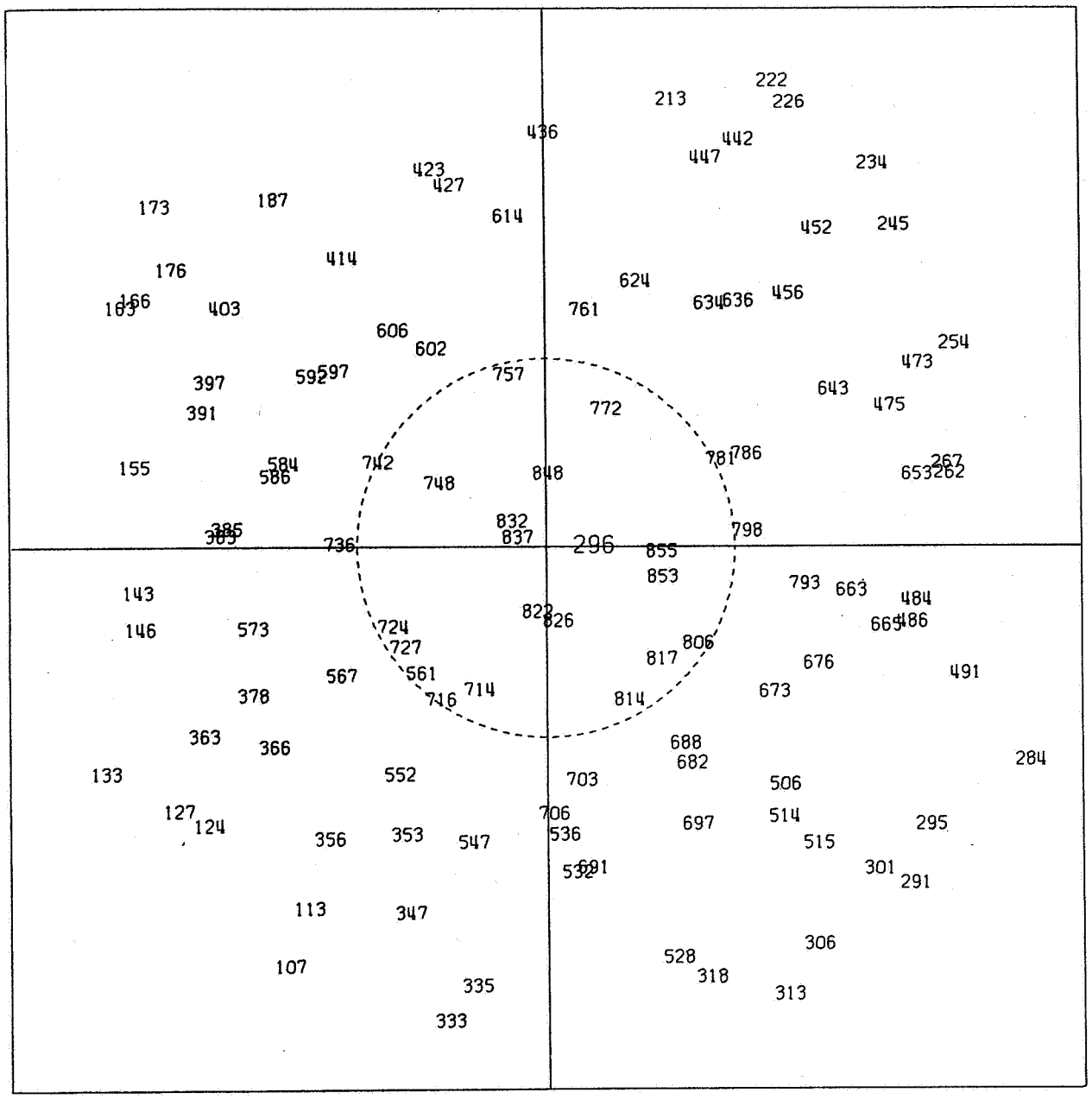

Fig. 2.1 Plate 2559: 6^{o} Circle Around Plate Center

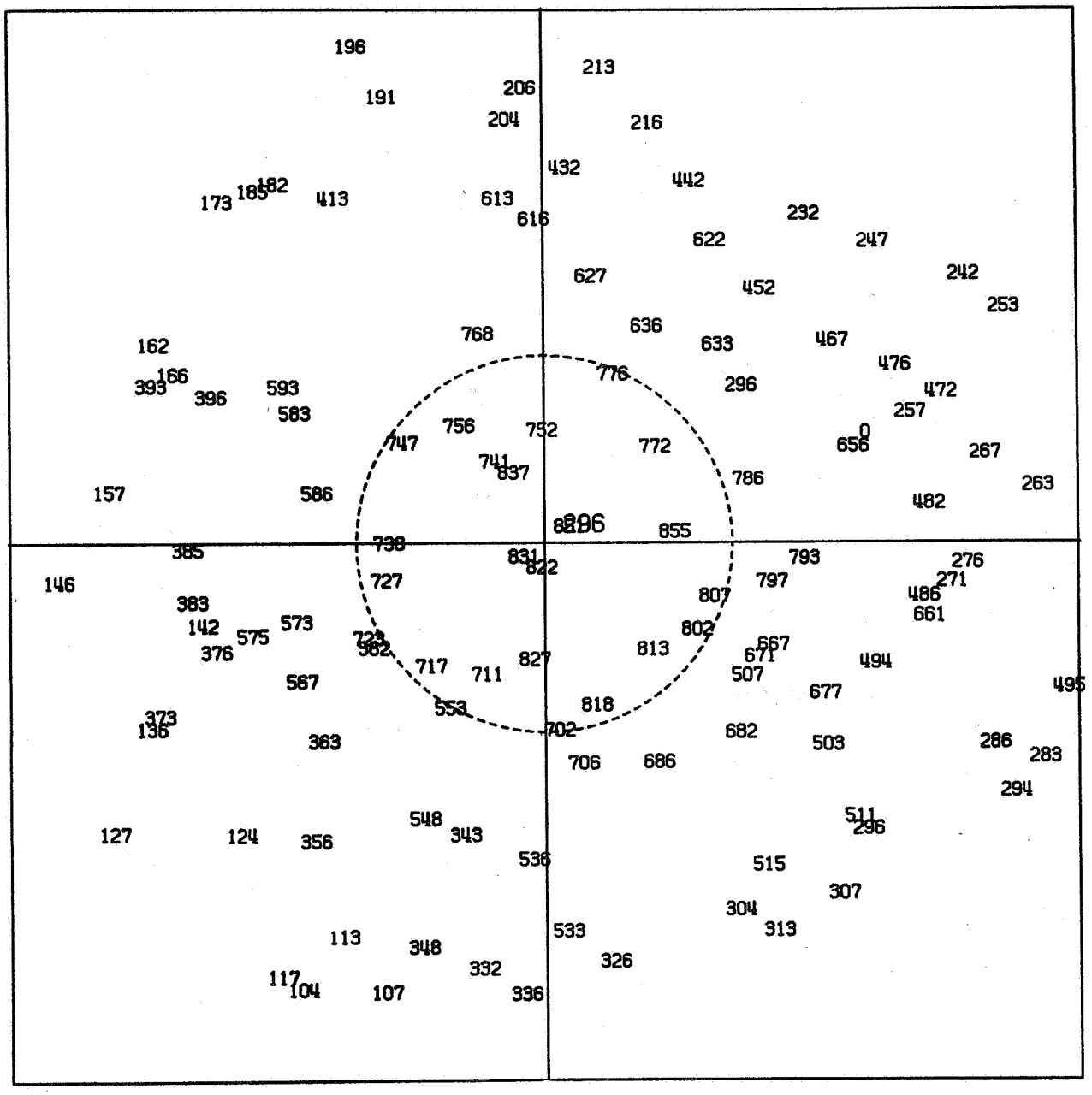

Fig. 2.2 Plate 5205: 6^{o} Circle Around Plate Center

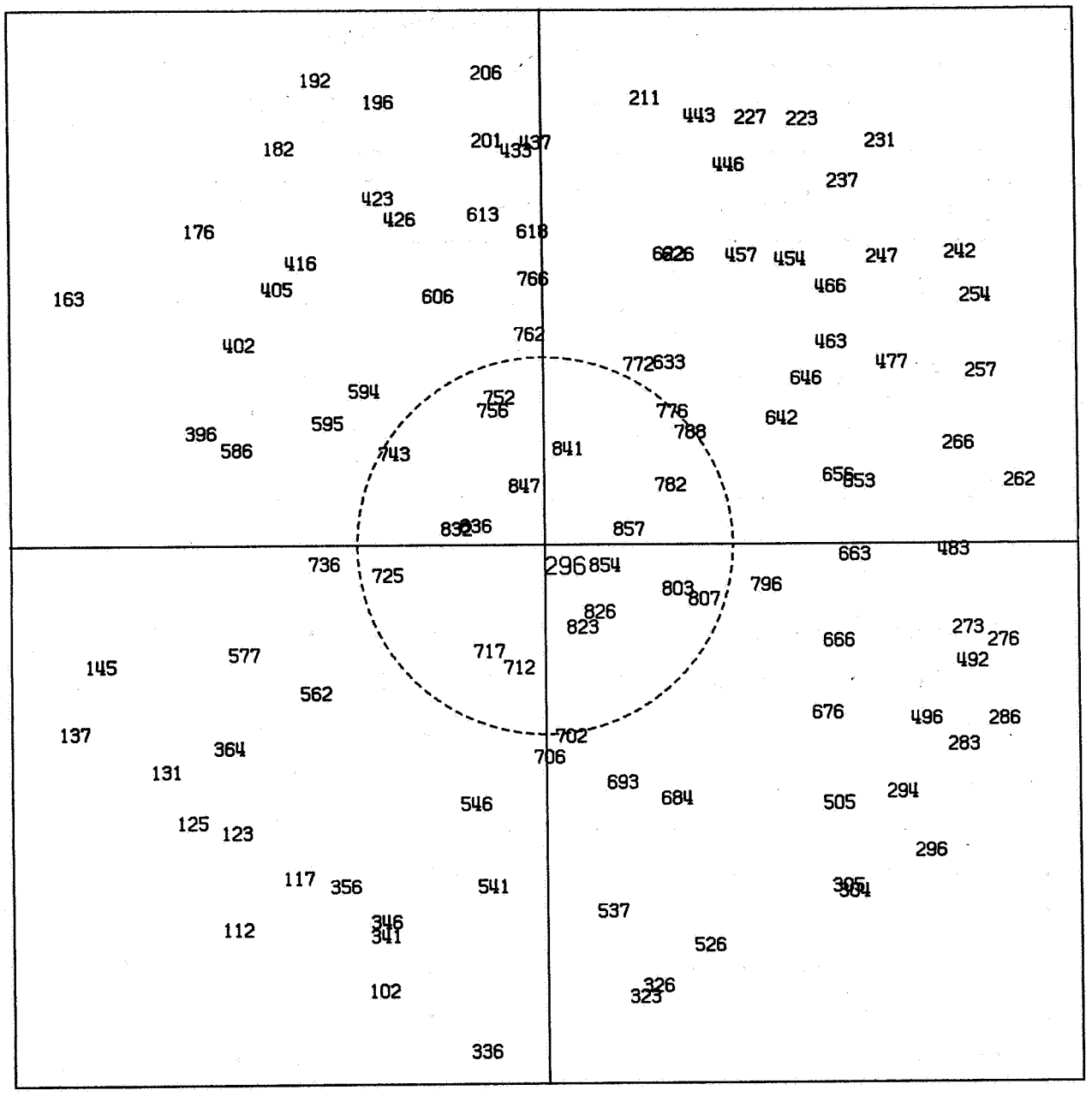

Fig. 2.3 Plate 6132: 6^{o} Circle Around Plate Center

Table 2.1

Photogrammetric and Astrometric Coordinates of a Satellite Image Near the Plate Center

PHOTOGRAMMETRIC					ASTROMETRIC	
					Measured	Mean
Plate		Hr/Deg	Min	Sec	Sec	Sec
2559	α	8	53	38.178	38.169	38.086
	δ	60	59	44.06	43.76	43.95
5205	α	3	24	4.863	4.857	4.831
	δ	53	20	43.16	43.39	42.34
6132	α	18	38	52.552	52.611	52.593
	δ	55	19	22.36	22.30	21.68

2.4 Evaluation

A comparison of the ESSA values with the results of the astrometric reduction substantiates Hornbarger's conclusion. Table 2.1 shows that the astrometric reduction, when used within a restricted area around the plate center, yields very nearly the same satellite coordinates as the photogrammetric reduction.

The mean departure of an astrometric coordinate from the photogrammetric is only 0".2 (0.3μm) when using the actual measured star coordinates as input. The maximum departure is 0".5.

Surprising to this author was the apparent decrease in accuracy when the mean star coordinates were used. From this small sample, no conclusion could be drawn; however, it did discourage further experimentation with mean star coordinates.

3. MULTIPLE SATELLITE DIRECTIONS ASTROMETRICALLY

The close agreement between the astrometric and photogrammetric satellite directions obtained at the plate center was as expected. This chapter describes an attempt to extend the astrometric reduction to areas away from the plate center.

The error sources discussed in section 2.1 are still present with similar magnitudes with one important exception. When applied to the entire plate, the astrometric reduction cannot absorb the varied and nonlinear lens distortions occurring outward from the plate center in cameras such as the BC-4.

The directions and magnitudes of these distortions are illustrated by Figs. 3.1, 3.2, and 3.3, reproduced from Hornbarger's report. Only a brief explanation of these figures is given here; for more information see [Hornbarger, 1968, p. 28]. The figures for one plate are included, those for the other two plates are very similar.

Starting with the updated (to observed place) catalog right ascensions and declinations, the ESSA orientation and lens distortions parameters were used to obtain a distorted set of plate coordinates. A residual, i.e., computed minus observed plate position, was calculated and plotted for each star. Fig. 3.1 shows the relatively small magnitudes and random directions associated with these residuals. The lengths of the vectors representing the residuals were scaled upward for plotting purposes. Fig. 3.2 shows the same type of residuals arising from the astrometric model when applied to the entire plate. They are large and systematic when compared to the photogrammetric. For comparison purposes, Fig. 3.3 is included. It shows the residuals when the astrometric reduction was applied to a limited number of stars around the plate center.

Obviously, if a single astrometric reduction were to be accomplished for the entire plate, large systematic errors would be expected in the satellite position when it is imaged away from the plate center. This applies to cameras with a wide field of view. In this chapter an alternate approach has been investigated.

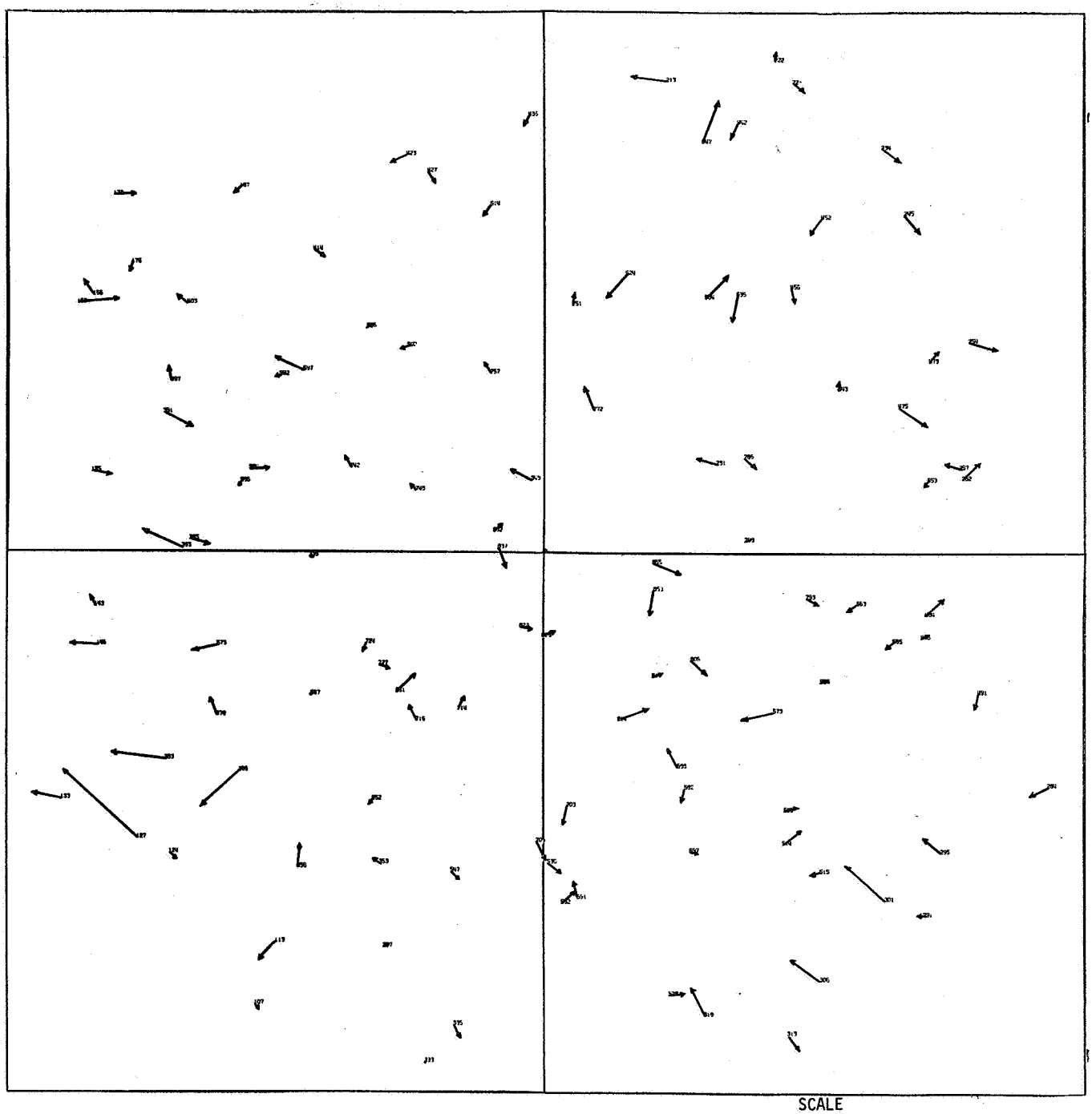

Fig. 3.1 Plate 2559: Photogrammetric Residuals

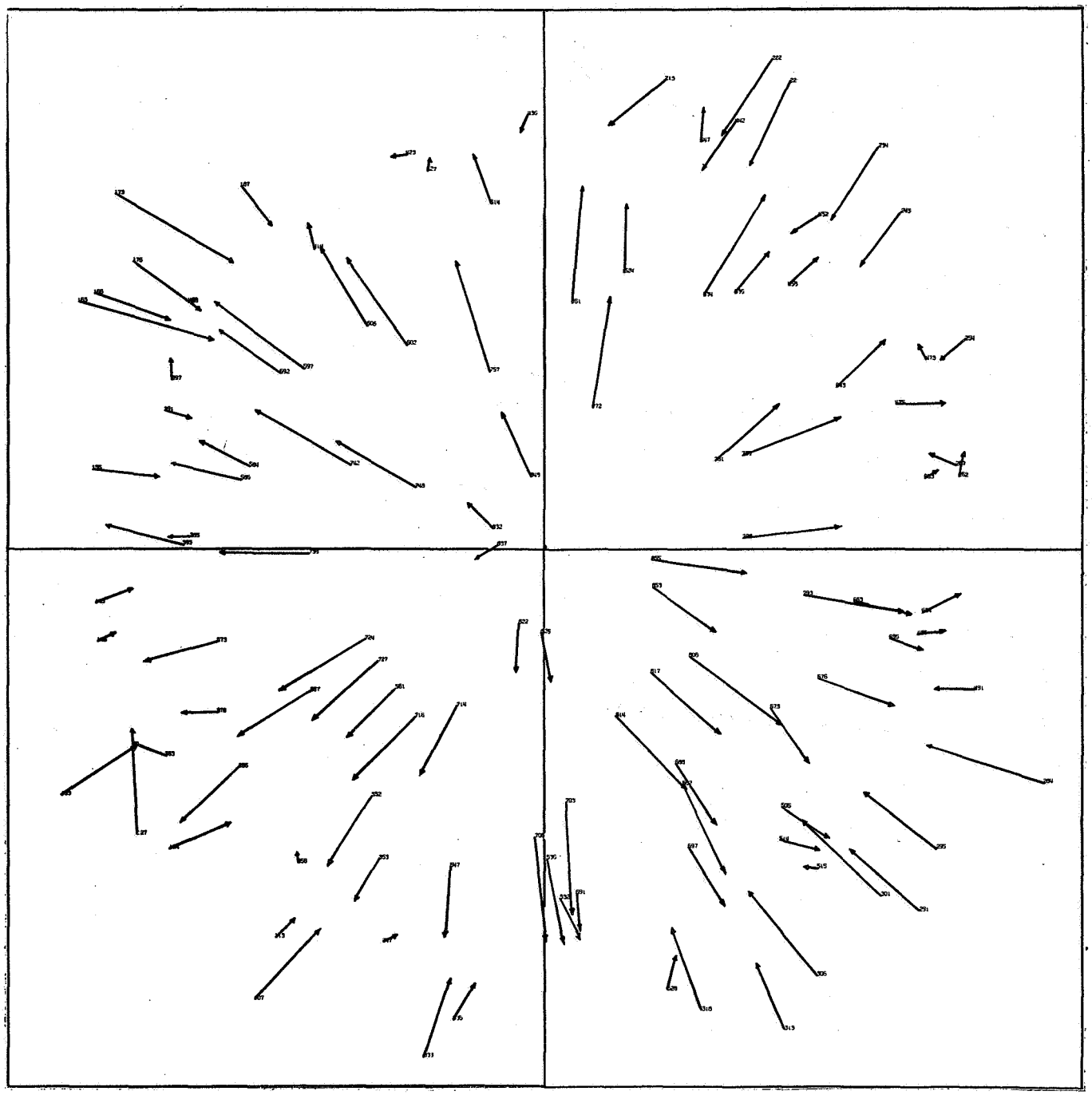

Fig. 3.2 Plate 2559: Astrometric Residuals

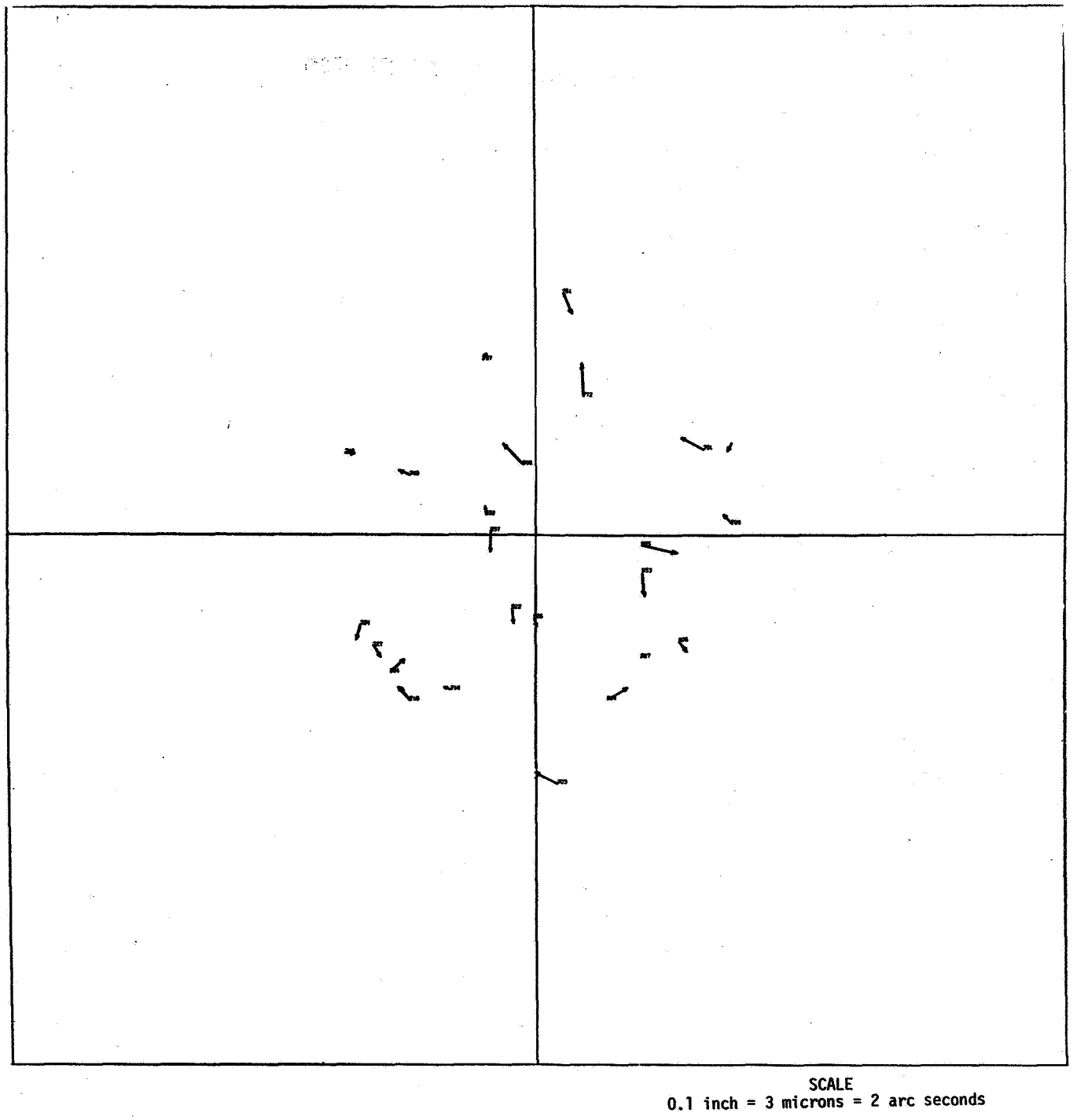

Fig. 3.3 Plate 2559: Astrometric Residuals, 6° Radius Around Plate Center

Several areas of each BC-4 plate were treated individually, reduced astrometrically, and a satellite direction obtained from each.

3.1 Procedure

The procedures used were similar to those described in Chapter 2. The astrometric model and reduction program were the same. The decision to treat several areas of the plate individually introduced two new problems. They are discussed in the following paragraphs.

3.11 Satellite Image Selection

The first requirement was to choose satellite images from the various plate areas. Two different sets of images were actually chosen. Table 3.1 below lists by number the images appearing in each set and the plates on which they appeared.

Table 3.1

Satellite Images Selected for Individual Astrometric Reductions

Set I						
Image / Plate	58	179	296	415	534	
2559	x	x	x	x	x	
5205		x	x	x		
6132		x	x	x		
Set II						
Image / Plate	42	126	211	296	382	469	549
2559	x	x	x	x	x	x	x
5205			x	x	x	x	
6132		x	x	x	x	x	

There were two criteria used in selecting the satellite images in each set. The first was that the images be more or less evenly spaced across the plate; that the satellite be imaged on all three plates was the second. The latter criterion was generated by the geometric theory of triangulation and its requirement for simultaneous observation of the satellite.

Set I is illustrated in Figs. 3.4, 3.5, and 3.6. It consists of a satellite image near the plate center and others spaced outward at 24-second intervals. The second set originated with the same central image but the interval between images was reduced to about 17 seconds (Figs. 3.7, 3.8, 3.9). The choice of these intervals produced at least three images common to all plates in Set I and at least four common images in Set II.

These particular time intervals were arbitrary and chosen only because they provided several evenly spaced images on the three available plates. The time required for the satellite to transit the field of view is, of course, a function of its range which, in turn, depends on the satellite orbit and camera location. A generalized method of segmenting the image trail would be by image numbers. They are directly correlated to time intervals by the "chopping" rate of the rotating shutters. In this study all references are to time, but it should be noted that the intervals discussed correspond to a specific number of satellite images. The same number of images may represent an entirely different time interval on another set of plates.

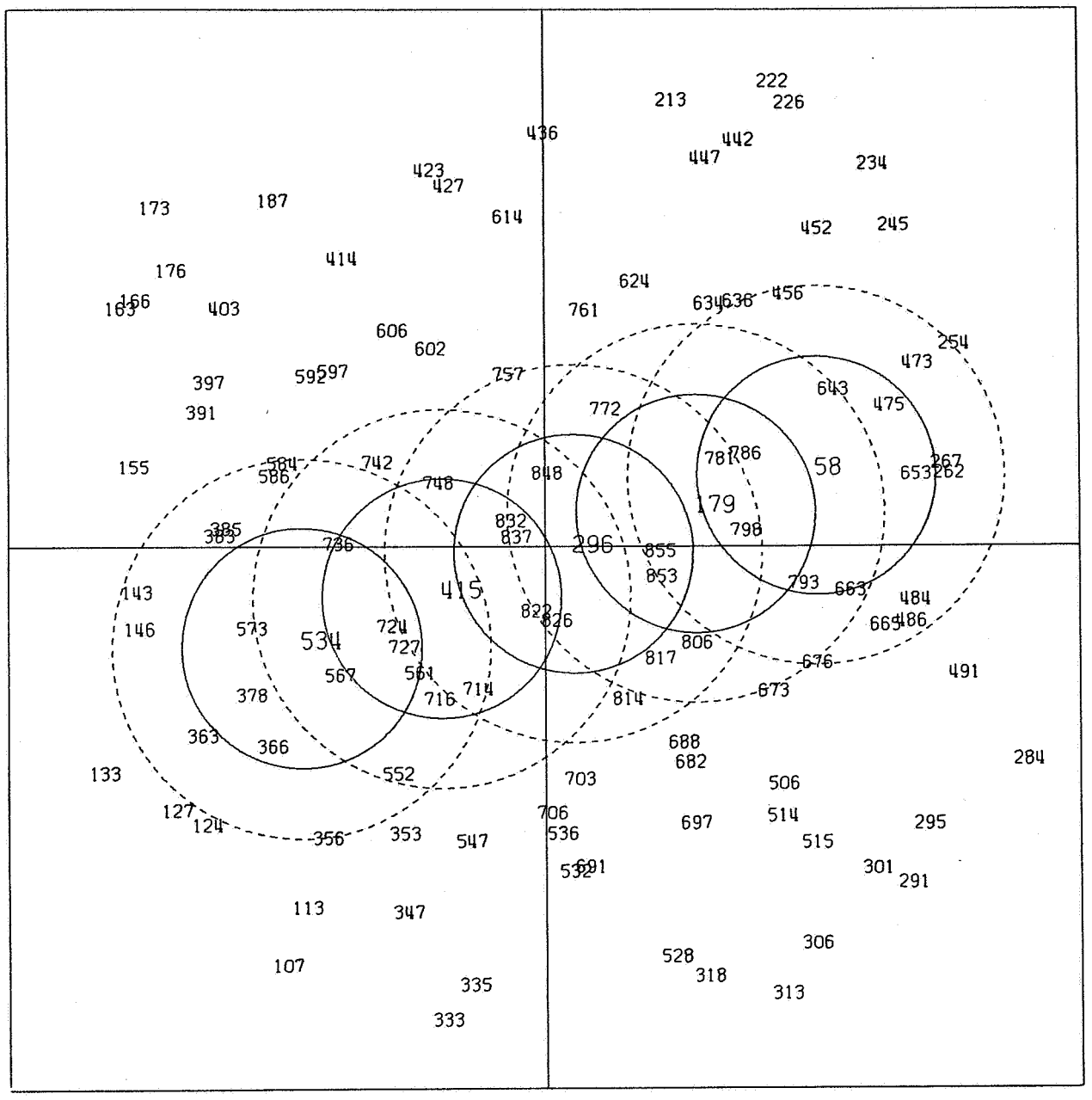

Fig. 3.4 Plate 2559: Set I Satellite, 24[s] Intervals 3.8° and 6° Circles

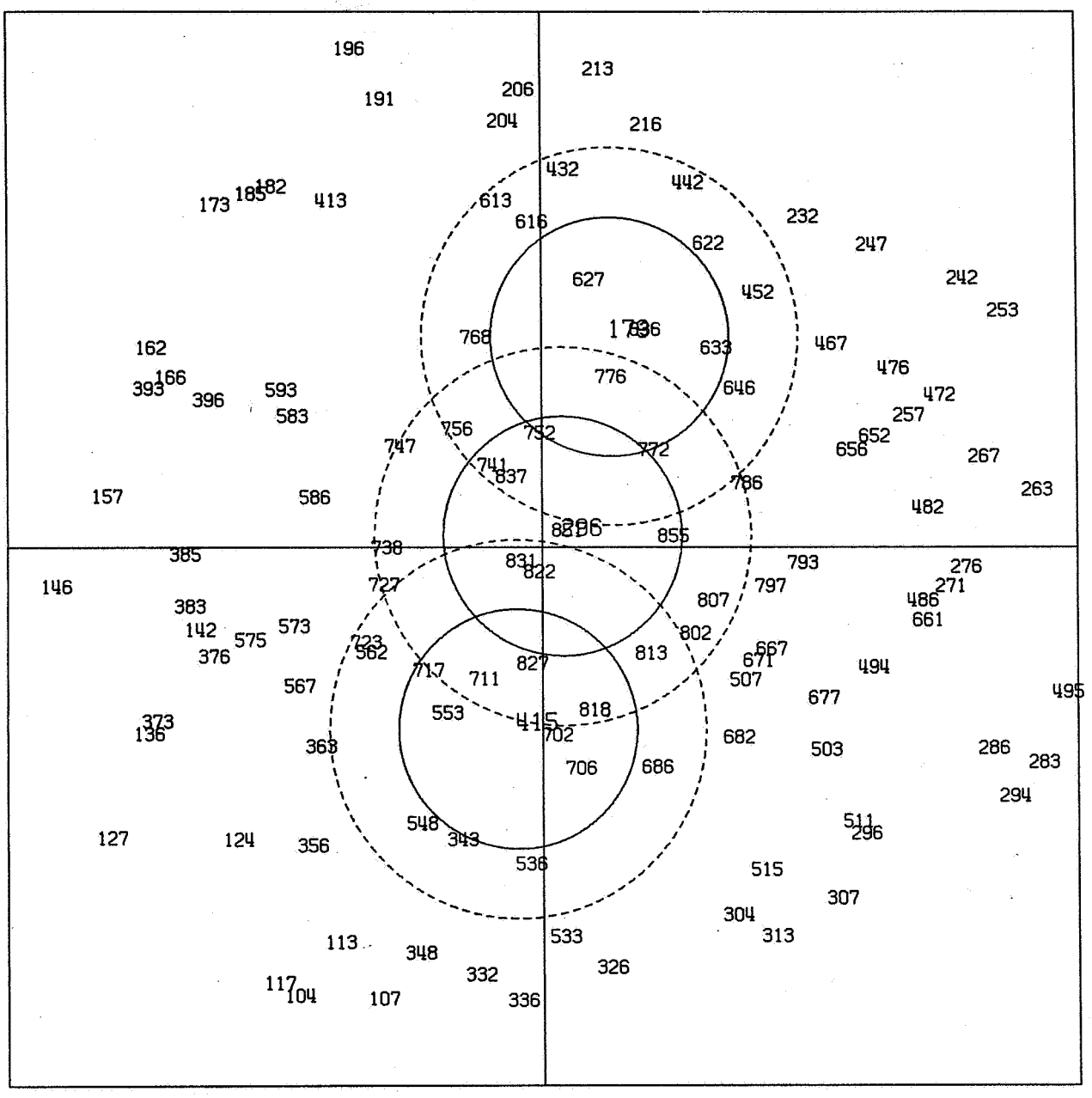

Fig. 3.5 Plate 5205: Set I Satellite, 24^s Intervals
3.8° and 6° Circles

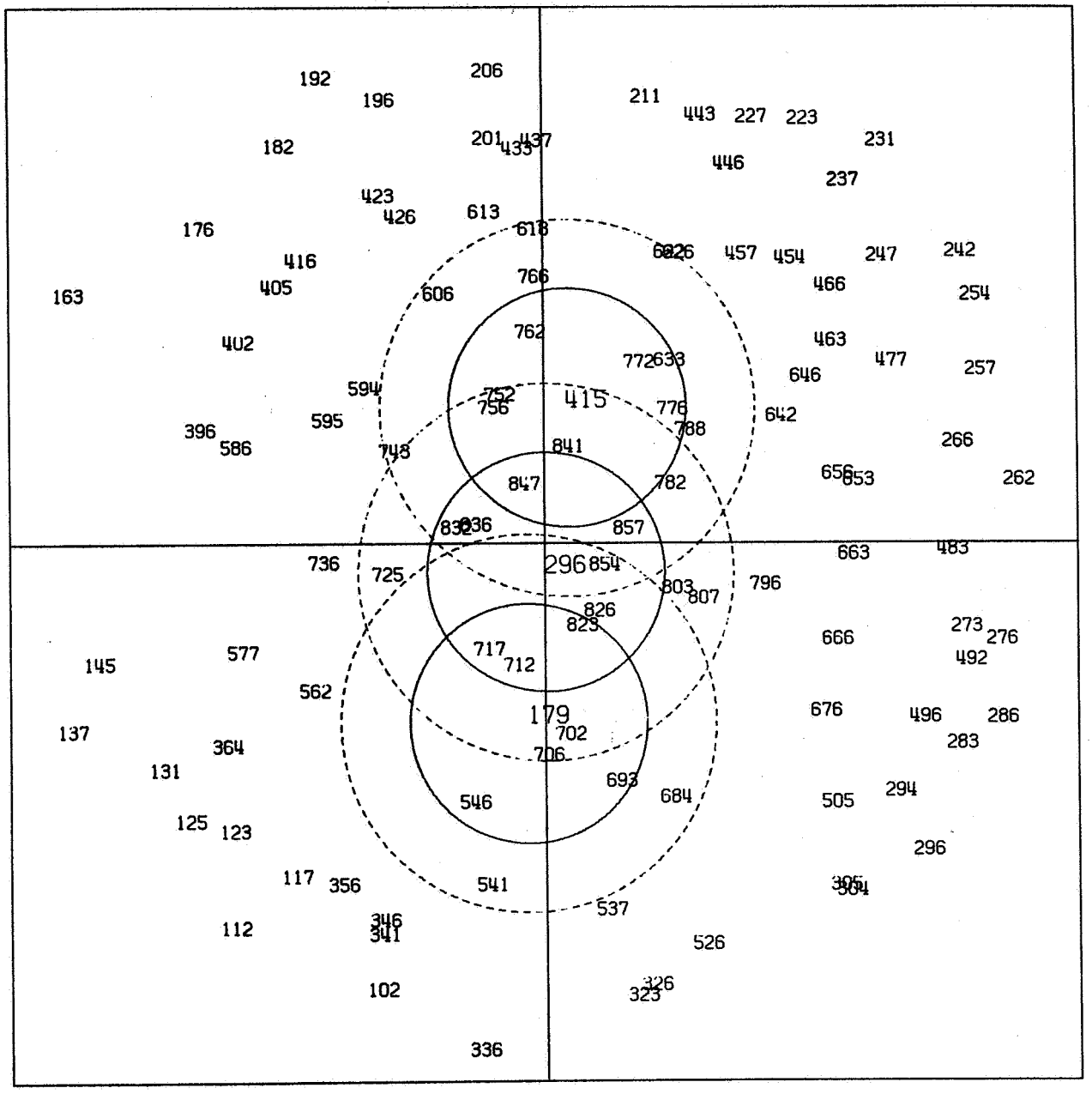

Fig. 3.6 Plate 6132: Set I Satellite, 24^s Intervals
3.8^o and 6^o Circles

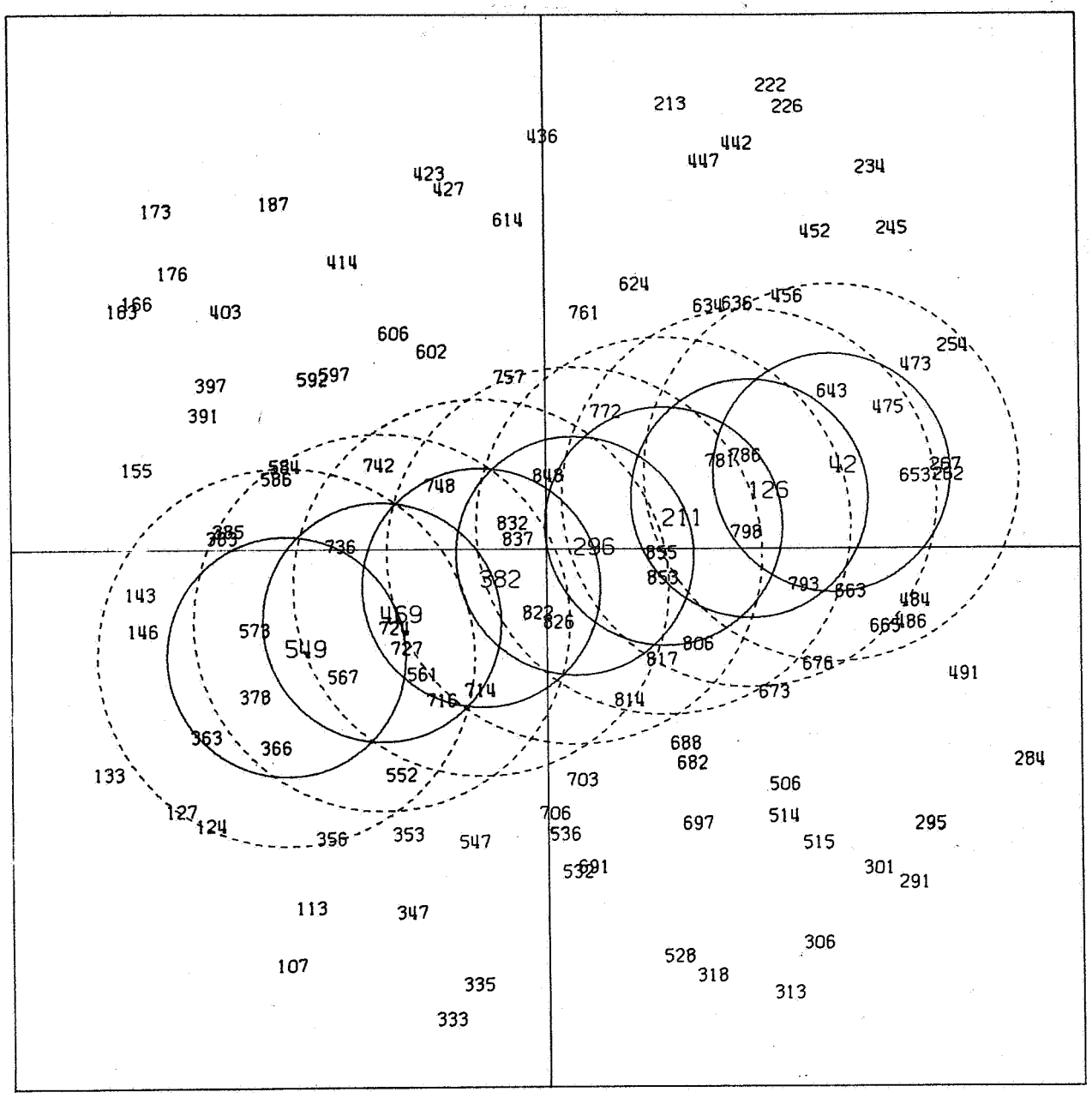

Fig. 3.7 Plate 2559: Set II Satellite, 17^s Intervals
3.8° and 6° Circles

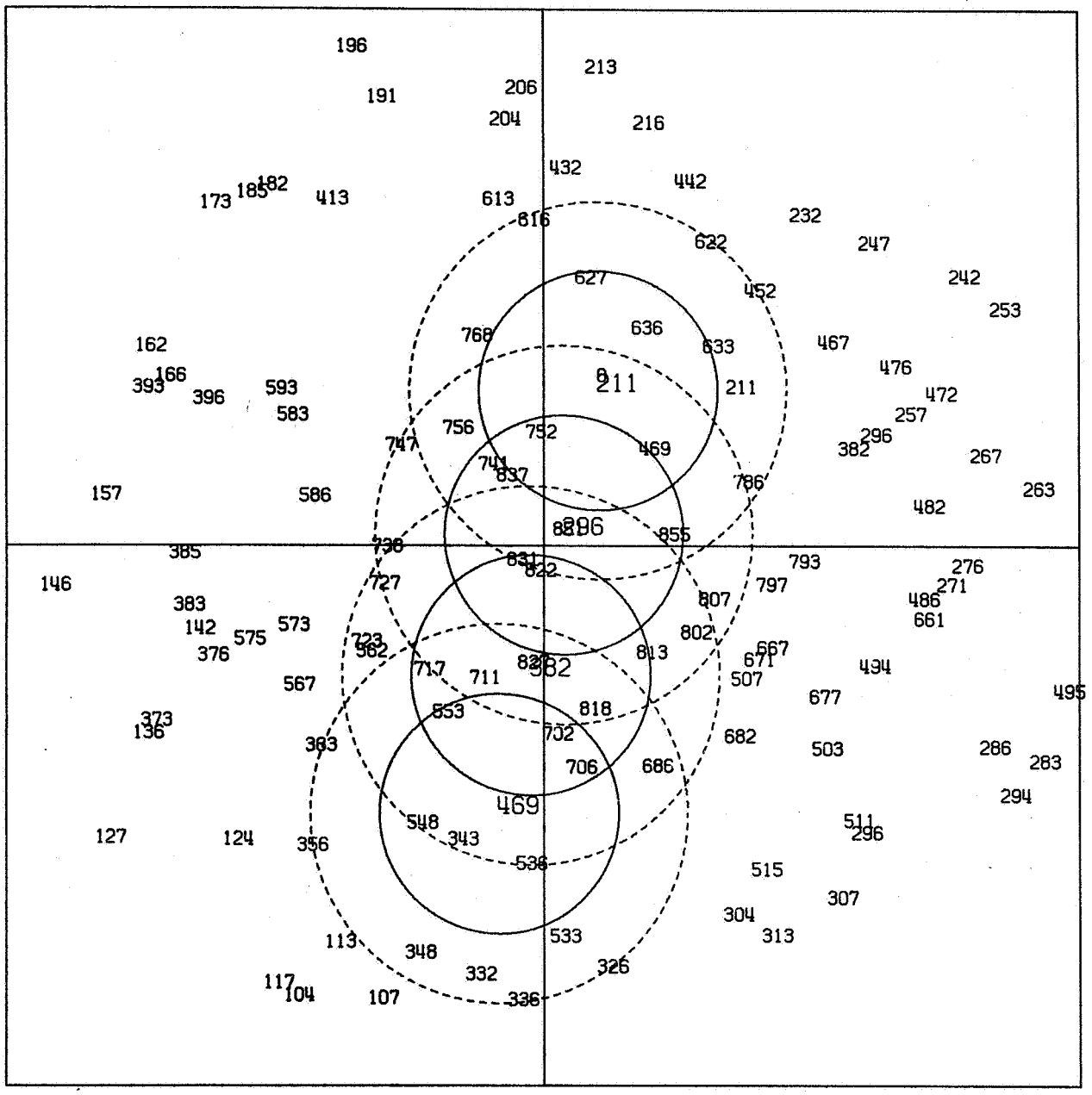

Fig. 3.8 Plate 5205: Set II Satellite, 17^s Intervals
3.8^o and 6^o Circles

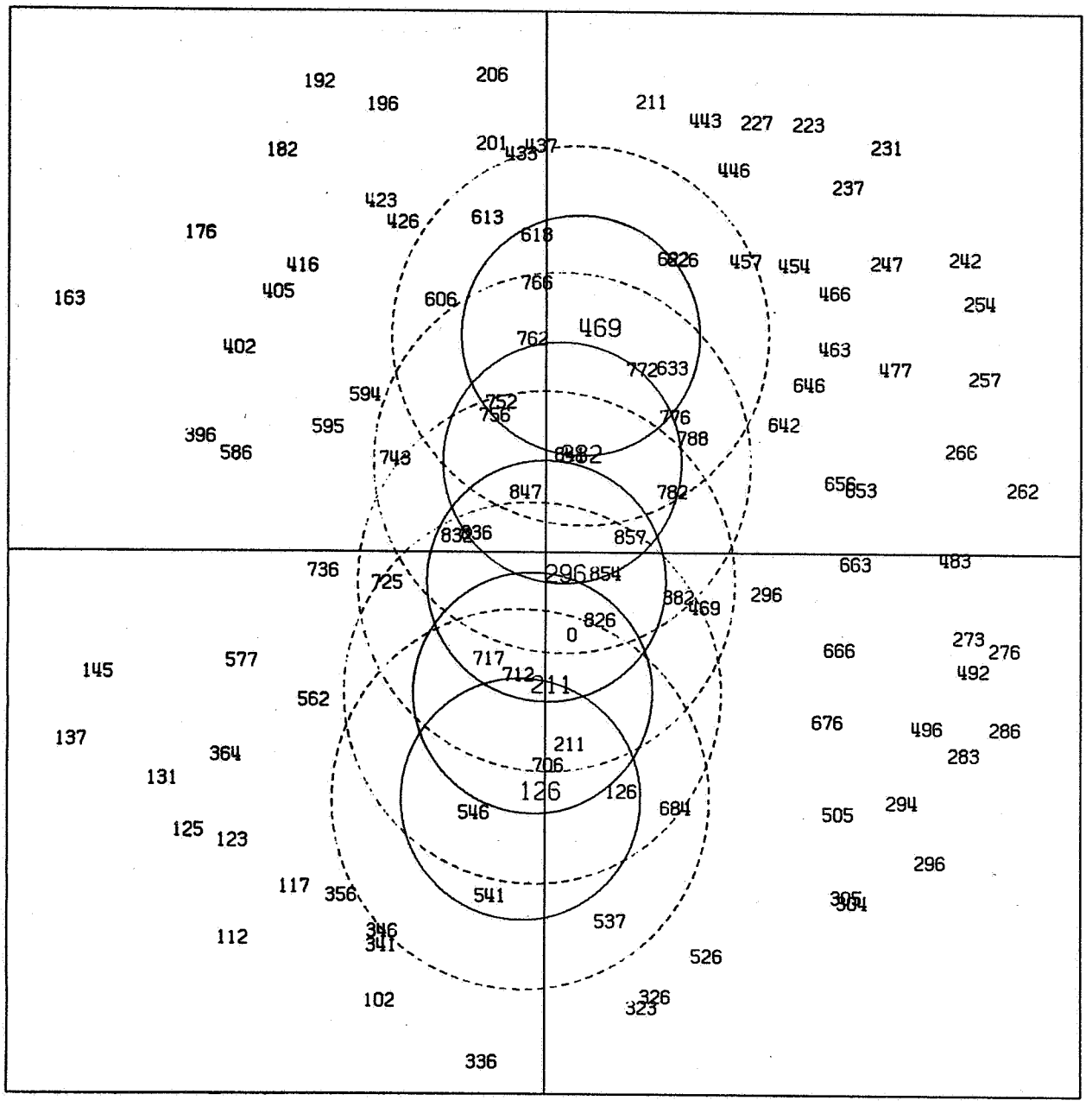

Fig. 3.9 Plate 6132: Set II Satellite, 17° Intervals
3.8° and 6° Circles

3.12 Plate Areas

The choice of the plate area to use with each satellite image was also somewhat arbitrary. The circle of six degree radius from Chapter 2 was the obvious choice and was one of the two used. The circle was constructed around each satellite image. This introduced two undesirable features.

An examination of Fig. 3.2 clearly indicates that any 6° radius circle away from the plate center would encompass nonlinear distortions. Secondly, Figs. 3.10 and 3.11 show that the 6° radius circles overlap so that the same stars appear in more than one plate area and would be used in the ensuing reductions. Systematic or random errors of the common stars, such as the star catalog, measured plate coordinates, etc., would enter the corresponding satellite directions which would then share the same bias.

It should also be pointed out that the same star may be imaged as several star trails on the BC-4 plate and used in the plate reduction. This could be considered as weighting each star proportionately to the number of times it appears. This is not likely to be significant in the ESSA reduction where nearly 100 known stars are carried. This duplication could be significant in smaller plate areas.

For example, on plate 5205 where 114 known stars are carried in the ESSA reduction, there are 89 different stars. In other words, 25 stars are used twice and 89 stars once. Comparable figures for plate 2559 are 111 stars and 92 different stars (one is used three times); for plate 6132, 106 stars and 90 different stars.

Relating these figures to the 6° areas of plate 2559: For Set I (Fig. 3.10) where the satellite images are spaced at 24-second intervals, seven stars would be used in three of the five astrometric reductions, ten more would appear in two reductions. In addition, seven stars would appear twice within the same plate areas.

In Set II (Fig. 3.11) where the satellite images are more closely spaced, these figures increase substantially. Again referring only to plate 2559, ten

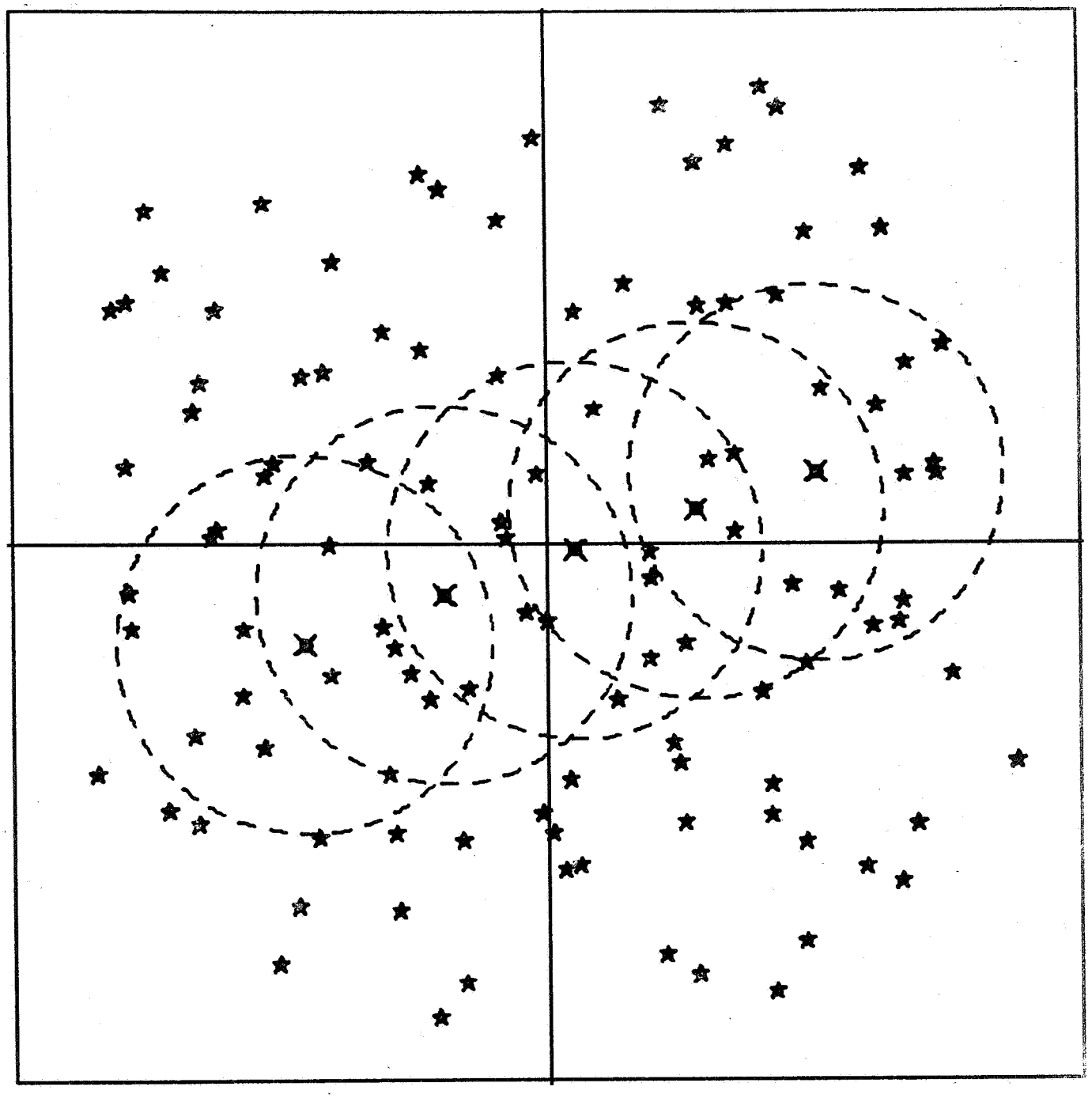

Fig. 3.10 Set I Satellites, 6^{o} Circles

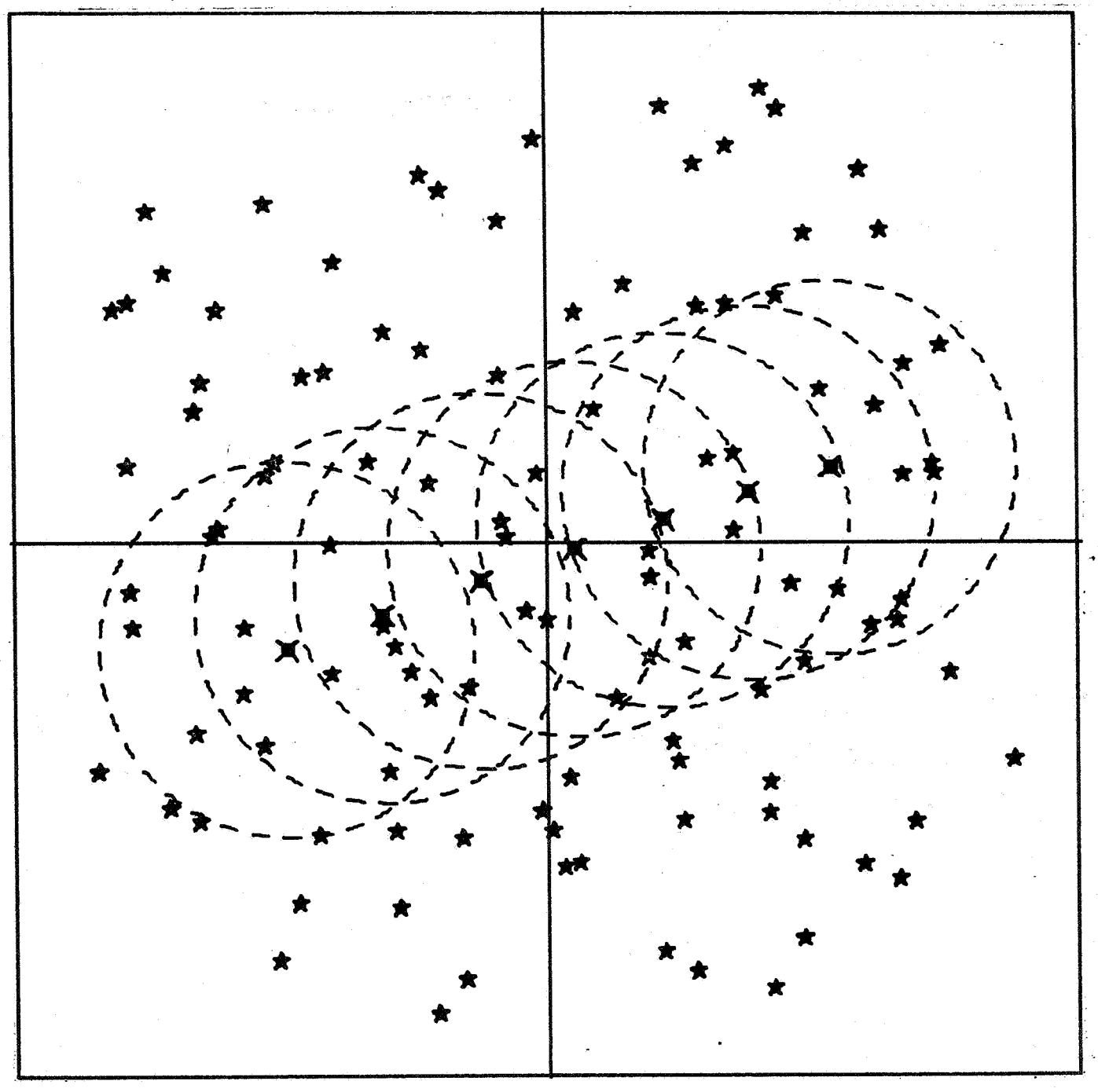

Fig. 3.11 Set II Satellites, 6^{o} Circles

stars would appear simultaneously in four of the seven plate areas, fourteen more would appear in three areas and many more would appear in two. These figures are not encouraging when the goal is to obtain observations that are at least reasonably independent.

For these reasons a smaller plate area seemed desirable and might have been expected to offer three immediate advantages:

(1) The lens distortions in a smaller plate area should be better accommodated by the astrometric reduction.

(2) By decreasing the plate area used, the number of stars carried in more than one reduction per plate would be reduced.

(3) A smaller plate area would reduce or eliminate the number of stars used twice in the same reduction.

The smaller plate area was chosen as a circle of approximately 3.8° radius around each satellite image. This radius provided at least six stars per satellite image and twelve observation equations to determine the eight unknown parameters of the astrometric model. Generally, eight to ten stars were within this area. Unfortunately when only six stars were available, they were usually not well distributed around the satellite image; when eight or more were available, the distribution was better. Expected advantage (1) could only be evaluated through the accuracy of the final satellite directions. Numbers (2) and (3) can be evaluated as for the 6° radius areas.

In Set I (Fig. 3.12) no stars appear in more than two reductions on the same plate and an average of three appear in the overlap areas of consecutive satellite images. Only one star is used twice in the same reduction.

As with the 6° circles, the figures are less encouraging for Set II (Fig. 3.13). Five stars appear simultaneously in three plate areas and nine more appear in two; in one area, two stars appear twice.

In summary, for satellite images at 24-second intervals (Set I) and circles of 6° radius, there is double and triple overlap of plate areas. If the radius is reduced to 3.8°, the triple overlap is eliminated. When using 17-second intervals

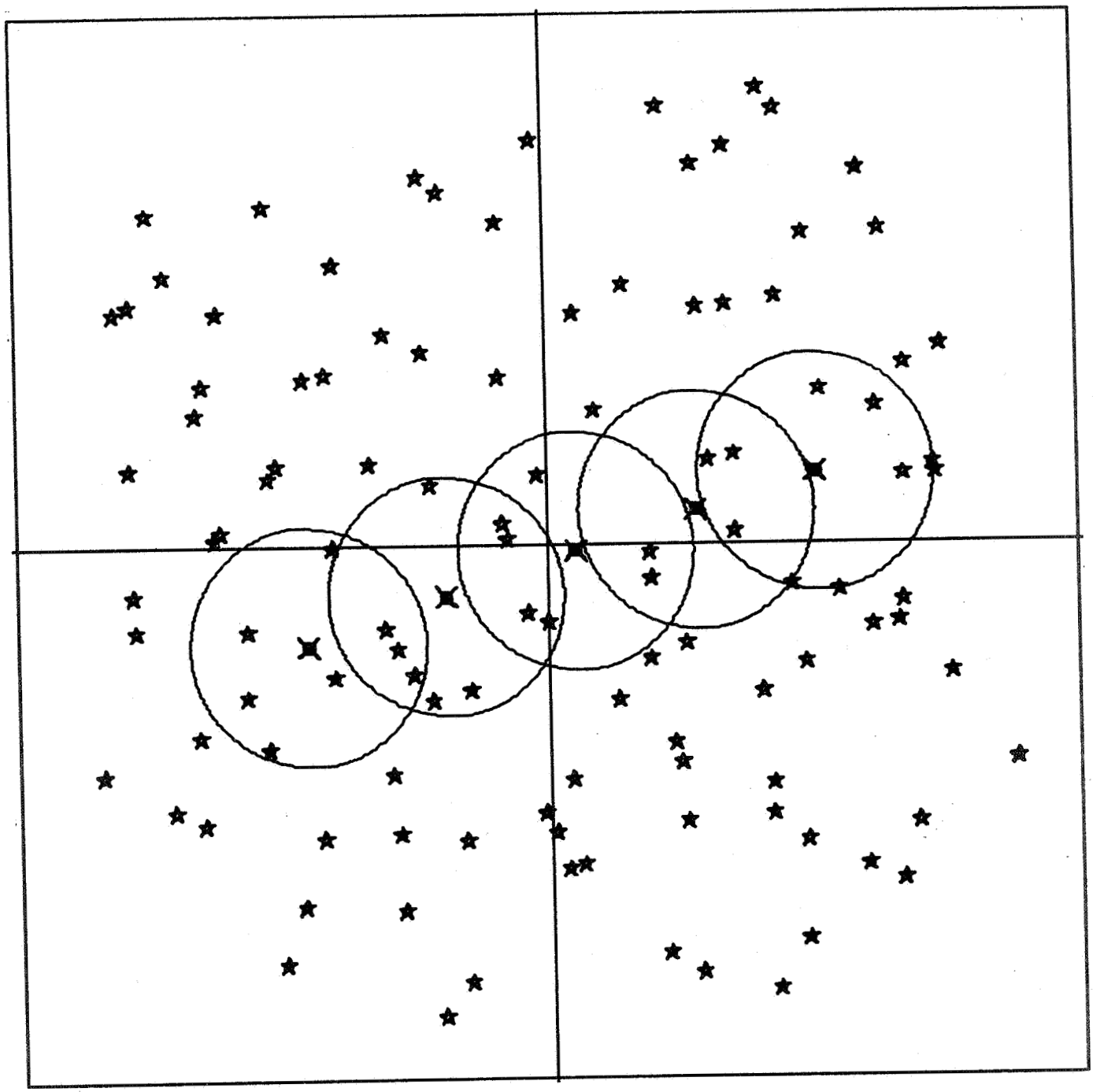

Fig. 3.12 Set I Satellites, 3.8° Circles

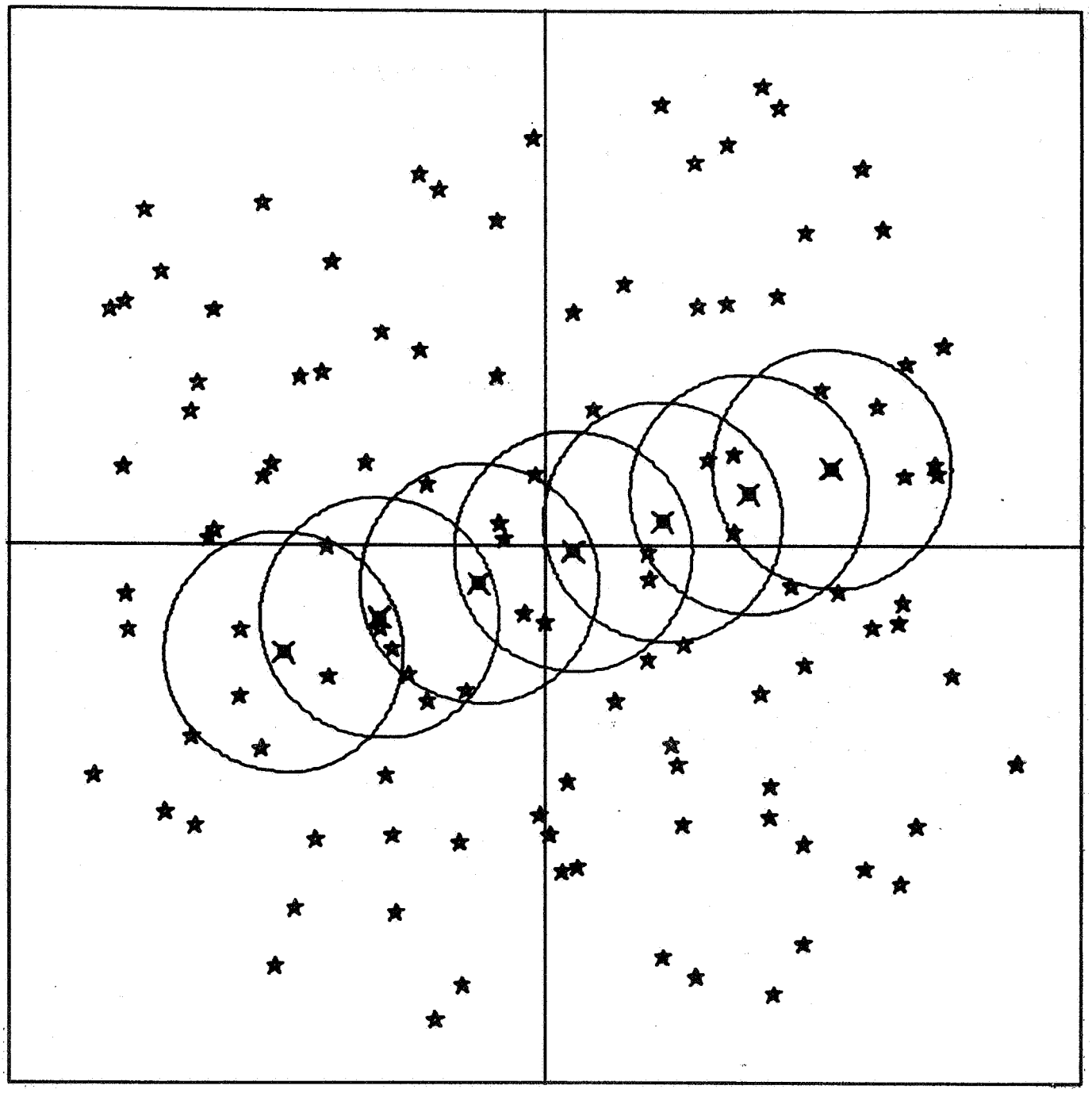

Fig. 3.13 Set II Satellites, 3.8° Circles

(Set II) and 6° circles, stars appear in both triple and quadruple overlap areas. Furthermore, the smaller plate areas significantly reduce the number of stars appearing twice in the same reduction.

From the above, it seems that Set I of the satellite images is more desirable than Set II; and in either case, the smaller plate area is preferable. The final accuracy of the satellite directions derived from the different sized plate areas was still an unknown. Therefore, the astrometric reduction was performed for all satellite images using areas of both 3.8° and 6° radius.

3.2 Results

The experimental results are summarized in Tables 3.2, 3.3, and 3.4 on the following pages. The photogrammetric coordinates given were computed by ESSA. The astrometric coordinates are given in terms of their departures from the photogrammetric coordinates—seconds of time for right ascension and seconds of arc for declination.

Table 3.2

Photogrammetric and Astrometric Satellite Directions
Plate 2559

	Right Ascension					Declination				
Image	Photogrammetric			Astrometric		Photogrammetric			Astrometric	
Set I	h	m	sec	3.8	6.0	°	'	"	3.8	6.0
58	9	56	12.925	-.055	-.329	59	20	25.42	-0.12	+0.04
179	9	26	16.073	+.053	-.054	60	24	59.28	-0.53	-0.06
296	8	53	38.178	-.036	-.009	60	59	44.06	-1.45	-0.29
415	8	17	39.502	+.101	+.186	60	58	54.67	-0.61	+0.09
534	7	40	30.543	+.075	+.226	60	15	04.81	+0.39	+0.75
Set II										
42	9	59	51.917	-.035	-.287	59	10	08.51	-0.15	+0.29
126	9	39	53.552	-.106	-.238	59	59	50.82	-0.99	-0.30
211	9	17	41.156	-.041	-.115	60	37	34.49	-1.36	-0.99
296	8	53	38.178	-.036	-.009	60	59	44.06	-1.45	-0.29
382	8	27	49.930	+.100	+.213	61	3	12.17	-0.29	-0.02
469	8	00	49.240	+.281	+.298	60	44	36.59	-0.94	+0.80
549	7	35	49.995	-.100	+.189	60	6	19.71	+0.71	+1.44

Table 3.3

Photogrammetric and Astrometric Satellite Directions

Plate 5205

	Right Ascension					Declination				
	Photogrammetric			Astrometric		Photogrammetric			Astrometric	
Set I	h	m	sec	$3^0.8$	$6^0.0$	°	′	″	$3^0.8$	$6^0.0$
179	3	43	36.244	-0.078	-0.155	59	11	22.57	+0.04	-0.78
296	3	24	4.863	-0.057	-0.006	53	20	43.18	-0.88	+0.21
415	3	10	3.090	-0.010	+0.011	47	31	21.02	-1.20	+0.79
Set II										
211	3	37	31.756	-0.074	-0.053	57	35	27.57	-0.16	-0.95
296	3	24	4.863	-0.057	-0.006	53	20	43.18	-0.88	+0.21
382	3	13	29.864	+0.083	+0.022	49	06	54.82	+1.02	+0.80
469	3	05	0.609	-0.044	+0.031	44	57	49.78	+0.02	+0.98

Table 3.4

Photogrammetric and Astrometric Satellite Directions

Plate 6132

	Right Ascension					Declination				
	Photogrammetric			Astrometric		Photogrammetric			Astrometric	
Set I	h	m	sec	$3^{0}_{.}8$	$6^{0}_{.}0$	0	'	"	$3^{0}_{.}8$	$6^{0}_{.}0$
179	18	05	12.282	-.003	+.054	54	47	50.89	-0.15	+0.20
296	18	38	52.557	+.042	+.054	55	19	22.35	+0.34	-0.06
415	19	16	11.981	-.069	-.105	55	09	26.22	+0.30	+0.34
Set II										
126	17	51	11.497	-.105	+.029	54	22	53.63	+0.49	+0.09
211	18	14	2,952	+.110	+.093	54	59	57.31	+0.63	-0.28
296	18	38	52.557	+.042	+.054	55	19	22.35	+0.34	-0.06
382	19	05	36.885	-.071	-.063	55	16	58.05	-0.16	-0.09
469	19	33	43.956	-.085	-.178	54	48	27.63	+0.37	+0.56

3.3 Evaluation

Two statistics were computed from the data available in the tables. The first was the standard deviation of the astrometric coordinates from the photogrammetric. It was computed from

$$\sigma_{\alpha,\delta} = \left[\frac{\Sigma (x_a - x_p)^2}{n - 1}\right]^{\frac{1}{2}}$$

where x_p was the photogrammetric coordinate, x_a was the astrometric coordinate, and n equaled the number of satellite images (24).

A σ_α and σ_δ were computed for both sets of satellite right ascensions and declinations. They were computed for each plate and for the entire sample.

The second statistic computed was the mean deviation. It was computed from

$$D_{\alpha,\delta} = \frac{\Sigma |x_a - x_p|}{n}$$

where the notation is the same as above. These were computed only for the entire sample. The computed values of the statistics are tabulated in Table 3.5 which follows.

Table 3.5

Standard and Mean Deviations of the Astrometric
from the Photogrammetric Coordinates
(numbers in parentheses exclude central image on each plate)

STANDARD DEVIATIONS

	Right Ascension (sec of time)							
	Plate 2559		Plate 5205		Plate 6132		All Plates	
	3°.8	6°.0	3°.8	6°.0	3°.8	6°.0	3°.8	6°.0
Set I	.075	.222	.069	.110	.057	.092	.091	.163
Set II	.138	.232	.076	.038	.096	.110	(.099)	(.213)
	Declination (sec of arc)							
	Plate 2559		Plate 5205		Plate 6132		All Plates	
	3°.8	6°.0	3°.8	6°.0	3°.8	6°.0	3°.8	6°.0
Set I	.85	.41	1.05	.80	.34	.28	.71	.62
Set II	1.03	.81	.78	.92	.48	.32	(.65)	(.66)

Table 3.5 (cont'd)

MEAN DEVIATIONS

Right Ascension		Declination	
$3^{\circ}.8$	$6^{\circ}.0$	$3^{\circ}.8$	$6^{\circ}.0$
.075	.123	.55	.47
(.080)	(.139)	(.51)	(.51)

It was known from the experimentation described in Chapter 2 that a plate area of 6° radius gave excellent agreement around the plate center. To remove this bias when evaluating the satellite directions away from the center, the standard and mean deviations were recomputed without satellite image 296. These values are listed in Table 3.5 in parentheses. No significant differences from the previous values are apparent.

A surprising and unexplained anomaly in the computed statistics is the relatively large standard deviation calculated for the satellite right ascensions from the 6° plate areas. This discrepancy is confirmed by the mean deviation statistic. The standard deviation of $0^{s}.091$ for the entire sample from the small plate areas corresponds to about $0''.7$ at an average declination. This value is compatible with the standard deviations associated with the declinations. The standard deviation in right ascension which was computed from the large plate areas appears much too large.

To test the significance of this discrepancy, the Sign Test for Paired Observations was performed. This is a distribution free test and specifically tests whether the median difference between two samples can be considered equal to zero. The hypothesis to be tested was: The plate areas of different size, when reduced astrometrically, produced the same mean departure from the photogrammetric coordinates. The statistic was computed for declination as well as right ascension and tested at the 10% significance level. The table used was from [Natrella, 1963, T-78]. Neither for right ascension nor declination could the hypothesis be rejected. There was no reason to believe that the average departures of the two samples (different plate areas) did actually differ.

The standard errors of unit weight arising from the astrometric adjustment were evaluated for the different plate areas. Tabulated in Table 3.6 for the satellites of Set I are the standard errors for 6° and 3.8° radius circles. Included also is the same statistic computed when all known lens distortions were removed from the star coordinates and the adjustment performed for the entire plate [Hornbarger, 1968, p. 95].

Table 3.6

Standard Errors of Unit Weight
($\pm\mu$m)

Plate	Image	$6^{\circ}.0$	$3^{\circ}.8$	Entire Plate
2559	58	3.22	2.93	3.06
	179	3.27	3.50	
	296	2.60	2.29	
	415	1.95	1.84	
	534	4.45	2.89	
5205	179	3.54	2.73	3.34
	296	3.22	2.85	
	415	3.34	3.08	
6132	179	1.92	2.24	2.26
	296	2.41	2.26	
	415	2.09	2.16	

In paragraph 3.12 it was theorized that the smaller plate areas might give better satellite directions than the larger. The experimental results do not seem to have supported this. The poorer distribution and fewer stars may have overcome any advantages of the smaller plate area, or possibly the area was still too large for the astrometric model to successfully accommodate the lens distortions. The standard errors of unit weight do not indicate a lack of accommodation however.

Of more importance is the fact that the smaller plate area did not produce results any less accurate than the larger. In the previously mentioned paragraph, two additional advantages were postulated for using the smaller areas; these were

subsequently proven to be correct.

The conclusion is that the smaller plate areas are preferable for the following reasons.

(1) There is no improvement in the accuracy of the satellite directions from the larger plate areas.

(2) Fewer stars are used in more than one reduction per plate, thereby decreasing the correlation between consecutive satellite directions.

(3) The number of stars appearing twice in the same reduction is small.

During this part of the investigation, an additional fact became evident. With proper choice of satellite images, each plate could have been divided into three entirely independent plates. They would be independent in the sense that three astrometric reductions could have been performed without using any star image in more than one reduction. This particular choice of satellite images was not compatible with other parts of the study so it was not attempted here.

The standard deviations in right ascension and declination listed in Table 3.5, when combined, result in a total standard deviation in arc of about one second. It is important to realize that this figure represents only a comparison of the astrometric and ESSA's photogrammetric coordinates. An estimate of the absolute error is unattainable.

A graphical comparison is made in Figs. 3.14 through 3.19. Plotted are photogrammetric minus astrometric coordinates; the astrometric coordinates are from the 3.8° areas. Also plotted on the figures are the SAO results from their astrometric reduction when they reduced the data from the same three plates [Hornbarger, 1968, Ch. 6 in thesis version].

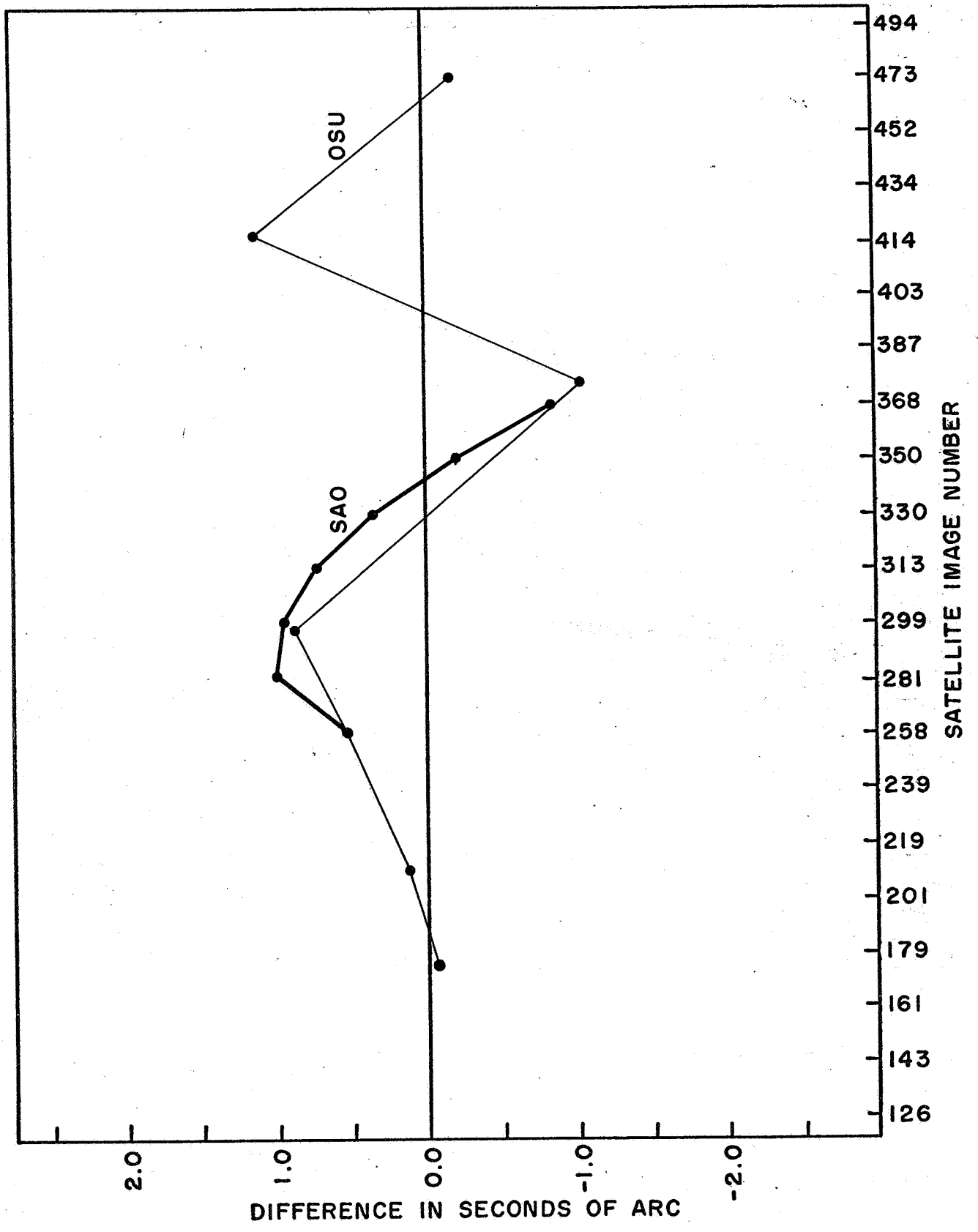

Fig. 3.14 Plate 2559: Right Ascensions (Photogrammetric - Astrometric)

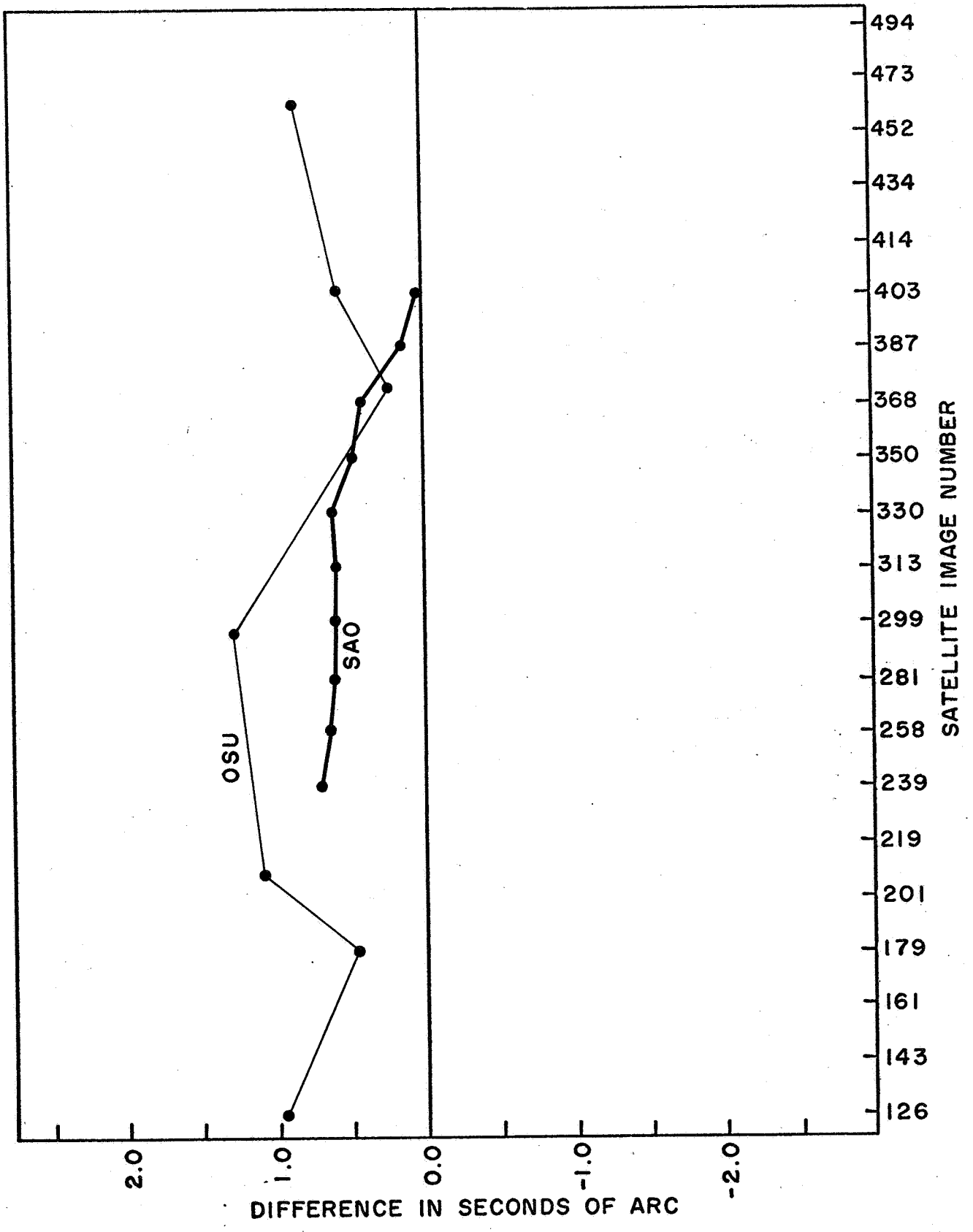

Fig. 3.15 Plate 2559: Declinations (Photogrammetric - Astrometric)

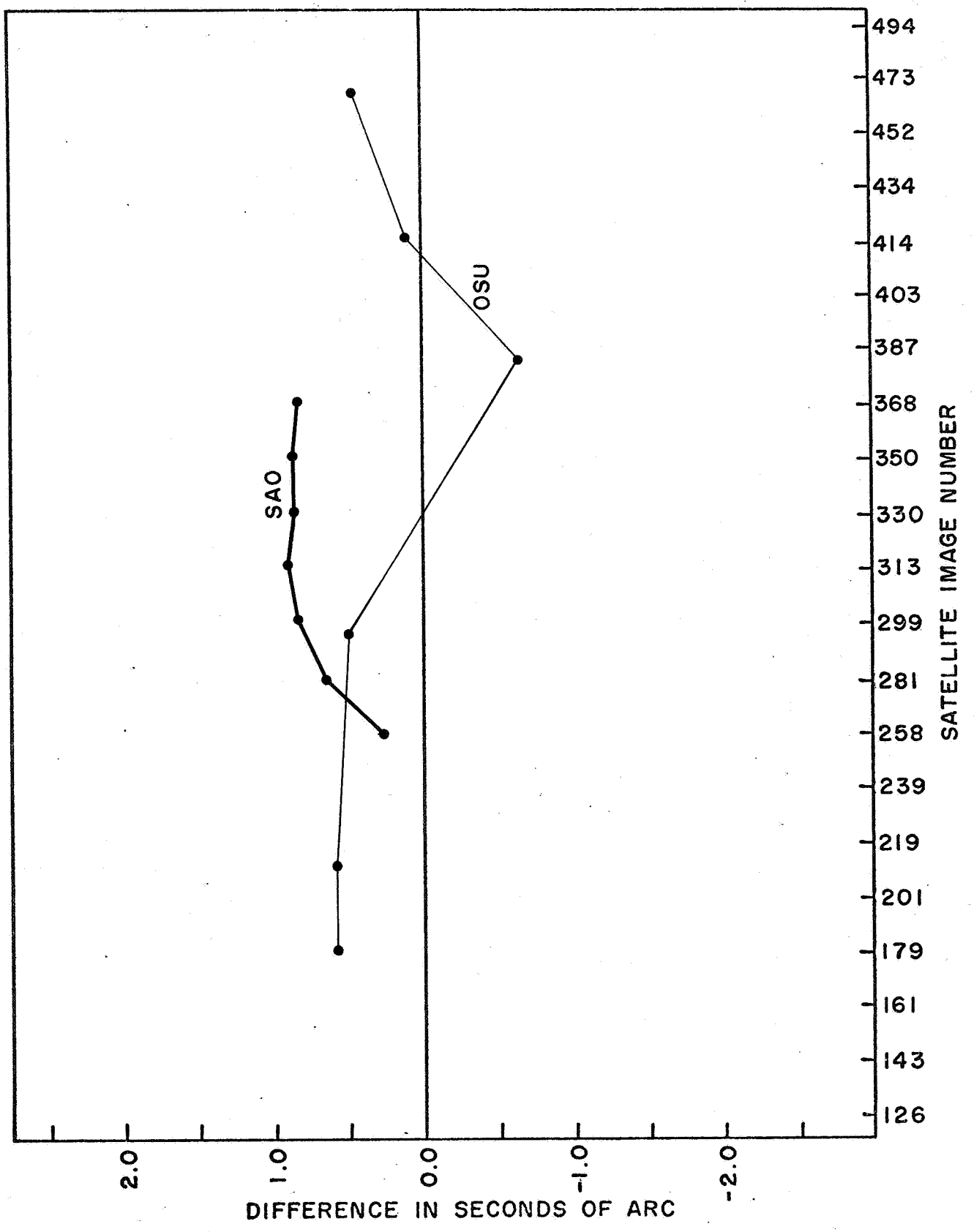

Fig. 3.16 Plate 5205: Right Ascensions (Photogrammetric - Astrometric)

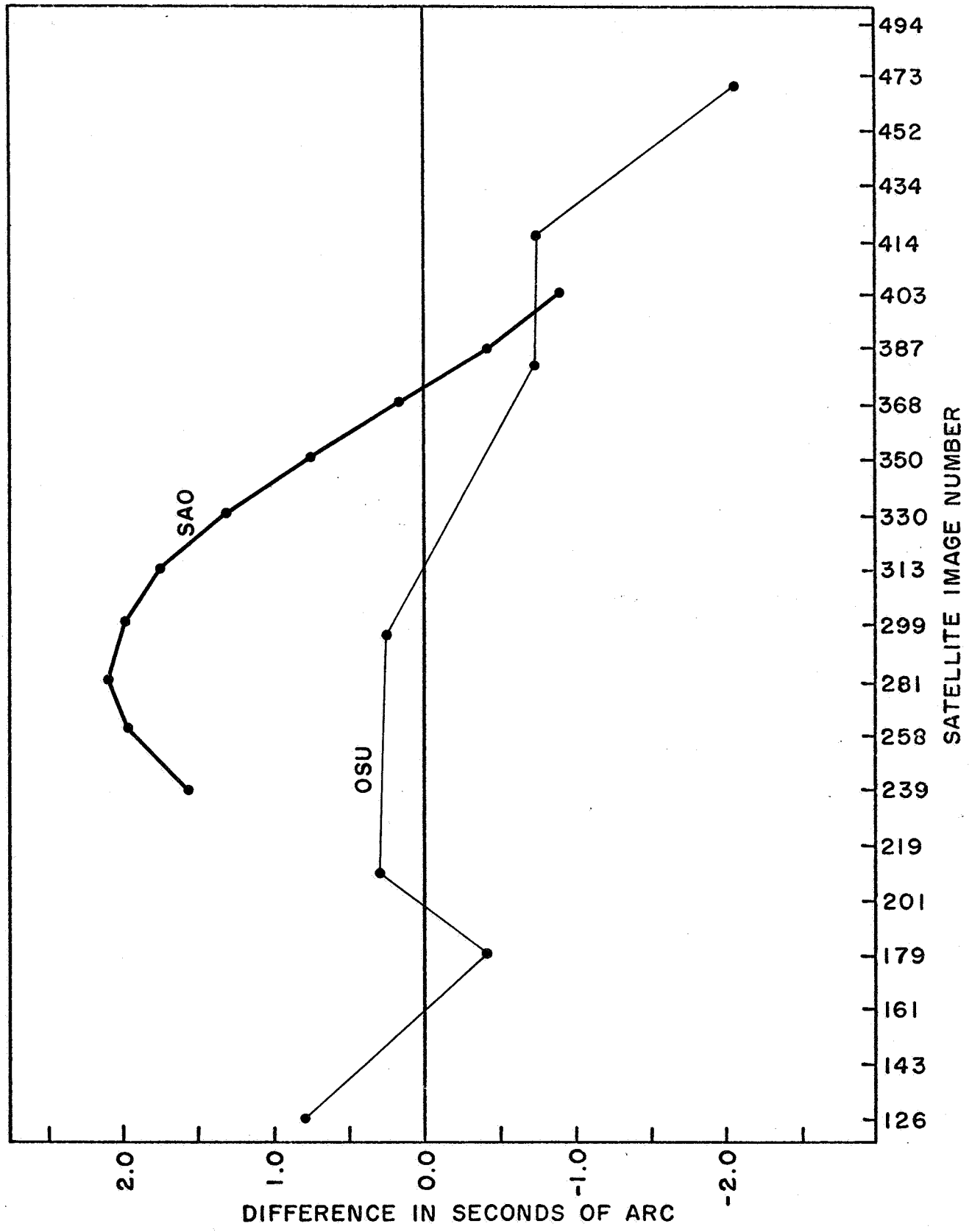

Fig. 3.17 Plate 5205: Declinations (Photogrammetric - Astrometric)

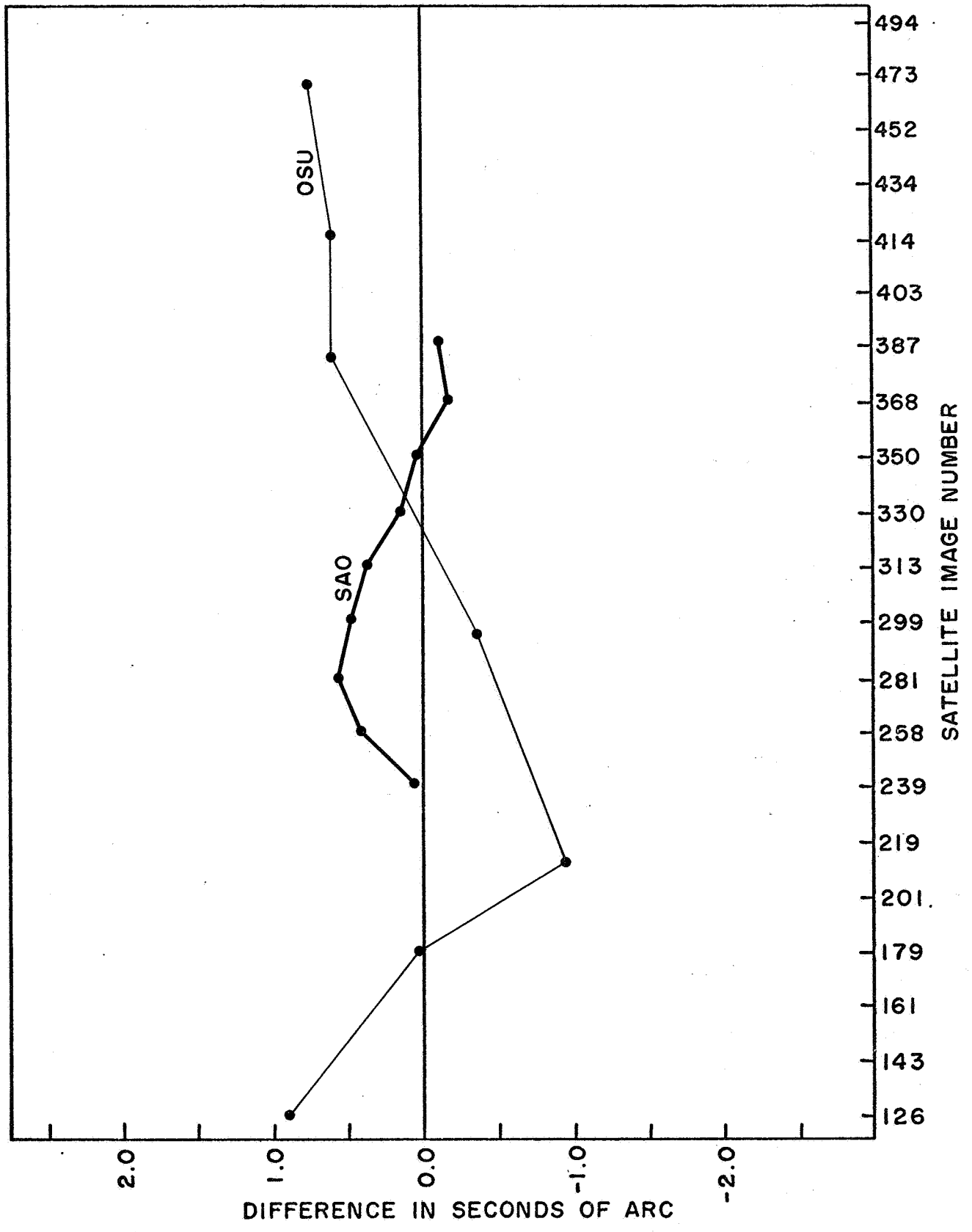

Fig. 3.18 Plate 6132: Right Ascensions (Photogrammetric - Astrometric)

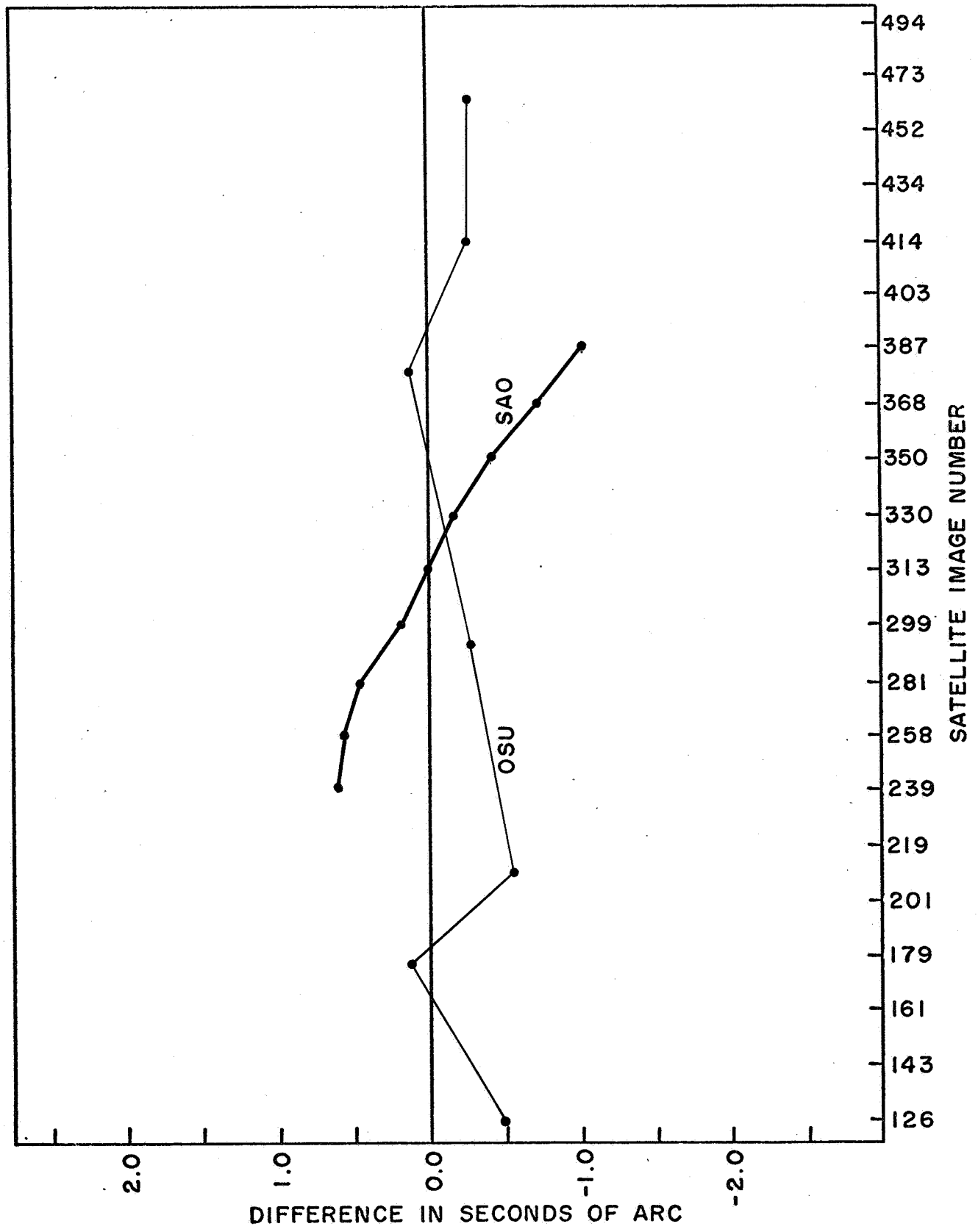

Fig. 3.19 Plate 6132: Declinations (Photogrammetric - Astrometric)

4. CURVE FITTING

The data compression technique of fitting a polynomial to the observations has several advantages, both theoretical and practical. It simplifies the light travel time corrections (satellite aberration), a necessary correction in the synchronization of observations. More important is the increase in accuracy that may be expected.

When considering the precision and accuracy of a final satellite direction, a significant improvement over a single satellite image may be realized by fitting a polynomial to several images. In effect, it can overcome the relatively large random errors inherent to a single image and may even tend to counteract small systematic errors which tend to randomness over the entire plate. The technique is not without its critics however. This is discussed in the following section; later sections detail this author's investigations and conclusions.

4.1 Theory and Application

The two agencies fitting polynomials to their observed data are the SAO and ESSA. Both use a similar approach, but the dissimilar nature of the data introduces significant differences in detail.

The functional relationship adopted is

$$Y_i \begin{Bmatrix} \xi, \eta \\ x, y \end{Bmatrix} = \beta_0 + \beta_1 t_i + \beta_2 t_i^2 + \ldots + \beta_n t_i^n$$

where the independent variable is time t. The dependent variables in the SAO reduction are the auxiliary coordinates ξ, η; in the ESSA reduction, they are the adjusted plate coordinates x, y [SAO Sp. Rept. 200, p. 64; Schmid, 1965b, p. 21].

Least-squares methods for estimating the coefficients β_i of the functional relationship are used in two situations:

(1) when it is known that the polynomial function describes the <u>true</u> relationship of the dependent variables to time, or

(2) when it can be assumed that the polynomial function approximates the true without significant error.

This relationship implies several assumptions [Natrella, 1963, pp. 6-14, 6-18].

(1) The dependent variables are statistically independent as are their errors of measurement.

(2) The dependent variables are effected by random errors; the errors have a zero mean and equal variances.

The functional relation of the satellite coordinates to time is not known to be polynomial. The assumptions concerning the dependent variables and their errors are not rigorously valid. Of importance then is whether the polynomial relationship is a sufficient approximation of the true relationship.

The sources and magnitudes of the random errors affecting the satellite images were discussed previously. It is assumed that the random errors are the major contributors to the uncertainty of a satellite coordinate; with proper precautions during data acquisition and reduction, this is a valid assumption. The question is: could the smaller systematic errors in single satellite images emerge to such a level to negate the assumption of a polynomial relationship and bias the results significantly. The conclusion is that it would not in the ESSA BC-4 data.

Systematic error does exist, but its magnitude is small when compared to random error. It may originate with residual bias of the comparator or its operator, uncompensated longer period atmospheric anomalies, etc. This systematic error will bias the resulting polynomial coefficients but not significantly when compared to the improved accuracy of the final satellite direction. Furthermore, some small systematic errors and their resulting bias may be or at least approach randomness when several plates (and polynomials) for a single camera station are considered.

It might be argued that some relationship other than the polynomial would be a better approximation. This may be true, but the entirely general nature of the time series polynomial is desirable. It requires no prior assumptions about the nature of the satellite's path across the plate.

If the assumption of a polynomial relationship is valid, the next area of interest is to determine the correct degree. It is well known that the shape of the polynomial curve is a function of its degree. Higher order polynomials and a large number of observations may overcome this to a certain extent. The SAO uses the polynomial as an interpolation tool; ESSA and this author use it primarily for other reasons but for interpolation also. It must be assumed that the polynomial of correct degree represents the best estimate of the satellite's path; a polynomial of incorrect degree cannot give the best estimate.

The SAO uses the quadratic form of the polynomial. At least four and normally seven sets of satellite coordinates are used, typically four or eight seconds apart [SAO Sp. Rept. 200, 1966, p. 64]. Four and eight second intervals between seven images correspond to arcs of 24 or 48 seconds respectively. Other available exposure rates correspond to 12 or 96 seconds for seven images. The limited number of images obviously restricts the degree of polynomial that could be used.

In contrast to the SAO quadratic, ESSA employs a fifth-degree polynomial to describe arcs of 75 to 120 seconds on the three BC-4 plates available. For the Pageos observations on the National Space Science Data Center tape, the observational period varies from less than three to over five minutes. No meaningful conclusions can be drawn from time alone, but it seems to this author that the choice of an arbitrary fixed degree polynomial to describe such a wide variety of observational situations is questionable.

Generally when a polynomial is used as an approximation to an unknown function, or as an interpolation formula, the correct degree is not known. An accepted method of evaluating how well the polynomial fits the data is through "Analysis of Variance" techniques. The author has encountered no narrative of this or other tests being performed on their polynomials by either the SAO or ESSA. It is assumed that when their data reduction techniques were formulated, the adequacy of these particular polynomials was investigated.

If the polynomial approximation is valid, the computed curve will either be

of correct degree and will give unbiased estimates of the coefficients or, if the degree is not correct, will lead to biased estimates [Natrella, 1963, p.6-19]. In the opinion of this author, the following conclusion is unavoidable. An arbitrary polynomial is equivalent to constraining the coefficients which in turn constrains the coordinates of any point computed from the polynomial. In statistical terminology, the word bias would be used in lieu of constraint.

If this is the intent of a fixed degree polynomial, the technical justification would be of interest. It certainly may exist, but it is not readily perceptible to this author. It does not seem likely that the nature and magnitude of such a constraint would be constant when applied to satellite image trails of variable lengths. If no such constraint is intended, the resulting bias seems unwarranted.

Higher order, unconstrained polynomials have been censured for fitting the observations too well, i.e., conforming to short period oscillations of the satellite image about the true path. This is a valid criticism—limiting the degree of the polynomial would restrict its ability to accommodate the oscillations. However, as stated above, this restraint would not apply equally to satellite image trails of varying length and hardly seems justified on this basis alone.

The technique of fitting higher order polynomials has been accused of "overparameterization." The term is used to imply that any parameters beyond the six elements that describe the satellite's orbit are superfluous. This is a difficult area to interpret. The coefficients of a polynomial are not independent parameters in any sense and additional terms are not detrimental per se. In the case of the six orbital elements, other parameters or constants not precisely known are assumed.

A criticism particularly applicable to the ESSA technique is that considerable knowledge is lost through the curve fitting procedure. Intuitively, it does seem that there should be more information on one of these BC-4 plates than can be represented by a single satellite direction. Each satellite position, in conjunction with the two observing stations, defines a plane in space. Any two of these planes define, in theory at least, the line joining the two stations. When all

images on the plate are compressed into a single satellite direction, the solution for the line becomes indeterminate. A solution is not practicable or attempted because of the unfavorable geometry of the spatial directions derived from a single plate. However, this particular criticism does suggest two cogent questions.

(1) If, in the future, a single observation per plate is to be accepted, can it be obtained by simpler methods without significant loss of accuracy?

(2) Is it possible to obtain more than one observation per plate? The greater number of observations should overcome any loss in the accuracy of a single satellite direction. If the additional observations could be made independent, an additional benefit would be gained.

These questions were discussed in terms of actual satellite images and an astrometric reduction in Chapters 2 and 3. In later sections, the curve fitting approach will be examined in the context of these two questions.

If a single satellite coordinate is to be interpolated from each polynomial, from what part of the curve should it be taken? Quoting from a recent report:

> If all observations are to be reduced to a single, smoothed ray, a central ray is not the optimum choice. As far as polynomial smoothing is concerned, greatest accuracies from a polynomial of moderate degree are not to be determined at the center of the span, but rather at a distance well out from the center [Brown, 1967, p. 96].

The quote is given in full here because of its direct consequence to the experimental results of this author. No justification for this statement could be found.

An investigation was made to determine from what part of the curve the best accuracy could be expected. The first problem was to define accuracy as it was used here. In the statistical sense, accuracy implies a knowledge of the true or reference value. It is a term used to define the closeness to or degree of agreement between the measurement and the true value [Natrella, 1963, p. 23-1; Mandel, 1964, p. 128; Hallert, 1966]. This would imply a knowledge or estimate of the satellite's undistorted path across the plate, neither of which seems to be available. Limits to the actual error of a report value, i. e., the magnitude and sign of its deviation from the true, can usually be inferred from the precision of

the measurement process with consideration given to any possible bias of the measurements [Natrella, 1963, p. 23-1]. It was in this sense that the accuracy of the polynomials was investigated.

Starting with the ESSA fifth degree polynomials (two per plate), the standard deviations of several fictitious points along the polynomials were computed. The standard deviations of x are plotted in Fig. 4.1, the same for y are plotted in Fig. 4.2. Recall that plate 2559 contained a much longer image trail than the other two. As can be seen, there are several inflections but no significant improvement away from the plate center for these fifth degree curves.

Next, standard deviations were computed at eleven points along polynomials of various degrees fitted to three trails of ninety consecutive satellite images from plate 6132. The results for all three trails have been listed in Table 4.1. In Figs. 4.3 and 4.4, the standard deviations of x and y for one of the image trails have been plotted. An inspection of the table illustrates the wide diversity that exists among trails for the same degree polynomials, and even between x and y polynomials from the same trail. The particular trail illustrated in Figs. 4.3 and 4.4 was chosen not because it was typical, but because of the contrast between the x and y polynomials. In the case of x, the third degree curve gave the smallest standard deviation all along the trail; for y, the second degree was best except at the center where the third degree gave equal precision. The inflections noted in the fifth degree polynomials were present here also and, as expected, were more pronounced.

One other connotation which might be applied to accuracy in reference to a polynomial is how well the curve fits the observations. It has already been pointed out that fitting too well is not to be desired. There is a statistic readily available to evaluate the goodness of fit—the estimate of σ^2 computed from the squared sum of the residuals. However, it does not give any information as to where the poorest fit occurred. There is no statistical tool to evaluate the curve in such a way, so the following procedure was developed.

The 450 residuals from the ESSA fifth degree curves for plate 2559 were

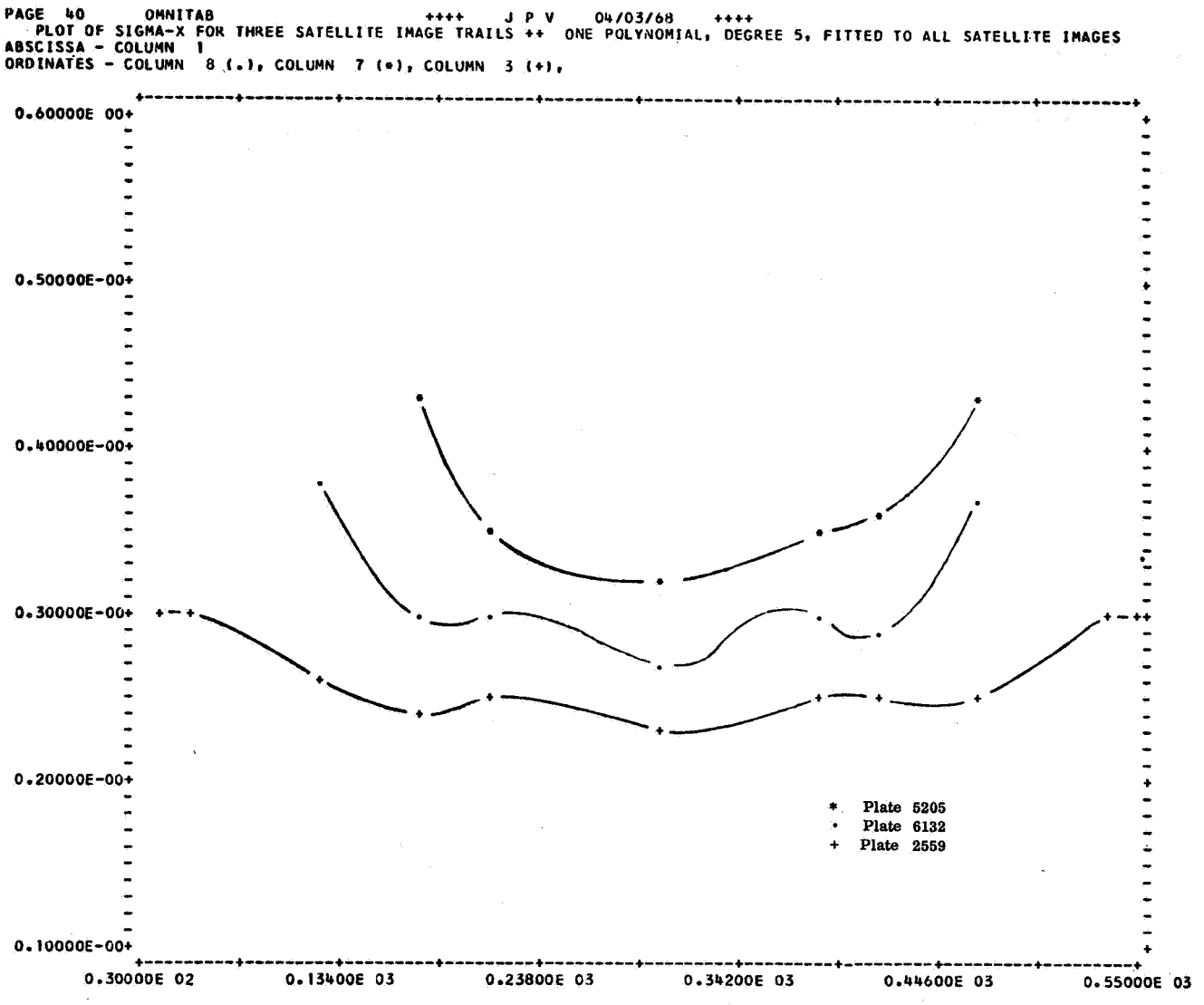

Fig. 4.1 Plot of Standard Deviations (σ_x) Along ESSA X Polynomials—Degree 5

Plate 2559 — 450 Images
Plate 5205 — 297 Images
Plate 6132 — 360 Images

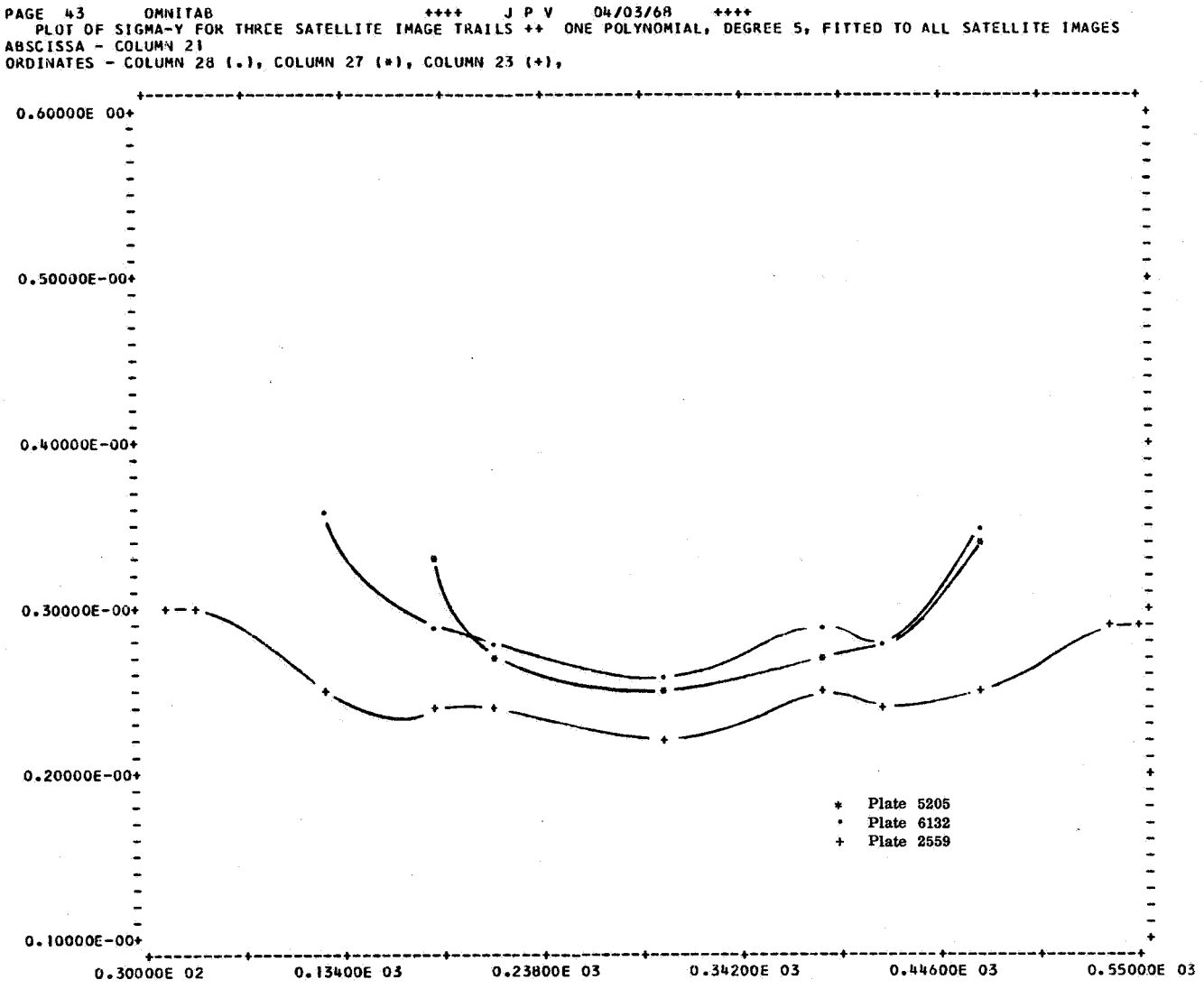

Fig. 4.2 Plot of Standard Deviations (σ_y) Along ESSA Y Polynomials—Degree 5

Plate 2559 — 450 Images
Plate 5205 — 297 Images
Plate 6132 — 360 Images

Table 4.1

Standard Deviations (σ_x, σ_y) at Points Along 90 Image Polynomials
Plate 6132

IMAGE TRAIL 1	SIGMA X				SIGMA Y		
POINT	DEGREE 2	DEGREE 3	DEGREE 4	POINT	DEGREE 2	DEGREE 3	DEGREE 4
-50.000	0.626	0.632	0.633	-50.000	0.618	0.630	0.635
-40.000	0.459	0.461	0.578	-40.000	0.453	0.460	0.579
-30.000	0.383	0.480	0.571	-30.000	0.378	0.479	0.571
-20.000	0.379	0.481	0.487	-20.000	0.374	0.479	0.488
-10.000	0.400	0.436	0.461	-10.000	0.395	0.435	0.462
0.980	0.411	0.392	0.481	0.980	0.406	0.390	0.482
10.000	0.402	0.400	0.468	10.000	0.397	0.399	0.468
20.000	0.378	0.440	0.445	20.000	0.373	0.439	0.446
30.000	0.368	0.461	0.490	30.000	0.363	0.460	0.491
40.000	0.419	0.450	0.553	40.000	0.413	0.448	0.553
IMAGE TRAIL 2							
-50.000	0.855	0.801	0.854	-50.000	0.798	0.892	0.922
-40.000	0.534	0.563	0.641	-40.000	0.562	0.572	0.692
-30.000	0.535	0.452	0.625	-30.000	0.451	0.573	0.675
-20.000	0.556	0.444	0.538	-20.000	0.443	0.575	0.580
-10.000	0.488	0.473	0.534	-10.000	0.471	0.523	0.576
0.979	0.451	0.487	0.562	0.979	0.486	0.483	0.606
10.000	0.477	0.474	0.535	10.000	0.473	0.511	0.577
20.000	0.528	0.448	0.527	20.000	0.446	0.565	0.568
30.000	0.539	0.457	0.617	30.000	0.456	0.578	0.666
40.000	0.546	0.570	0.669	40.000	0.568	0.585	0.722
50.000	0.812	0.807	0.812	50.000	0.805	0.870	0.876
IMAGE TRAIL 3							
-50.000	1.024	0.853	0.920	-50.000	0.638	0.752	0.811
-40.000	0.727	0.517	0.599	-40.000	0.453	0.455	0.528
-30.000	0.567	0.488	0.602	-30.000	0.353	0.430	0.531
-20.000	0.538	0.505	0.521	-20.000	0.335	0.445	0.459
-10.000	0.571	0.477	0.503	-10.000	0.356	0.420	0.444
0.978	0.604	0.435	0.553	0.978	0.376	0.383	0.488
10.000	0.603	0.438	0.548	10.000	0.375	0.385	0.483
20.000	0.573	0.479	0.502	20.000	0.357	0.422	0.442
30.000	0.542	0.508	0.527	30.000	0.337	0.448	0.465
40.000	0.573	0.493	0.615	40.000	0.357	0.434	0.545
50.000	0.734	0.522	0.609	50.000	0.457	0.460	0.537

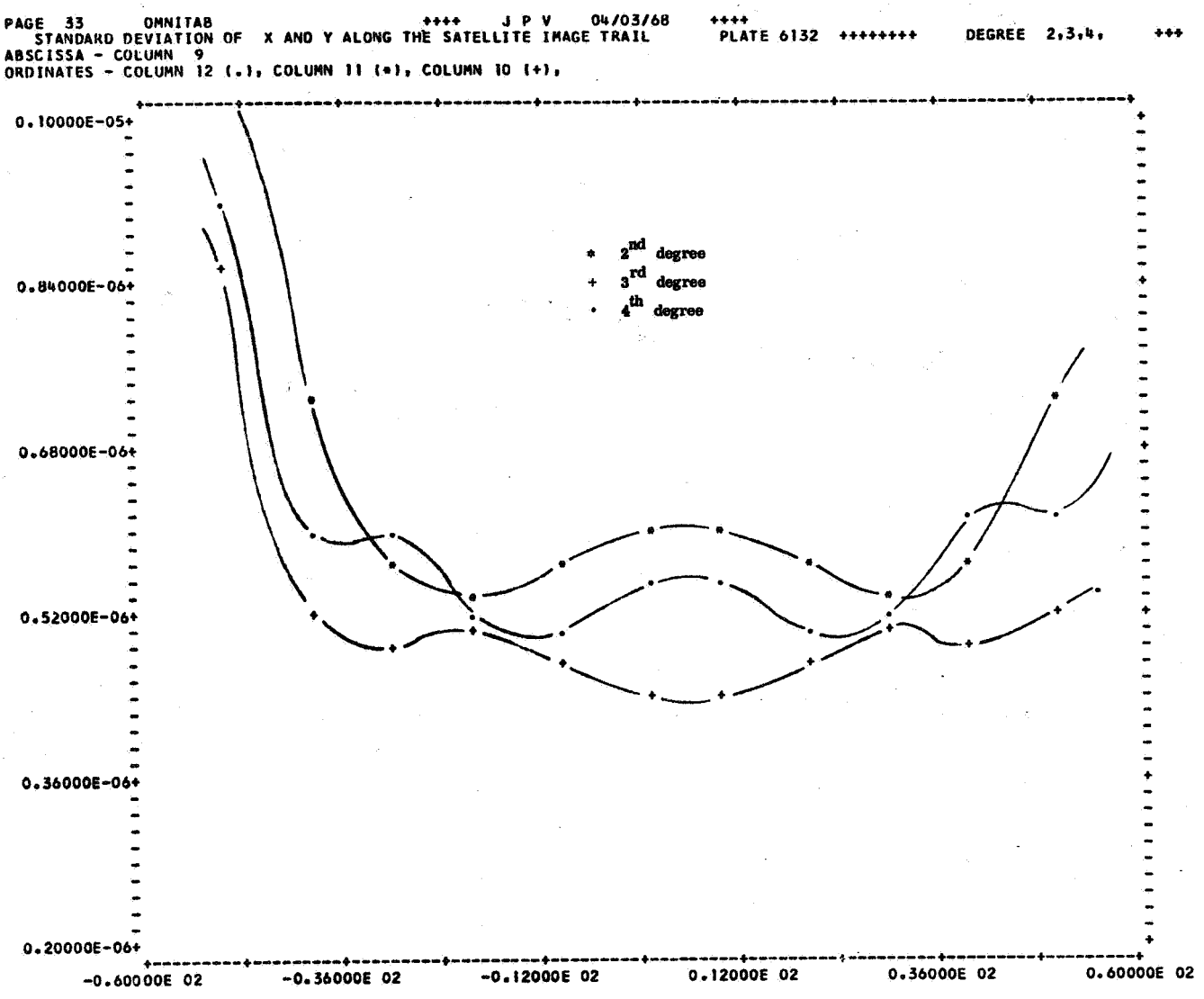

Fig. 4.3 Plot of Standard Deviations (σ_x) Along X Polynomials of Various Degrees Fitted to 90 Satellite Images — Plate 6132

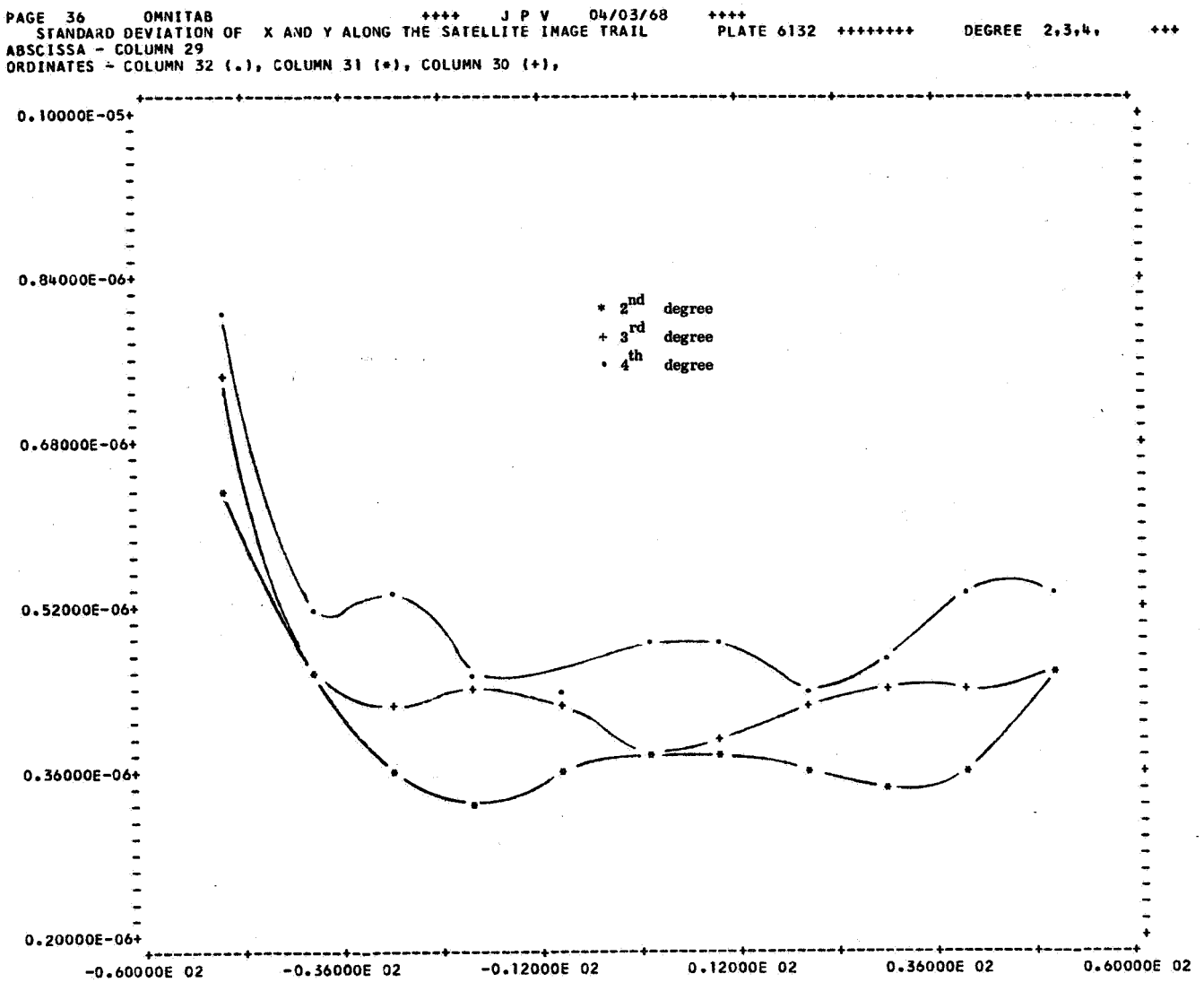

Fig. 4.4 Plot of Standard Deviations (σ_y) Along Y Polynomials of Various Degrees Fitted to 90 Satellite Images — Plate 6132

plotted (Figs. 4.5, 4.6). The plot was repeated using the residuals from five third degree curves, ninety images in each (Figs. 4.7, 4.8). In both cases, the residuals smaller than one-half sigma were not plotted—sigma taken as the standard deviation from the ESSA curve fits.

The conclusion drawn from the investigation was that no general statement about relative accuracies (sigmas) along a polynomial is valid. A better statement would have been that the accuracy of a polynomial fitted to a particular set of data is a function of the number of observations, the degree of the polynomial and the point of interest on the polynomial. Of course, consistency of the data is the overriding factor but was not the question here. The investigation did point out that the entire subject was pertinent to curve fitting as an interpolation function.

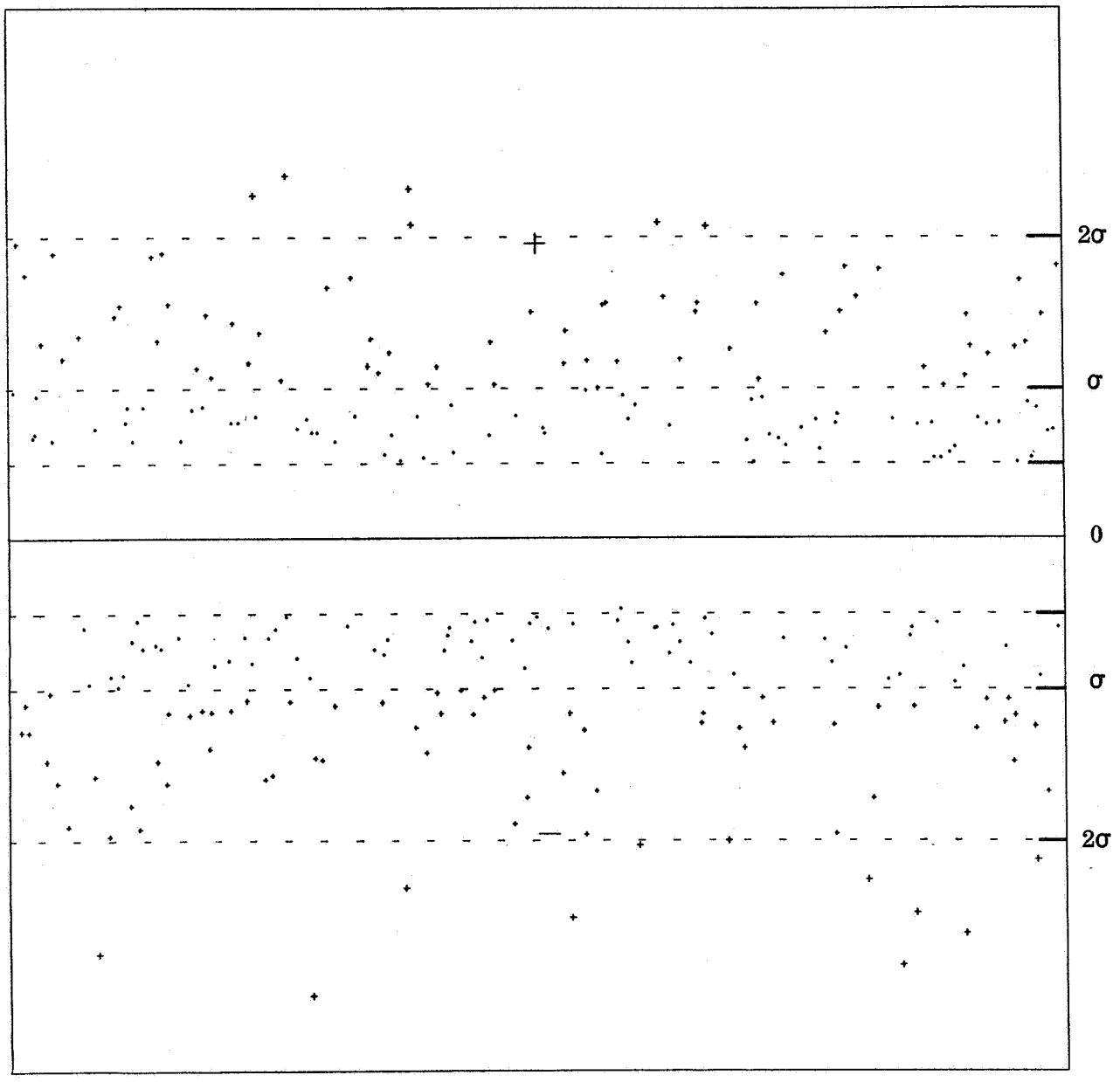

Fig. 4.5 Plot of X Residuals — Plate 2559
ESSA Polynomial—Degree 5—450 Images
σ_x from curve fit = 2.55 μm

(Residuals less than $\frac{1}{2}\sigma_x$ not plotted; one residual greater than 9 μm did not plot)

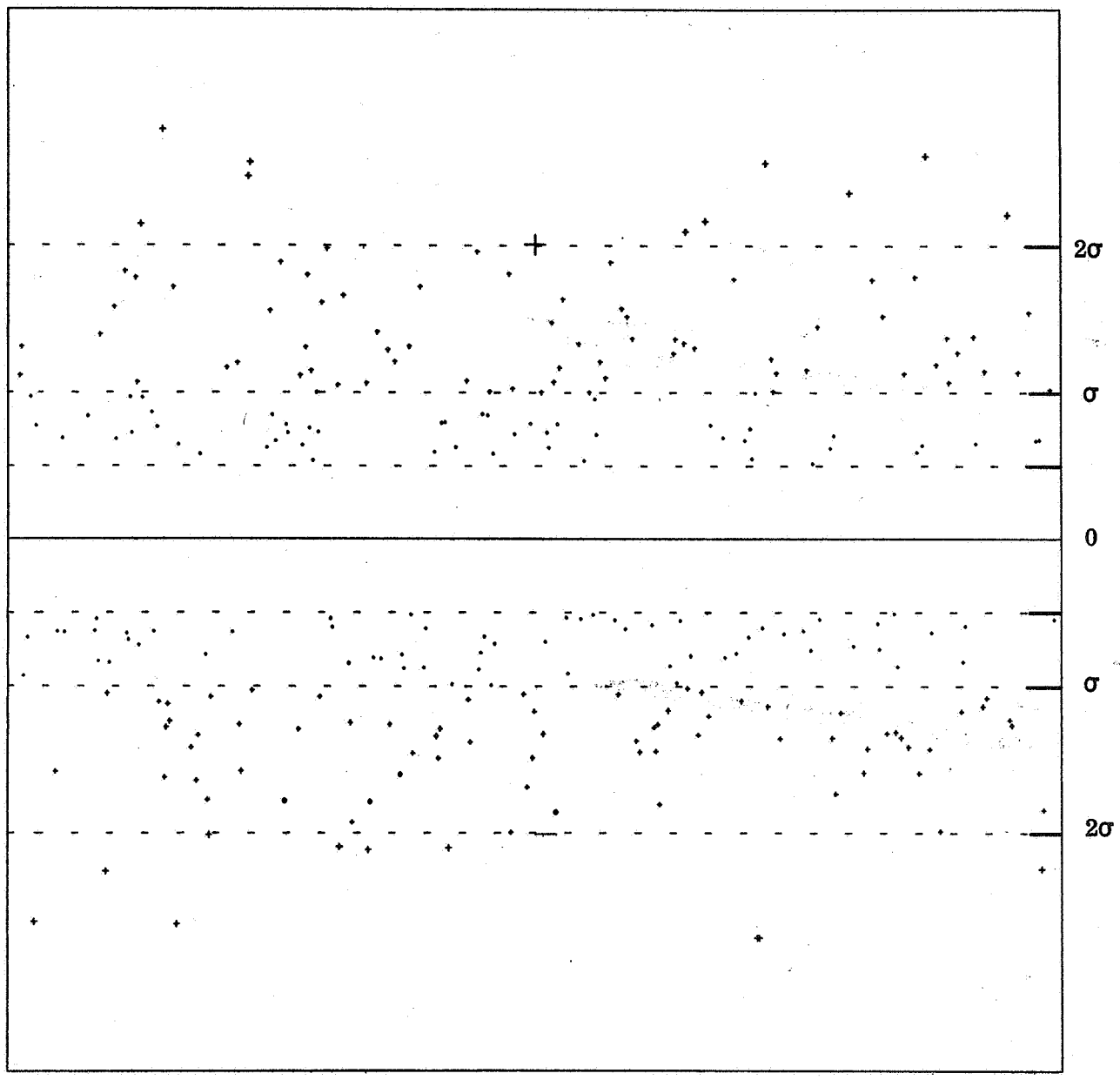

Fig. 4.6 Plot of Y Residuals — Plate 2559
ESSA Polynomial — Degree 5 — 450 Images
σ_y from curve fit = 2.49 μm
(Residuals less than $\frac{1}{2}\sigma_y$ not plotted)

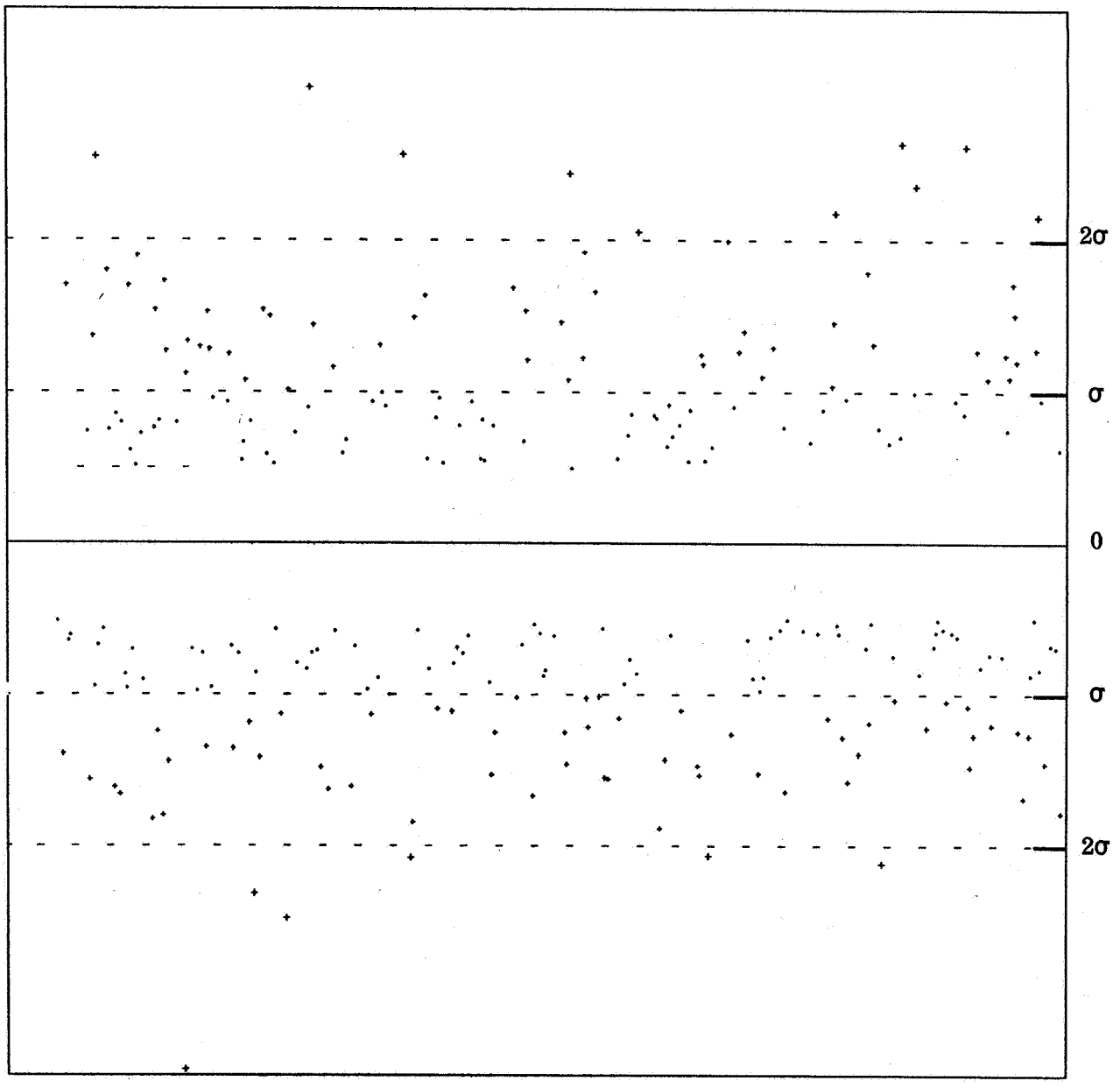

Fig. 4.7 Plot of X Residuals — Plate 2559
5 Consecutive 90-Image Polynomials — Degree 3
(Residuals less than 1.28 μm not plotted)

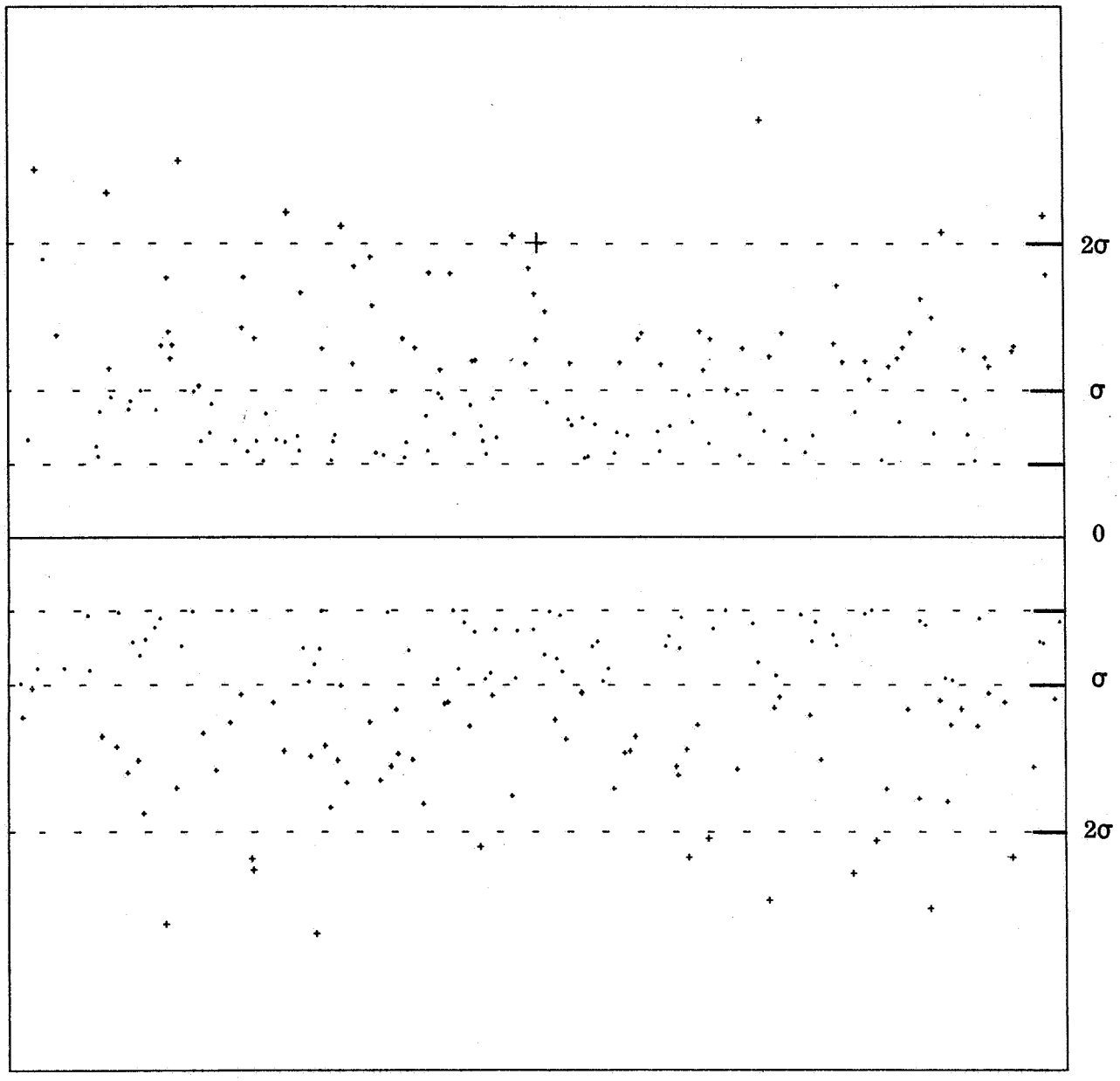

Fig. 4.8 Plot of Y Residuals — Plate 2559
5 Consecutive 90-Image Polynomials — Degree 3
(Residuals less than 1.25 μm not plotted)

4.2 Polynomial Selection

The goal of more than one satellite direction from a BC-4 plate precluded fitting a polynomial to all satellite images. The alternative was to divide the satellite image trail into several segments and fit a polynomial to each. This introduced several new unknowns.

How many images would be required to reach an optimum precision level? What degree polynomial would be required to adequately describe the fewer images? It had already been shown that these two subjects were not independent and must be evaluated together. How would the resulting precision compare to the ESSA "long" polynomials? This was an important factor in evaluating the expected accuracies of the final satellite directions.

Would the several directions be independent observations? Accepting a single photogrammetric reduction for the entire plate, they would not be independent. However, they would be no more dependent than the satellite directions derived from the flashes of an active satellite appearing on a single plate. Assuming an astrometric reduction accomplished for a limited area around each segment of the image trail, the resulting satellite directions would approach independence. The experimentation was begun with satellite trails of sixty images and repeated for ninety image trails. The ninety image trails centered on the individual satellite images of Set I described earlier, while the sixty image trails centered on the images of Set II. Within each set, the image trails did not overlap. The choice of sixty and ninety images was not arbitrary; the reasons advanced in an earlier chapter for selecting the particular images of Sets I and II applied here also.

The decision to use a specific number of images was based on the previous conclusion that a fixed degree polynomial should only be used to describe a specific arc length (time interval). The fixed number of images per polynomial required some images on each plate to be discarded. The sixty image trails offered an immediate advantage in that more satellite directions per plate would be available.

Polynomials of degree one through five were fitted to each of the image trails. The dependent variables were the adjusted plate coordinates as given by ESSA; time was the independent variable. The plate coordinates were first rotated into an orthogonal coordinate system with the x-axis approximating the satellite's direction of motion. The polynomials were then fitted to the rotated coordinates. This procedure is followed by ESSA and is discussed in a later section of this chapter.

After the polynomials were fitted to the observational data, they were evaluated by analysis of variance techniques. Analysis of variance is usually applied to polynomials as follows [Natrella, 1963, p. 6-19].

(1) Fit polynomials of degree 2 through degree n to the data.

(2) Evaluate the error sum of squares for the subsequent polynomials. If the reduction due to fitting the (i+1) degree term is not significant on the basis of the F-test, then the polynomial of degree (i) is accepted as the best fitting polynomial.

A summary of the results are given in Tables 4.2 and 4.3; the computed value of the F statistic and the standard deviations from the curve fits are listed. See [Natrella, 1963; Mandel, 1964] for analysis of variance theory, its applications and the mathematical formulation of the F statistic.

It was required to choose a significance level for the tests. A lower significance level implied a smaller "critical region"; a smaller "critical region" implied a smaller probability of a computed F statistic falling within the region [Mandel, 1964, pp. 164-171]. In the evaluation, this meant that the same (i+1) degree polynomial might be accepted as best fitting at a higher significance level (larger critical region) and rejected at a lower significance level. For preliminary evaluations, two levels were selected—the 10% and the 1%.

First evaluated were the sixty image polynomials. For the appropriate degrees of freedom, the critical values associated with the 10% and 1% significance levels were approximately 2.8 and 7.1 [Biometrika Tables for Statisticians, Vol. 1, 1966]. An inspection of Table 4.2 for the sixty image polynomials shows that the

Table 4.2

60 Image Polynomials — Analysis of Variance

		Plate 2559				Plate 5205			
		X		Y		X		Y	
Trail	Degree	F. Stat.	σ_x	F. Stat.	σ_y	F. Stat.	σ_x	F. Stat.	σ_y
1	2	1 561.41	2.760	271.61	2.110				
	3	0.23	2.779	.12	2.126				
	4	0.08	2.802	.75	2.131				
	5	0.01	2.827	.07	2.149				
2	2	2 174.68	2.887	140.82	2.835				
	3	0.66	2.895	2.80	2.789				
	4	0.04	2.920	0.08	2.812				
	5	0.20	2.942	0.35	2.829				
3	2	3 887.79	2.341	179.31	2.642	8 110.75	3.156	176.68	2.200
	3	0.98	2.341	2.71	2.602	0.97	3.159	0.86	2.203
	4	0.19	2.358	.13	2.622	2.84	3.112	4.52	2.136
	5	0.58	2.367	.28	2.639	3.29	3.049	0.35	2.155
4	2	5 785.21	2.570	295.83	2.370	4 094.76	2.939	108.83	1.934
	3	4.96	2.483	0.00	2.391	1.03	2.938	1.47	1.925
	4	0.69	2.490	0.22	2.408	0.99	2.937	0.08	1.941
	5	0.36	2.504	0.28	2.424	0.05	2.963	0.01	1.959

Table 4.2 (cont'd)

		Plate 2559				Plate 5205			
		X		Y		X		Y	
Trail	Degree	F. Stat.	σ_x	F. Stat.	σ_y	F. Stat.	σ_x	F. Stat.	σ_y
5	2	7 719.17	2.467	310.16	2.628	2 795.17	3.235	062.66	2.297
	3	3.96	2.405	4.13	2.562	1.77	3.211	0.01	2.317
	4	0.59	2.414	1.69	2.546	0.00	3.240	0.33	2.332
	5	1.69	2.399	1.80	2.528	0.00	3.270	4.32	2.264
6	2	7 474.75	2.364	350.53	2.151	3 355.26	2.762	056.54	2.549
	3	0.34	2.377	0.34	2.164	0.00	2.787	2.55	2.515
	4	0.14	2.396	0.01	2.183	1.89	2.764	1.22	2.510
	5	0.29	2.411	0.13	2.201	0.53	2.776	0.93	2.511
7	2	7 573.24	2.550	318.92	2.392				
	3	0.90	2.552	0.01	2.413				
	4	0.11	2.572	0.22	2.429				
	5	0.02	2.596	0.00	2.452				

Table 4.2 (cont'd)

Plate 6132

Trail	Degree	X F. Stat.	X σ_x	Y F. Stat.	Y σ_y
1					
2	2	7 850.36	2.627	525.21	2.379
	3	2.88	2.582	0.01	2.400
	4	0.08	2.604	0.02	2.421
	5	0.00	2.628	7.33	2.293
3	2	7 190.52	2.545	312.73	2.862
	3	1.58	2.531	0.81	2.869
	4	0.28	2.548	8.45	2.693
	5	0.11	2.569	0.12	2.714
4	2	6 155.98	2.939	181.64	3.059
	3	4.32	2.867	3.89	2.984
	4	4.96	2.775	1.58	2.968
	5	3.00	2.725	0.33	2.987
5	2	8 924.86	2.628	453.69	2.453
	3	0.01	2.652	1.84	2.439
	4	0.01	2.675	6.16	2.333
	5	0.30	2.693	0.83	2.337
6	2	18 067.67	2.956	786.14	2.332
	3	3.30	2.902	0.14	2.349
	4	3.96	2.829	1.04	2.348
	5	1.38	2.819	0.11	2.367
7					

quadratic term was always significant and the cubic sometimes significant at the 10% level. On the other hand, the choice of the 1% significance level would have eliminated the cubic term from all of the sixty image polynomials. This was a rather unsatisfactory basis from which to attempt any general conclusions. Furthermore, an inspection of the F's associated with the polynomials of higher degree than cubic indicated that there was considerable error remaining.

The F statistics and standard deviations from the curve fits for the ninety image polynomials are tabulated in Table 4.3. In this case, the cubic was generally significant. Again, the cubic could be accepted as entirely suitable at the 1% level (also the 5%) but not at the 10% level. The thirty additional degrees of freedom did not appreciably change the critical values of F.

To compare the encountered values of the F statistic with the expected values from samples of this size, the following procedure was used. The critical values of F were plotted for the various significance levels and appropriate degrees of freedom. This gave a plot analogous to the Cumulative Distribution Function (CDF) of the F distribution. Treating F as a random variable, expected values of F ($E\{F\}$) were obtained by interpolation from the plot of the CDF. This is illustrated below. As a first order approximation, the two samples were con-

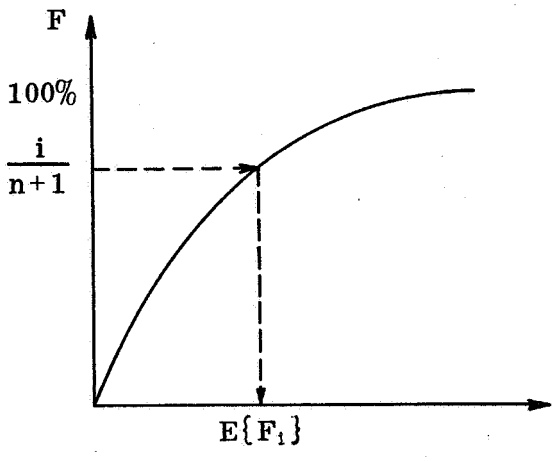

sidered as Order Statistics (a uniform distribution) of size n. An expected value of F was interpolated for each probability interval of $i/(n+1)$, the result was an expected value for each F statistic from sample sizes of 22 and 32.

Table 4.3

90 Image Polynomials — Analysis of Variance

		Plate 2559				Plate 5205			
		X		Y		X		Y	
Trail	Degree	F. Stat.	σ_x	F. Stat.	σ_y	F. Stat.	σ_x	F. Stat.	σ_y
1	2	12 353.15	2.939	1 103.80	2.488				
	3	0.63	2.945	5.97	2.420				
	4	0.97	2.946	0.74	2.423				
	5	0.22	2.959	0.77	2.426				
2	2	20 484.42	2.601	1 079.52	2.625	68 555.07	3.282	1 208.30	2.351
	3	1.93	2.587	2.60	2.602	19.01	2.992	2.54	2.330
	4	0.27	2.598	0.07	2.616	0.69	2.997	2.19	2.314
	5	0.43	2.607	2.36	2.595	2.64	2.969	0.02	2.327
3	2	38 900.89	2.434	1 659.54	2.390	32 478.48	3.086	728.60	2.236
	3	5.91	2.369	0.00	2.404	9.60	2.441	4.96	2.186
	4	2.14	2.353	1.77	2.393	0.33	2.953	0.00	2.199
	5	0.70	2.357	0.04	2.407	0.00	2.970	1.42	2.194
4	2	59 754.02	2.377	2 070.69	2.461	29 348.28	3.181	832.28	2.441
	3	8.84	2.278	3.26	2.429	14.58	2.954	0.05	2.455
	4	0.66	2.283	0.91	2.431	0.02	2.971	3.01	2.427
	5	2.25	2.266	1.45	2.424	0.00	2.988	1.61	2.418
5	2	51 334.18	2.741	2 213.95	2.380				
	3	11.50	2.586	0.48	2.387				
	4	0.36	2.596	0.15	2.399				
	5	0.04	2.611	0.01	2.413				

Table 4.3 (cont'd)

		Plate 6132			
		X		Y	
Trail	Degree	F. Stat.	σ_x	F. Stat.	σ_y
1					
2	2	58 190.97	2.626	2 845.52	2.593
	3	10.58	2.491	8.71	2.484
	4	1.02	2.490	0.40	2.493
	5	0.02	2.505	0.55	2.499
3	2	51 912.54	3.129	1 783.24	3.119
	3	17.02	2.894	2.03	3.101
	4	1.52	2.887	0.21	3.116
	5	7.89	2.777	2.25	3.093
4	2	102 521.30	3.800	4 466.48	2.367
	3	87.23	2.696	0.47	2.374
	4	0.61	2.702	0.42	2.382
	5	1.78	2.690	1.94	2.369
5					

Next, the computed values of F were arranged by magnitude. This ordering was accomplished for the 32 F statistics which tested the significance of the cubic term in the 60 image polynomials. These ordered F statistics were plotted against the expected values. These appear in Fig. 4.9 as °. If the values would plot as a straight line of slope one, it would tend to indicate that the computed F's were compatible with a true F distribution. This, in turn, would lend support to the conclusion that the curves were truly quadratic. This procedure was repeated for the 22 F statistics which tested the significance of the quartic term in the 90 image polynomials. They were plotted in Fig. 4.9 as • . As can be seen, the F's from the quartic term approximated the straight line very well—considerably better than the F's testing the cubic term in the shorter polynomials.

On the basis of these tests, two conclusions were drawn.

(1) The third degree polynomial fitted to ninety satellite images adequately described the satellite path over limited areas of the three plates.

(2) Of the two polynomials studied, the third degree fitted to ninety images was preferable to the second degree fitted to sixty images.

The standard deviations from the curve fit tabulated with the F statistics in Tables 4.2 and 4.3 provided an area of comparison between the shorter polynomials of lower degree and ESSA's long fifth degree curves. The standard deviations, as given by ESSA, were (in μm):

	x	y
plate 2559	2,55	2.49
plate 5205	2.98	2.30
plate 6132	2.79	2.64

A visual comparison can be made through the residual plots for plate 2559 (Figs. 4.5 through 4.8).

The larger standard deviation in x is usually attributed to image smear or other factors that degrade the measuring accuracy in the direction of motion [Brown, 1967, p. 121]. Recall that the adjusted plate coordinates were transformed into a

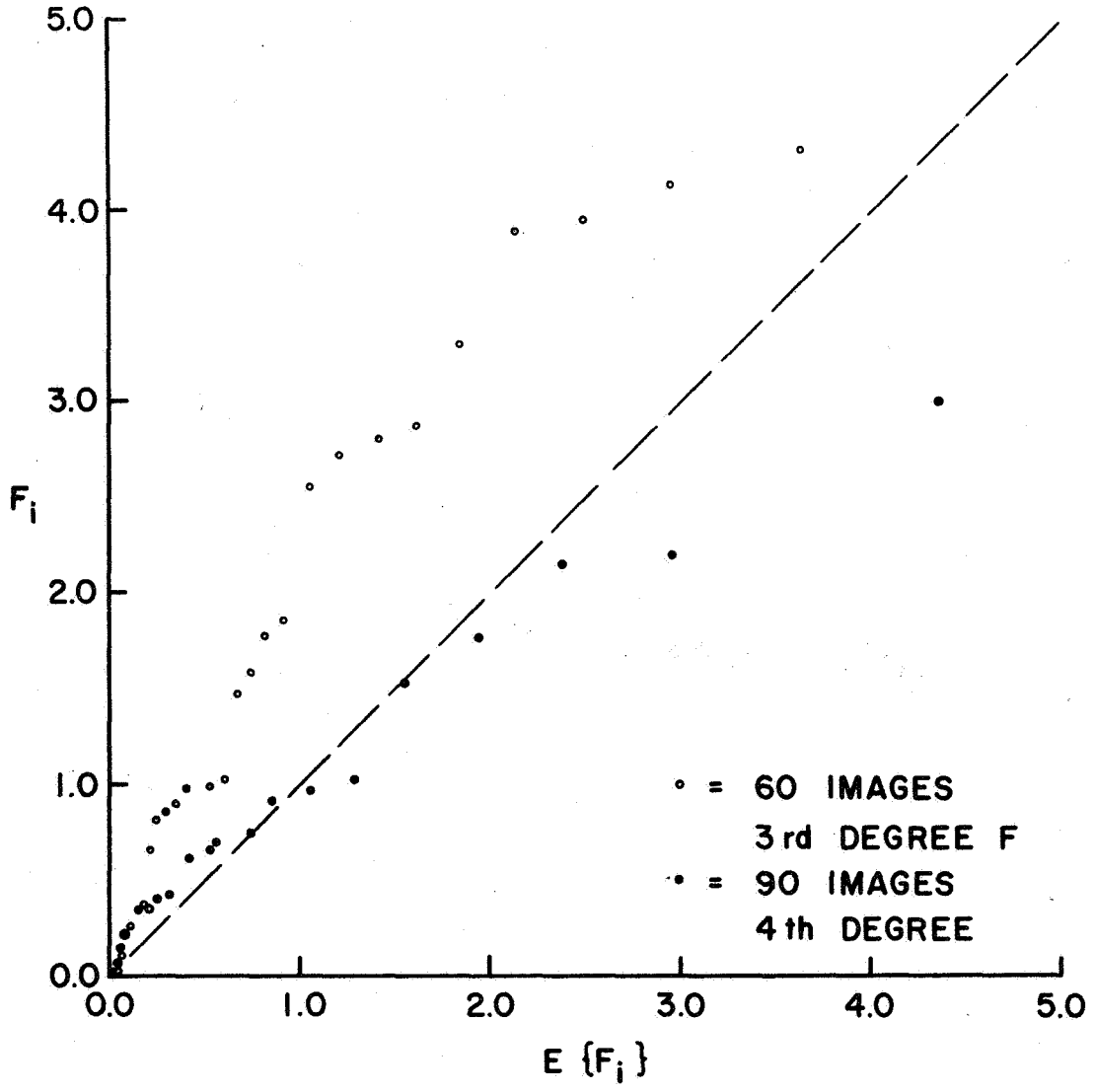

Fig. 4.9 Computed vs. Expected Values of F Statistic

coordinate system in which the x-axis was aligned with the direction of motion. This rotation was performed to isolate the degradation of measurement accuracy in just one coordinate.

On the plates where ESSA's standard deviations were relatively large, at least some of the shorter polynomials reflected the same relatively large values. However, the large standard deviations were not consistent across the entire plate. A comparison of the x and y polynomials across an entire plate raised an interesting point. If the systematic degradation of accuracy along track was due to the causes postulated, there were also periodic or other systematic errors which easily dominated the measuring error in some areas of the plate. These errors certainly acted in a direction perpendicular to the satellite track.

4.3 Polynomials Fitted to Photogrammetric Data

Polynomials had been fitted to the satellite trails of ninety and sixty images described in the last section. The dependent variables were the adjusted x and y coordinates from the ESSA photogrammetric reduction. The independent variable, expressed as an image number, was time. In the ESSA procedure, each satellite image is precisely time correlated; the integer image number is a more convenient form of the independent variable than the conventional units of time.

A simultaneous observation time was selected near the center of each image trail. Fictitious observation times which corresponded to the true observation times were computed. They included corrections for light travel time and station clock error (see section 5.32). Sets of coordinates equivalent to fictitious satellite images and corresponding to the fictitious observation times were interpolated from the polynomials. For the ninety image trails, the third degree polynomial coefficients were used.

The computed coordinates are tabulated in Tables 4.4 and 4.5. Listed with the short polynomial results are the fictitious satellite coordinates computed from the ESSA long polynomial. Only the departures in μm of the short polynomial

Table 4.4

Computed Coordinates and Standard Deviations
(μm)

Plate 2559	ESSA POLYNOMIAL				SHORT POLYNOMIAL			
Point Number	degree 5 X	σ_x	450 images Y	σ_y	degree 3 X	σ_x	90 images Y	σ_y
57.98700	45 719.26	.30	11 866.65	.30	+.47	.47	-.18	.39
178.98635	25 447.39	.24	5 585.44	.24	+.03	.41	-.37	.42
295.98510	4 873.95	.23	- 1 108.30	.22	+.51	.38	+.30	.39
414.98400	-17 220.80	.24	- 8 611.80	.24	-.08	.37	+.41	.39
533.98330	-40 717.16	.29	-16 928.25	.29	-.09	.41	+.25	.38
					degree 2		60 images	
41.98700	48 326.50	.30	12 676.64	.30	+.21	.55	+.73	.42
125.98695	34 440.67	.25	8 418.54	.25	-.11	.58	+.25	.57
210.98600	19 923.02	.25	3 816.70	.24	-.81	.45	+.39	.51
295.98510	4 873.95	.23	- 1 108.30	.22	+.78	.49	-.07	.45
381.98430	-10 963.60	.25	- 6 454.75	.25	+.04	.47	-.27	.50
468.98355	-27 694.14	.25	-12 277.28	.25	+.23	.45	-.01	.41
548.98330	-43 791.55	.30	-18 040.83	.29	-.17	.51	+.06	.48

Table 4.5

Computed Coordinates and Standard Deviations
(μm)

Plate 5205	ESSA POLYNOMIAL				SHORT POLYNOMIAL			
Point Number	degree 5 X	σ_x	297 images Y	σ_y	degree 3 X	σ_x	90 images Y	σ_y
178.97325	11 496.48	.43	35 307.67	.33	+.13	.48	+.12	.38
295.97380	3 447.03	.32	1 853.93	.25	+.29	.46	+.45	.34
414.97460	-4 139.90	.36	-30 505.26	.28	-.01	.47	-.13	.39
					degree 2		60 images	
210.97340	9 230.92	.35	25 974.86	.27	-.12	.61	-.25	.42
295.97380	3 447.03	.32	1 853.93	.25	+.38	.57	+.67	.37
381.97435	-2 091.24	.35	-21 678.89	.27	-.58	.64	+.40	.45
468.97500	-7 408.62	.43	-44 730.40	.33	-.04	.53	+.54	.49
Plate 6132					degree 3		90 images	
178.98005	-2 762.79	.30	-30 250.24	.29	+.15	.39	-.50	.39
295.97875	267.05	.27	- 4 973.64	.26	-.50	.45	+.21	.48
414.97765	4 004.26	.29	22 670.91	.28	+.49	.43	+.38	.38
					degree 2		60 images	
125.98070	-3 947.82	.38	-41 166.89	.36	.00	.50	+.17	.45
210.97970	-1 992.61	.30	-23 505.02	.28	+.17	.49	-.59	.55
295.97875	267.05	.27	- 4 973.64	.26	+.01	.57	-.10	.59
381.97790	2 896.03	.30	14 787.32	.29	-.01	.52	+.81	.48
468.97715	5 945.93	.37	35 966.03	.35	-.12	.56	-.10	.44

coordinates from the long are given. This does not imply which is the more accurate; it presents easily interpretable figures.

The maximum difference between a fictitious image coordinate computed from the long polynomial versus the ninety image polynomial was 0.51 μm. The mean difference was 0.27 μm or 0".17. When considering both x and y coordinates together, the largest total difference was approximately 0.6 μm or less than 0".5. This indicates that the shorter polynomials gave nearly the same interpolated values as the longer polynomial.

Within each image trail, different degree polynomials had varying effects on the interpolated coordinates. Table 4.6 illustrates this; it is the computer output from the curve fit program for plate 5205. It lists the coordinates (in meters) of the fictitious satellite images as interpolated from polynomials of degree one through five. For example, the x coordinates of image 295.97380 had a range of only 0.03 μm (degree one excluded) and it matters little from which degree curve the interpolated value was taken. On the other hand, the x coordinate of image 414.97460 varies by over 0.5 μm. The analysis of variance techniques described and used earlier makes the choice of degree automatic. Furthermore, confidence in the interpolated value is increased.

Another comparison between the various polynomials was made through the precision estimates (σ_x, σ_y) for the coordinates of the fictitious points. The precision figures are listed in Tables 4.4 and 4.5 also. The x and y coordinates of a fictitous satellite image computed from the shorter image trails did suffer a significant decrease in precision. It averaged about 60% for an image near the plate center for the ninety image third-degree polynomials and less away from the center. The loss of precision was somewhat greater for the sixty image quadratic polynomials.

The precision of points all along the fifth-degree curves had previously been examined. Similar calculations were undertaken for all third-degree curves. Without exception, the best precision estimate was at or very near the center of the curve. Limited experimentation with the quadratic curves indicated that the

Table 4.6

Predicted Values of Fictitious Satellite Images
(in meters)

Plate 5205

---------- PLATE 5205 ----------

THE CURVE IS DIVIDED INTO THREE SEGMENTS 90 IMAGES EACH

FIVE POLYNOMIALS WERE FITTED DEGREE 1 THROUGH 5

PREDICTED VALUES OF THE FICTITIOUS POINTS

X COORDINATE

DEGREE	178.97325	295.97380	414.97460
1.	0.1152796E-01	0.3468443E-02	-0.4117566E-02
2.	0.1149656E-01	0.3447336E-02	-0.4139836E-02
3.	0.1149661E-01	0.3447320E-02	-0.4139888E-02
4.	0.1149693E-01	0.3447351E-02	-0.4140380E-02
5.	0.1149694E-01	0.3447341E-02	-0.4140349E-02

Y COORDINATE

DEGREE	178.97325	295.97380	414.97460
1.	0.3539750E-01	0.1913510E-02	-0.3044722E-01
2.	0.3530770E-01	0.1854393E-02	-0.3050495E-01
3.	0.3530779E-01	0.1854375E-02	-0.3050513E-01
4.	0.3530743E-01	0.1854570E-02	-0.3050496E-01
5.	0.3530746E-01	0.1854573E-02	-0.3050497E-01

best values occurred outward from the center. This provided an additional reason for choosing the cubic polynomial over the quadratic.

With particular reference to the ninety image third-degree polynomials, the experimental results are summarized as follows. The interpolated fictitious satellite coordinates are very nearly the same from either the long or short image trails. The short image trails yield larger precision estimates, but at least three reliable satellite directions per plate are now available.

4.4 Polynomials Fitted to Astrometric Data

The procedures used here are based on the recommendations of previous sections; namely, plate areas of 3.8° radius and third-degree curves fitted to ninety satellite images. Each image trail consisted of the same ninety satellite images discussed in the last section. The fictitious satellite images also were the same. The astrometric reductions were reaccomplished for the 3.8° radius plate areas; output of the adjustment program now consisted of right ascensions and declinations for the ninety satellite images within the area. These satellite directions were then corrected for phase angle and differential refraction (for a description of these corrections, see Chapter 5).

To these ninety final right ascensions and declinations (in radians), first- through fifth-degree polynomials were fitted. Based on the previous experimentation, it was assumed that the third-degree curve would be adequate. To verify this, analysis of variance techniques were again used to evaluate the polynomials.

Generally the cubic term was significant at any level. The quartic term was significant at the 10% significance level in three of the twenty-two polynomials. Two of three quartic terms would have been eliminated at any lower significance level but the third would have retained significance through the 1% level. The two largest F statistics, which tested the significance of the quartic term, were associated with the same image trail from plate 5205.

This presented the alternatives of using a fourth-degree curve for one or two interpolation functions and cubics for the remainder, or accepting the cubic for

all. The decision was to accept the cubic for all image trails. This was done for two reasons. The one F statistic was so much larger than the others, it appeared there had been a computational problem in the plate reduction or curve fit. Furthermore, when reduced photogrammetrically, the same satellite coordinates had been accommodated adequately by the third-degree polynomials. The final interpolated value would have changed only 0^s.004 if the fourth-degree curve would have been used.

A right ascension and declination (in radians) for the fictitious satellite image were interpolated from the third-degree curves. These were transformed back into equatorial coordinates and are tabulated in Table 4.7. The precision estimates are given in seconds of time and arc as well as μm. Also included in the table are the departures of the photogrammetric from the astrometric coordinates as computed from the ESSA and ninety image polynomials.

Two other slightly different approaches to the curve fitting could have been taken. Lambeck implies a fit to the declination and to the right ascension multiplied by the cosine of the declination ($\delta, \alpha \cos\delta$) [Lambeck, 1967, p. 82]. This would not offer any apparent advantages other than smaller dependent variables. It would have required two additional computational steps.

The SAO transforms the coordinates into an auxiliary system before the curve fit. This is done to avoid computational problems if the satellite is imaged near the celestial pole. An auxiliary system which could be used with the BC-4 data is the standard coordinate system. The maximum satellite declination on the three plates studied was near 61° so the use of the auxiliary system was not required.

The version of the Omnitab language available and used in the curve fitting was limited to single precision arithmetic. It is believed that double precision would have improved the final accuracies of this section; the use of double precision is recommended. In single precision on the IBM 7094, the eighth significant figure is in doubt. When curve fitting to radians of right ascension and declination, the seventh and eighth significant figures are obviously important to the final accuracies and could be considerably altered by round-off errors.

5. SATELLITE IMAGE CORRECTIONS

A satellite position interpolated directly from the stellar background of a photographic plate may not be considered a final satellite direction. Such an interpolated position could be considered equivalent to a fictitious satellite at infinite range whose only motion is the diurnal motion of the celestial sphere. The satellite is at finite range and possesses an orbital motion of its own. Therefore, the satellite position interpolated from the photographic plate is not the true position and must be corrected.

There are three corrections required to bring an interpolated satellite position to its true or final position. First, the satellite has a velocity with respect to the observer; the satellite will be displaced or aberrated by an amount dependent upon the satellite's relative velocity. Second, the satellite being at a finite range, astronomic refraction applied to its observed coordinates will not result in the actual satellite position. It must be further corrected for a differential refraction arising from the finite range. Third, a passive satellite's geometric center will not coincide with the observed center since only a portion of the satellite is illuminated by the sun. These corrections are discussed in reverse order.

5.1 Phase Correction

The portion of a large passive satellite which is both sun illuminated and visible to an observer on the earth is continually changing much as the moon goes

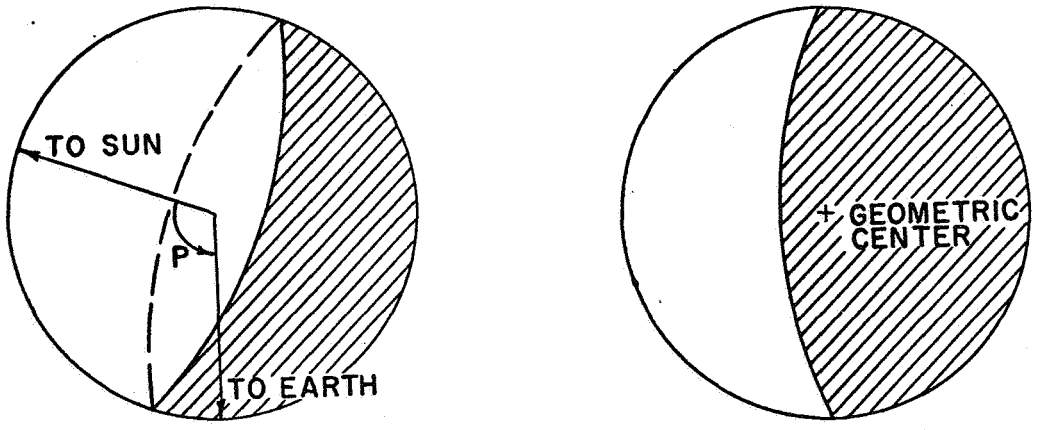

SPACE VIEW EARTH VIEW

through its phases. As a result, the visible center will, in most cases, not coincide with the geometric center.

The mathematical formulation for the correction used in this study is from [Schmid, 1964]. Of interest here is the case of a spherical reflective satellite such as the balloon satellites Echo and Pageos. In a form convenient for computer computation, the expressions are

$$\Delta\alpha = \frac{-R}{r \cos\delta_s} \left[\frac{1 - \cos P}{2\,(1 - \cos^2 P)}\right]^{\frac{1}{2}} \cos\delta_S \sin(\alpha_S - \alpha_s)$$

$$\Delta\delta = \frac{R}{r \sin\delta_s} \left[\frac{1 - \cos P}{2\,(1 - \cos^2 P)}\right]^{\frac{1}{2}} [\cos\delta_S \cos(\alpha_S - \alpha_s) + \cos P \cos\delta_s]$$

where the square root is taken always positive, r is the range from observer to satellite, α_S and δ_S are the sun's right ascension and declination, α_s and δ_s are the satellite's right ascension and declination, R is the satellite radius, and P is the angle at the satellite between the vectors to the sun and to the observer. Cos P may be computed from

$$\cos P = -(\cos\alpha_S \cos\delta_S \cos\alpha_s \cos\delta_s + \cos\alpha_S \sin\delta_S \cos\alpha_s \sin\delta_s + \sin\delta_S \sin\delta_s) \ .$$

The sun's equatorial coordinates may be taken from the American Ephemeris and Nautical Almanac or computed approximately from the following expressions [Badekas, 1967].

$$\alpha_S = 282^\circ.373 + 0^\circ.98562\ (\text{MJD} - 39\,493.5) + 1^\circ.9166 \sin[0^\circ.98562\ (\text{MJD} - 39\,493.5)] - 2^\circ.4666 \sin[2(282^\circ.373 + 0^\circ.98562\ (\text{MJD} - 39\,493.5))]$$

$$\sin\delta_S = \sin[282^\circ.373 + 0^\circ.98562\ (\text{MJD} - 39\,493.5)] \times 0.39785$$

MJD is the Modified Julian Date and is computed

$$\text{MJD} = \text{JD} - 2\,400\,000.5 \ .$$

The reference epoch of the equations is 1967 January 3.5.

5.2 Parallactic Refraction Correction

Parallactic refraction ΔZ is defined as the difference between the apparent position of the satellite and its actual position as shown in the following figure. The notation is self explanatory.

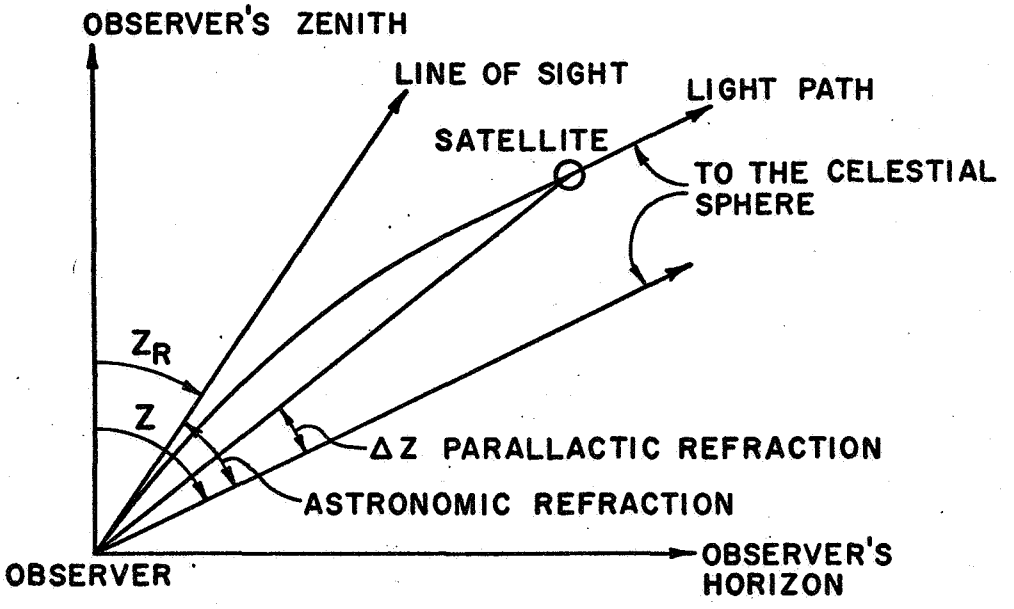

The formulation used in this study and at ESSA is attributed to Hellmut Schmid [Hotter, 1967, p. 31]. The correction is computed from

$$\Delta Z = \frac{2.2330 \tan Z_R}{r \cos Z_R} \frac{206265}{1 + 0.003665\, T_s} \frac{P_s}{P_0}$$

where r is the range to the satellite, Z_R is the refracted zenith distance, T_s is the station temperature in degrees centigrade, P_s is the station barometric pressure (mm of Hg), and P_0 is standard barometric pressure (760 mm of Hg).

5.3 Satellite Aberration Correction

Let the light be reflected from a passive satellite at the time t_1. The right ascension and declination of the satellite at this instant are represented by α_1, δ_1. The light arrives at the camera at the time t_2. During the time interval $t_2 - t_1$, the satellite has moved forward along its orbital path to the position α_2, δ_2.

The differences between the coordinates α_2, δ_2 and α_1, δ_1 are due to the relative velocity of the satellite with respect to the observer and are termed the components of parallactic aberration.

The parallactic aberration correction required may be accomplished in two ways. The first is to correct the satellite's coordinates from their values at t_1, which are recorded on the plate, to their values at the time t_2. The second method is to antedate the observation time from t_2 by the light travel time to t_1.

In this study, the goal has been to obtain simultaneous observations, from two or more ground stations, of a passive satellite. When using individual images, the satellite coordinates will have to be corrected as mentioned above and as is described in section 5.31. When polynomials have been fitted to several images, a light travel time correction may be applied somewhat differently as described in section 5.32.

A subject related to the satellite aberration correction is timing. The two must be considered together when simultaneous observations of a passive satellite are desired.

Each station clock defines its own time system which generally differs from the desired UT1. The station clocks (and time systems) are synchronized to UTC through a portable crystal clock and their rate is determined from VLF phase comparisons. Therefore, associated with each photographic plate is a correction to the station clock time to refer it to UTC and another correction from UTC to UT1 which is the same for all station clocks.

The two corrections may be applied as a single correction to the station clock times of the satellite observation or they may be considered when computing the fictitious simultaneous satellite image from a curve fit. The fundamental relationship between the observation time, as recorded in the station clock time system (T_{sc}), and the time the light was emitted or reflected from the satellite ($UT1_s$) may be expressed

$$T_{sc} + \Delta T = UT1_s + (r/c)$$

or

$$T_{sc} = UT1_s + (r/c) - \Delta T$$

where ΔT is the required correction to the station clock time to refer it to UT1, r is the range to the satellite, and c is the velocity of light.

The satellite aberration and station clock corrections are discussed together since, in practice, they may be applied at the same time.

5.31 Individual Image Correction

In some designated time system, the observed light is reflected from the satellite at a time $UT1_s$. It will reach station A at a time $UT1_A$ in the same time system where $UT1_A = UT1_s + (r/c)$. It will reach station B at a time $UT1_B$ computed similarly; r/c is the light travel time correction. For a simultaneous observation, the satellite position of interest is the one imaged at $UT1_A$ and $UT1_B$ on the two plates. To this point, the correction is straightforward.

The problem arises because, most likely, there will not be a satellite image recorded at either $UT1_A$ or $UT1_B$. Even if it were possible to synchronize the station clocks to the required accuracy, it would be impossible to vary the chopping rate of the shutters to give an image precisely at $UT1_s + (r/c)$. The quantity r/c is continuously changing as the satellite passes through the field of view.

The practical solution is to correct the position of an actual satellite image. This may be done by calculating a rate of change per unit time (α', δ') for the satellite coordinates and multiplying it by the time interval (δt) required to bring a recorded image to the time $UT1_s + (r/c)$. This method has been derived in detail in [Veis, 1960, p. 116]. Veis' formulation alone is not applicable to simultaneous observations of passive satellites as it only updates the satellite coordinates to what they should be at the observation time. What is required are the satellite coordinates at the time the light was reflected from the satellite.

A formulation applicable here is

$$\Delta\alpha = \frac{d\alpha}{dt}\,\delta t = \alpha'\,\delta t$$

$$\Delta\delta = \frac{d\delta}{dt}\,\delta t = \delta'\,\delta t$$

where $\Delta\alpha$ and $\Delta\delta$ are the corrections to an actual satellite image's coordinates.

δt is any difference between the actual station clock epoch of observation and the desired epoch at the station $(UT1_s + (r/c))$.

The simplest way to compute $\Delta\alpha$ and $\Delta\delta$ is to first transform each station clock time system into a common time system (such as UT1). This is done by correcting the station clock time of observation by ΔT, now each recorded image has an epoch of observation in this common time system. The simultaneous observation epoch may also be selected in the same time system.

For example: assume $UT1_s$ is designated the epoch of the simultaneous observation. Light reflected from the satellite at this time will reach the observing stations at time $UT1_s + (r/c)$. If the si- ultaneous observation is to occur, a satellite image should be recorded at this instant. Suppose, at one station, the camera shutter opened and an image was recorded at a time δt later $(UT1_s + (r/c) + \delta t)$. The required corrections to the observed satellite coordinates would be

$$\Delta\alpha = \alpha' (-\delta t)$$
$$\Delta\delta = \delta' (-\delta t)$$

where δt is applied with appropriate sign.

In practice, there is no need to transform the station clock time system to the common time system by correcting the observation times. This correction may be applied directly when computing δt. Let $UT1_s$ be the desired observation time at the satellite, UT1 be the desired observation time at the station ($UT1 = UT1_s + (r/c)$), and T'_{sc} be the time, in the station clock time system, that an image was actually recorded (shutter opening time). Then

$$UT1 = T'_{sc} + \Delta T + \delta t = UT1_s + (r/c)$$

where all times are now referred to the UT1 time system. This may be rewritten as

$$\delta t = UT1_s + (r/c) - (T'_{sc} + \Delta T) \ .$$

This method of correcting for station clock error and light travel time may be applied in any coordinate system. Its use is not restricted to the equatorial coordinates discussed here.

The author is not aware of any agency using these or similar expressions at the present. However, the satellite directions derived in Chapters 2 and 3 of this report would have to be thus corrected to be used as simultaneous observations in the geometric mode. For this reason, a brief investigation was undertaken to examine the expected accuracy of the corrections computed from the above equations.

The first step was to determine an α' and δ' to use in the equations. It has been postulated that these quantities can be obtained with sufficient accuracy from the plate itself [Veis, 1960, p. 116; Mueller, 1964, p. 316]. The rates of change of α and δ vary greatly across the plate. This raised the question of how long a time interval (dt) should be used to determine $d\alpha/dt$ and $d\delta/dt$. The interval must be short enough to be sensitive to the rapid variations of the α' and δ', yet long enough to overcome the errors that may occur in individual satellite coordinates. The best computational results were obtained with time intervals of $2^s.0$. A satellite image $1^s.0$ prior to and another $1^s.0$ beyond the satellite image of interest were used to calculate the rates of change. This exact interval and spacing could not always be duplicated due to missing images but it was approximated as closely as possible.

A $\Delta\alpha$ and $\Delta\delta$ were computed for the previously discussed satellites of Sets I and II, plate 2559. The important fact to note is that the α' and δ' used in the above expressions were computed from satellite images actually recorded on the plate. δt was set equal to r/c which made the expressions analogous to Veis' formulation. This was not necessary—any arbitrary time interval or intervals could have been substituted.

The computed values of $\Delta\alpha$ and $\Delta\delta$ were checked in the following manner. The best available estimate of the satellite's true path across the plate was represented by the ESSA fifth-degree polynomials. They were directly correlated to time through the image numbers. Two groups of fictitious satellite image coordinates (x and y) were generated from the ESSA polynomials for plate 2559. One group corresponded to the observation times UT1 of the images of Sets I and II.

A second group was generated for times UT1 + (r/c). Both groups of x and y coordinates were transformed into equatorial coordinates and a $\Delta^*\alpha$ and $\Delta^*\delta$ calculated as the differences between the two groups. These quantities should have been accurate estimates of the changes in the satellite right ascension and declination during the time interval r/c.

The experimental results are listed in Table 5.1. The columns labeled α' and δ' show the large magnitudes and rapid variation of these quantities across the plate. The $\Delta\alpha$ and $\Delta\delta$ agree very closely with $\Delta^*\alpha$ and $\Delta^*\delta$. The conclusion was: If this correction were carefully and precisely computed from the observed right ascensions and declinations, it would not introduce large errors into the final satellite directions.

Table 5.1

Computation of Satellite Coordinate Corrections
for Time Interval r/c

IMAGE	$\frac{r}{c}$	α'(s/s)	$\Delta\alpha^s$	$\Delta^*\alpha^s$	δ'("/s)	$\Delta\delta$"	$\Delta^*\delta$"
42	.00720	-67.5224	-.486	-.495	195.774	1.41	1.41
58	.00720	-69.4472	-.505	-.500	186.871	1.34	1.36
126	.00719	-75.3981	-.546	-.542	157.809	1.13	1.13
179	.00707	-78.9775	-.568	-.558	131.127	.93	.90
211	.00700	-82.1653	-.580	-.575	108.384	.76	.75
296	.00682	-88.0971	-.605	-.606	46.277	.32	.32
382	.00666	-92.4538	-.619	-.616	-24.629	- .16	- .16
415	.00660	-93.4355	-.620	-.617	-59.467	- .39	- .36
469	.00651	-93.6911	-.617	-.610	-111.192	- .72	- .68
534	.00646	-93.7629	-.610	-.605	-166.099	-1.07	-1.09
549	.00646	-93.0100	-.608	-.601	-184.104	-1.19	-1.18

$\Delta\alpha$, $\Delta\delta$ computed from actual satellite images

$\Delta^*\alpha$, $\Delta^*\delta$ computed from ESSA polynomials

5.32 Fictitious Satellite Image Correction

The satellite aberration and station clock corrections are greatly simplified when polynomials are fitted to the recorded images and fictitious satellite images are interpolated from them. The correction for satellite aberration may now be applied as a light travel time correction.

The general procedure is to designate an epoch at the satellite in some reference time system. The corresponding epoch in the station clock time system may then be computed by applying the corrections for light travel time and station clock error. This station clock epoch can be transformed into a satellite image number, i.e., fictitious satellite image. The coordinates of this fictitious satellite image are then interpolated from the polynomial. Recall that the independent variable of the curve fit is image number; this is actually the station clock time system expressed in a different manner.

The mathematical formulation expressing the general procedure can be developed very simply. Let an arbitrary station clock epoch be represented by T_{sc} and its correction to UT1 be represented by ΔT. Then

$$T_{sc} + \Delta T = UT1$$

or

$$T_{sc} = UT1 - \Delta T \ .$$

The satellite image number corresponding to the epoch T_{sc} is computed from

$$IN = (T_{sc} - T_r) \times C \ .$$

T_r is a reference epoch in the station clock time systems; C is the number of images recorded per unit time. T_r is computed from the time (t_1) that the first satellite image is recorded by

$$T_r = t_1 - (1/C) \ .$$

The first satellite image recorded is not necessarily recorded by each observing station. This formulation for the reference epoch simply means that the first image will have the number 1 associated with it rather than 0. If $T_{sc} - T_r$ is an integer multiple of the chopping rate of the camera shutter (1/C), the shutters

will be open and an actual satellite image recorded.

A satellite image number corresponding to a specified UT1 epoch is

$$IN = (UT1 - \Delta T - T_r) \times C \ .$$

The satellite image represented by this number corresponds to the satellite position at $UT1_s$ where $UT1_s = UT1 - (r/c)$. $UT1_s$ is the time the light left the satellite and r/c is the light travel time. The expression may, therefore, be rewritten as

$$IN = (UT1_s + (r/c) - \Delta T - T_r) \times C \ .$$

This gives the relationship between a designated simultaneous observation epoch at the satellite ($UT1_s$) and the satellite images actually recorded on the photographic plate.

If the station clock time of the simultaneous observation is desired, it can be computed from

$$T_{sc} = UT1_s + (r/c) - \Delta T \ .$$

Given the image number corresponding to the simultaneous observation, the equivalent station clock time may be computed from

$$T_{sc} = \frac{IN}{C} + T_r \ .$$

The practical application of these formulas can best be shown through an example. This is the method used to compute fictitious satellite images in this study. This procedure is a simplification of the ESSA procedure as deduced from their computational form. This form accompanied the data from the three BC-4 plates. The data is taken from the first 90-image polynomial on plate 2559. The formulation already described and used in this example is

$$IN = (T_{sc} - T_r) \times C$$

or

$$IN = (UT1_s - \Delta T + (r/c) - T_r) \times C \ .$$

(1) Select a simultaneous observation time ($UT1_s$) at the satellite. $UT1_s = 1^h30^m50^s.80000$

(2) Apply the station clock correction (ΔT). $-.00980$

(3) Compute r/c. $\frac{2160.36725}{300{,}000} = .00720$

(4) Compute the observation time at the station (T_{sc}) in the station clock system. $T_{sc} = UT1_s - \Delta T + (r/c)$. $1\ 30\ 50.79740$

(5) The reference epoch (T_r) for this event was $-\ 1\ 30\ 39.20000$

(6) The time elapsed since the reference epoch. $T_{sc} - T_r = 11.59740$

(7) C = 5. 5 images are recorded per second. (Chopping interval is $0^s.2$.) $\times\ 5$

(8) The final fictitious satellite image number is 57.98700

The coordinates of this fictitious satellite image may now be interpolated from the polynomial.

6. CONCLUSIONS

Several precise satellite directions may be obtained from a BC-4 plate on which a passive satellite is imaged. This can be accomplished in two ways.

(1) The satellite image trail from a photogrammetrically reduced plate is divided into segments. A polynomial is fitted to each; from this polynomial, a final satellite direction is interpolated.

(2) Astrometric reductions are accomplished within several small areas of the plate. A curve is then fitted to the right ascensions and declinations of the satellite images within this small plate area. A final satellite direction is interpolated from the curve.

The astrometric reduction (projective equations model) when applied to a small plate area will give individual satellite directions very similar to those determined photogrammetrically. In this study, the only pre-reduction corrections applied were to the stellar coordinates and were for refraction and diurnal aberration. More realistically, some camera lens distortion parameters should be nearly constant and could be determined. In practice, the plate coordinates would be corrected for the known lens distortions before the reduction, and even better results would be expected from the projective equations.

The projective equations, as used here, sometimes suffered from a weak determination of the parameters. In some cases there were only 0.5 degrees of freedom per unknown parameter. Furthermore, the star distribution within the plate area was not uniform in all cases. These two deficiencies could be corrected by altering the pre- and post-calibration program to produce more star images, by using more than one image per star trail or by placing particular emphasis on measuring and identifying sufficient and well distributed stars within the area of interest.

Any single satellite image, no matter how carefully reduced, can still be affected by large random errors. These random errors are more influential in

short focal length cameras, but still impose significant limits on the expected accuracies in cameras with longer focal lengths. Through a curve fitting procedure, the random errors of an individual satellite direction can be suppressed to a level where the systematic errors probably dominate. At the present, only a passive satellite can provide the number of observations required to fully exploit this technique.

On each plate, the precision estimates (σ_x, σ_y) of the satellite directions derived from the several polynomials compared favorably to the σ_x, σ_y for a satellite direction from a single polynomial. This can be illustrated simply, if not rigorously, by computing the precision of the mean of the five satellite directions from plate 2559 and comparing it to the precision of the single direction computed by ESSA. This is not rigorous in that the correlation between the several satellite directions was not determined.

The mean value is a linear function of the type [Hogg and Craig, 1965, p. 148].

$$Y = \sum_{1}^{5} k_i X_i$$

where k_i is equal to 1/5 in this case. The variance estimate of the mean takes the form

$$\sigma^2 = \sum_{1}^{5} k_i^2 \sigma_i^2 + 2 \sum_{i<j} \sum k_i^2 \rho_{ij} \sigma_i \sigma_j$$

where ρ is the correlation coefficient between the several satellite directions. The variance estimates of the x and y coordinates were computed. Assuming the correlation to be 1 (an unrealistically high estimate), the standard deviations (in μm) of the mean x and y coordinates were approximately 0.32 and 0.31 respectively. Assuming a correlation of 0.3, the standard deviations would about equal those given by ESSA for their single satellite directions (near 0.22 μm for both coordinates).

In the case of the astrometric reduction, where the correlation should approach zero, the standard deviation estimates of a mean right ascension and declination (in μm at plate scale) were approximately 0.17 and 0.18 respectively. These figures only illustrate that it is not mandatory to suffer a loss of overall

precision from the shorter polynomials. Of more importance is the accuracy, the number, and the geometry of the additional satellite directions made available.

The experimental results have led to the following recommendations.

(a) That shorter image trails and lower degree polynomials be considered for use with ballistic camera (BC-4) observational data. This would result in additional observations per plate.

(b) That the theory and limitations of polynomial fitting be recognized in any such program and a continuing evaluation of the polynomials be made using established statistical methods.

No specific recommendations have been made in the area of the photogrammetric vs. the astrometric plate reduction technique. It has been demonstrated that the astrometric reduction usually yields satellite coordinates very close to the photogrammetric, but it must be assumed that the latter are the more accurate.

To offset the loss of accuracy, the astrometric reduction is simpler and faster, requires fewer plate measurements, and provides the opportunity for additional observations per plate. Furthermore, plates that would be unusable for a photogrammetric reduction, due to partial cloud cover, etc. might yield one or two completely reliable sets of astrometrically derived coordinates. In any particular project, the final accuracies desired, the time and resources available, and certainly the cameras and associated equipment should determine the reduction technique to be used.

REFERENCES

Baarda, W. (1967). "Statistical Concepts in Geodesy." Publications on Geodesy, New Series, No. 4, Vol. 2, Netherlands Geodetic Commission, Delft, Netherlands.

Badekas, John. (1967). "Phase Correction for Spherical Specular Satellite." Unpublished paper, The Ohio State University Department of Geodetic Science.

Biometrika Tables for Statisticians. (1966). Third Edition, Vol. 1 (H. O. Hartley and E. S. Pearson, eds), Cambridge University Press.

Brown, Duane C. (1964). "An Advanced Reduction and Calibration for Photogrammetric Cameras." Prepared for the Air Force Cambridge Research Laboratories, Office of Aerospace Research, United States Air Force, Bedford, Massachusetts, January.

Brown, Duane C. (1967). "Review of Current Geodetic Satellite Programs and Recommendations for Future Programs." Prepared for the National Aeronautics and Space Administration, June.

Hallert, Bertil H. (1960). Photogrammetry. McGraw-Hill Book Company, Inc., New York.

Hallert, Bertil H. (1966). National Science Foundation Lecture, The Ohio State University, Columbus, Ohio, November 3-4.

Hogg, Robert V. and Allan T. Craig. (1965). Introduction to Mathematical Statistics. The Macmillan Company, New York.

Hornbarger, Daniel H. (1968). "Comparison of Astrometric and Photogrammetric Plate Reduction Techniques for a Wild BC-4 Camera." The Ohio State University Department of Geodetic Science Report No. 106, March. (A more extensive version of this report also exists as a Master of Science thesis submitted to the Graduate School of The Ohio State University.)

Hotter, Frank D. (1967). "Preprocessing Optical Satellite Observations." The Ohio State University Department of Geodetic Science Report No. 82, April.

Lambeck, Kurt. (1967). "Precise Geodetic Position Determination with Aid of Artificial Earth Satellites." Doctoral Thesis, University of Oxford, England.

Mandel, John. (1964). The Statistical Analysis of Experimental Data. Interscience Publishers, New York.

Markowitz, Wm. (1963). "Timing of Artificial Satellite Observation for Geodetic Purposes." The Uses of Artificial Satellites for Geodesy (G. Veis, ed), North Holland Publishing Company, Amsterdam, Netherlands.

Mueller, Ivan I. (1964). Introduction to Satellite Geodesy. Frederick Ungar Publishing Co., Inc., New York.

Natrella, Mary G. (1963). Experimental Statistics. National Bureau of Standards Handbook No. 91, United States Department of Commerce, United States Government Printing Office, Washington, D. C.

Schmid, Erwin. (1964). "Phase Correction for Sun-Reflecting Spherical Satellite," United States Coast and Geodetic Survey, ESSA.

Schmid, Hellmut H. (1959). "A General Analytical Solution to the Problem of Photogrammetry." Ballistic Research Laboratories Report No. 1065, Aberdeen Proving Ground, Maryland, July.

Schmid, Hellmut H. (1965a). "Accuracy Aspects of a World-Wide Passive Satellite Triangulation System." Photogrammetric Engineering, American Society of Engineering, Vol. XXXI, No. 1, January.

Schmid, Hellmut H. (1965b). "Precision and Accuracy Considerations for the Execution of Geometric Satellite Triangulation." Second International Symposium: The Use of Artificial Satellites for Geodesy. National Technical University, Athens, Greece.

Schmid, Hellmut H. (1966). "The Status of Geometric Satellite Triangulation at the Coast and Geodetic Survey." Presented to the ACSM/ASP Convention, Washington, D.C., March.

Smart, W.M. (1962). Textbook on Spherical Astronomy. Fifth edition. Cambridge University Press.

Smithsonian Astrophysical Observatory. (1966). "Geodetic Parameters for a Standard Earth." (C.A. Lundquist and G. Veis, eds). SAO Special Report No. 200, Vol. 1.

United States Coast and Geodetic Survey. (1965) "Satellite Triangulation in the Coast and Geodetic Survey." Technical Bulletin No. 24, February.